ELECTRON CAPTURE AND LOSS AND IONIZATION

IN IONIC AND ATOMIC IMPACT PHENOMENA

F. J. DE HEER

ELECTRON CAPTURE AND LOSS AND IONIZATION IN IONIC AND ATOMIC IMPACT PHENOMENA

ELECTRON CAPTURE AND LOSS AND IONIZATION

IN IONIC AND ATOMIC IMPACT PHENOMENA

PROEFSCHRIFT

TER VERKRIJGING VAN DE GRAAD VAN DOCTOR IN DE WIS- EN NATUURKUNDE AAN DE RIJKSUNIVERSITEIT TE LEIDEN OP GEZAG VAN DE RECTOR MAGNIFICUS DR A. E. VAN ARKEL, HOOGLERAAR IN DE FACULTEIT DER WIS- EN NATUURKUNDE, TEGEN DE BEDENKINGEN VAN DE FACULTEIT DER WIS- EN NATUURKUNDE TE VERDEDIGEN OP WOENSDAG 6 JUNI 1956 TE 15 UUR

DOOR

FREDERIK JACQUES DE HEER

GEBOREN TE EINDHOVEN IN 1926

1956

WED. G. VAN SOEST - AMSTERDAM

Promotor: Prof. Dr J. Kistemaker

Aan de nagedachtenis van mijn vader

Aan mijn vrouw

In overeenstemming met de wens van de Faculteit der Wis- en Natuurkunde van de Leidse Universiteit volgt hierbij een overzicht van mijn universitaire studie.

Ik begon mijn studie in september 1945 aan de Amsterdamse Universiteit, waarna ik in december 1948 mijn kandidaats examen letter D en in maart 1952 het doctoraal examen experimentele natuurkunde aflegde. De tentamens in de statistische en quanten mechanica werden mij afgenomen door Prof. Dr. J. de Boer, het tentamen elektriciteitsleer door Prof. Dr. S. A. Wouthuysen.

In de jaren 1948-1952 werkte ik op het van der Waals laboratorium onder leiding van Prof. Dr. A. M. J. F. Michels aan de absorbtie spectrografie. Wij voerden metingen uit voor sterk gecomprimeerd CO_2 gas in het ultraviolette gebied en bestudeerden bandverbreding en bandverschuiving.

In maart 1952 begon ik de in dit proefschrift beschreven onderzoekingen op het Laboratorium voor Massaspectrografie onder leiding van Prof. Dr. J. Kistemaker. De opzet van het onderzoek werd tevens besproken met Prof. Dr. C. J. Bakker en het onderzoek maakte deel uit van het program van de Stichting voor Fundamenteel Onderzoek der Materie in welke organisatie ik in januari 1955 als gewoon medewerker werd aangesteld. Het onderzoek werd tevens gesubsidieerd door de Philips Gloeilampen Fabrieken in Eindhoven.

Vanaf october 1955 werkte ik voor een deel van mijn tijd mede aan het reactor project bij de Kema, onder leiding van Dr. J. J. Went.

Bij de experimenten over vangst, verlies en ionisatie doorsneden werd ik gedurende de laatste twee jaren geassisteerd door W. Huizenga. De metingen werden uitgevoerd tesamen met W. Huizenga, P. van Deenen, C. Visser, de staf van de isotopen separator onder leiding van Drs. P. K. Rol en andere medewerkers van het laboratorium. Bij de uitwerking der resultaten werd een groot deel van het rekenwerk verricht door Ir. G. Braam.

Bij de constructie van het apparaat werd behalve van Prof. Dr. J. Kistemaker technisch advies en hulp verkregen van W. Hoogvorst, leider van de Centrale Werkplaats van het Gemeente Energiebedrijf in Amsterdam, van Meester J. P. J. Janssen, Dr. C. J. Zilverschoon en Alphons de Meere.

De electronica werd gebouwd in overleg met J. P. J. Nabben en J. Schutten waarbij een groot deel van het uitvoerend werk voor rekening kwam van de volontairs G. v. d. Heide en P. van Deenen.

Het manuscript voor dit proefschrift werd getypt door mijn vrouw en het tekenwerk werd verzorgd door J. Duin.

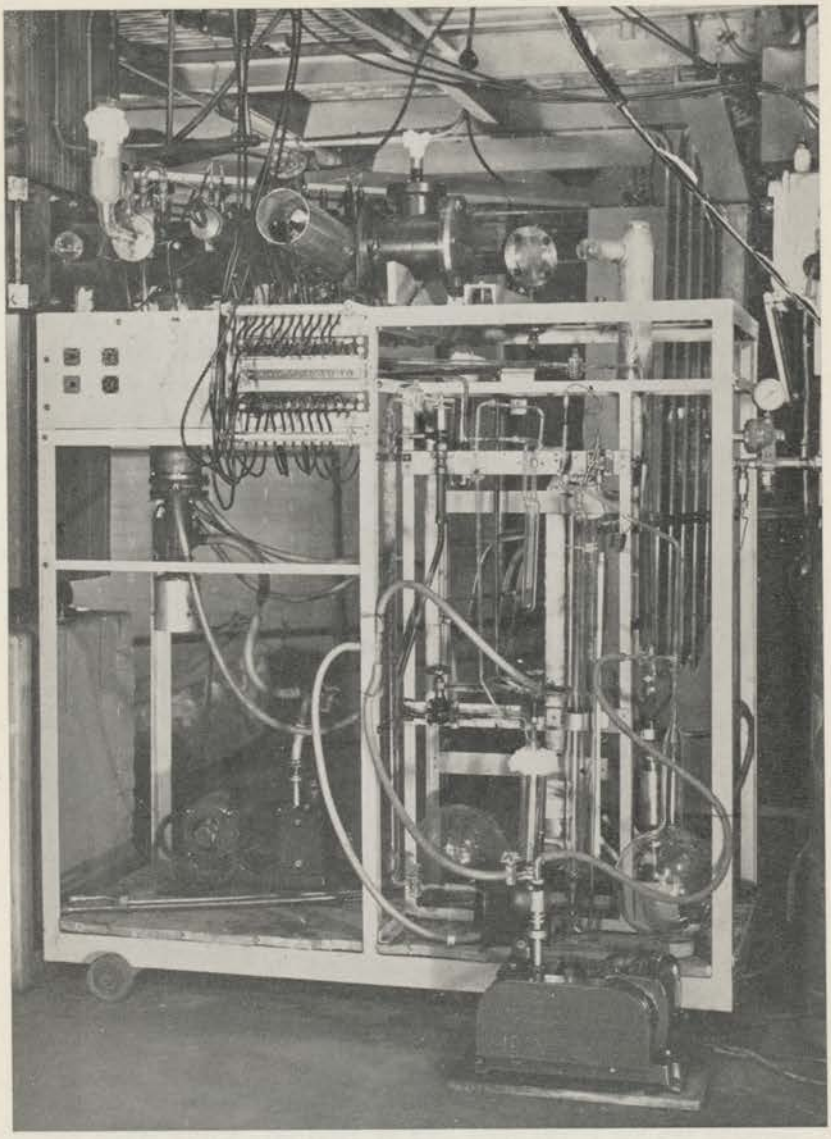

The apparatus used in the capture, loss and ionization cross-section measurements at the collector side of the isotope separator.

INTRODUCTION.

Ionic and atomic impact phenomena are of importance in the production of stable isotopes, which is the main object of our laboratory. The production of the isotopes is performed in a magnetic isotope separator and is described in the dissertation of Zilverschoon[Z1]. In order to show reactions in which we are interested, we shall give a short description of the separator, sometimes used as a source of ions in our capture, loss and ionization experiments.

As a starting-point we take the isotope separation of uranium. Natural uranium consists of the isotopes U^{238} and U^{235}, which we want to separate from each other, as we have schematically indicated in fig. 1.

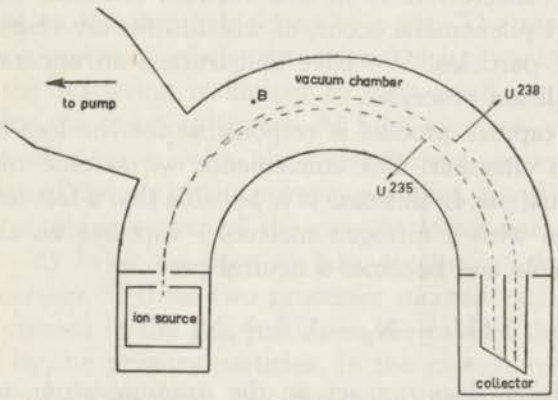

Fig. 1.
The isotope separator in schematical design.

The material is brought into the ion source in the form of uranium tetrachoride. By heating this compound we get gaseous UCl_4 and by bombarding the gas with electrons we produce U^{238} and U^{235} ions. The ion source is maintained at a high tension of about twenty kilovolts. At a certain distance from the exit slit we have placed an earthed electrode by which the ions are extracted

from the ion source and are accelerated into the vacuum chamber. (In reality a lens electrode system is used). In consequence of the presence of a strong magnetic field B ($\pm$ 3000 Gauss), perpendicular to the plane of the paper, the particles describe a path with radius R determined by the equilibrium between the Lorentz and the centrifugal force:

$$R = \frac{1}{B}\sqrt{\frac{2mV}{e}}$$

in which B is the magnetic field, V the acceleration voltage, e the charge of the ions and m the mass of the particle. Having passed through 180 degrees, the particles are gathered at the collector, consisting of two chambers. The equation we have given for R shows us that the lighter isotope U^{235} has to arrive at the left hand chamber, and so on. The space between ion source and collector, the "vacuum chamber", is evacuated so that a separation is realized at a pressure of about 4×10^{-5} mm Hg. Because of the residual gas, only a part of the ions leaving the ion source can reach the collector. It is in this vacuum chamber that the different impact phenomena occur, of which some are responsible for the loss of particles. We have constructed an apparatus to study these collision processes.

At first the capture process is responsible for the loss of ions in the vacuum chamber. For convenience we assume nitrogen being the residual gas. In this case it is possible that a fast uranium ion, in collision with a nitrogen molecule, captures an electron from the molecule and becomes a neutral particle:

$$U^+ + N_2 \rightarrow U^{\not 0} + N_2^+$$

The Lorentz force does not act on the uranium atom, so that the atom follows the tangent of the circular path and is lost for the production.

A second process of great importance in the separation is the ionization of the residual gas molecules:

$$U^+ + N_2 \rightarrow U^+ + N_2^+ + e^-$$

As a consequence of the ionization process, electrons are created in the vacuum chamber. The negative space charge of these

electrons, hampered by the strong magnetic field, prevents a strong spreading of the beam of positive particles and is advantageous for a good resolving power of the separator.

Another process by which the particles are lost is the elastic or inelastic scattering over large angles. In case of the combination U^+, N_2 one can predict that the scattering is limited to small angles, the maximum scattering angle Φ_{max} being given by

$$\sin \Phi_{max} = m/M = 28/238 \therefore \Phi_{max} \sim 7^\circ$$

Following the neutral particles formed by the capture process, these may lose an electron again in collision with a nitrogen molecule, giving rise to the so called loss process:

$$U + N_2 \rightarrow U^+ + e^- + N_2$$

This is also a kind of ionization process where the fast atoms are ionized by the nitrogen gas molecules.

The different processes mentioned have also an important influence on the stopping power of a gas. The capture, loss and ionization processes involve an internal energy exchange and in so far as the scattering is limited to very small angles, they only determine the stopping power. At high energies, of the order of millions of electron volts, the predominent process, namely the ionization of the gas by the primary particles, is mainly responsible for the stopping power of the gas. At lower energies as in our case (1—25 keV), we have to take account of the capture and loss processes. If these two processes succeed each other, an ion pair is created in the gas, just as in the case of the ionization of the gas by the primary particles. In the capture process, the loss of energy is often small, but the main energy loss occurs in the loss process, where the neutral beam particle is ionized by the gas atom. We can assign a comparable influence on the stopping power to the ionization and loss process. In these two processes the energy loss is of the order of thirty electron volts per collision.

In the following chapters we describe the capture, loss and ionization cross-section determinations for different combinations of accelerated ions and gases.

Chapter I.

HISTORICAL REVIEW OF THE EXPERIMENT.

In this chapter we give first a short summary of the different applied methods to determine the capture, loss and ionization cross-sections, secondly we mention in our literature review, which investigators have used these methods, and at last we give some results of capture, loss and ionization cross-sections to orientate ourselves about their order of magnitude.

§ 1.1. Experimental methods.

A. Capture of electrons:

$$X^+ + Y \rightarrow X + Y^+$$

A beam of ions X^+ is shot into a collision chamber, filled with a certain gas Y (fig. 1.1). In consequence of a magnetic field B,

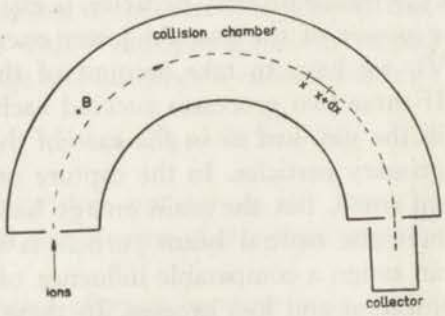

Fig. 1.1.
The capture cross-section determination.

perpendicular to the plane of the paper, the charged particles are turned off and follow a circular path. At the collector we can measure the current of the ions. The ions, becoming neutral by

capturing an electron in collision with a gas atom will not reach the collector. Assuming that at the point x n_x^+ charged particles are present, the change in this number between x and x + dx is given by

$$dn_x^+ = -\alpha_c\, n_x^+\, dx \qquad (1.1.1)$$

α_c represents the probability that the ion captures an electron in the unit length.

After integration over the path length L we get:

$$n_{x=L}^+ = n_{x=o}^+ \exp(-\alpha_c L) \qquad (1.1.2)$$

$n_{x=o}^+$ and $n_{x=L}^+$ are respectively the number of ions at x = o, entering the collision chamber and the number of ions at x = L, arriving at the collector. In vacuo we have $n_{x=o}^+ = n_{x=L}^+$. The number $n_{x=L}^+$ is determined in vacuo and at different gas pressures in the collision chamber by measuring the collector current under these circumstances. From (1.1.2) we see that we can calculate α_c which is linearly pressure dependent.

The results of capture, loss and ionization measurements are very often given by the cross-section σ in stead of using the probability α. Sometimes the quantity λ is used, representing the mean free path length for the process. The relation between σ, α and λ is given by

$$\alpha = 1/\lambda = N\sigma \qquad (1.1.3)$$

which shows us the linear pressure dependence of α.

N is the number of gas atoms per cc.

The equation $\alpha = 1/\lambda$ is almost trivial and is derived from the definition of these quantities.

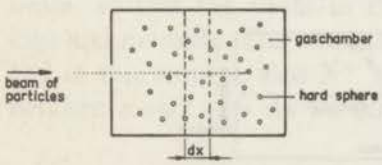

Fig. 1.2.
Derivation of $\alpha = N\sigma$

To derive $\alpha = N\sigma$, we assume that we are shooting particles of infinitely small dimension into a chamber filled with particles, which we may represent by hard spheres (fig. 1.2) and that the velocity of the beam particles is much larger than that of the hard spheres. We calculate the chance that a beam particle hits a hard sphere. For that purpose we consider a gas strip of thickness dx, so thin that there are no two spheres inside the strip, which cover

each other in the direction of the arriving beam. The chance of collision in length dx is now given by the ratio of the total cross-section of the hard spheres present in the gas strip and the cross-section of the strip itself:

$$\alpha \, dx = \frac{N\sigma \; O \; dx}{O}$$

N is the number of hard spheres per cc, O is the cross-section of the gas strip and σ is the cross-section of one hard sphere ($\sigma = \pi r_1^2$ if the radius of the sphere is equal to r_1). From the equation we see at once that $\alpha = N\sigma$.

If the beam of particles were to consist of hard spheres with radius r_2, and the gas molecules were represented by hard spheres with radius r_1, σ would be equal to $\pi (r_1 + r_2)^2$. For inelastic collisions σ is used in the same manner, without taking into account exactly the size of each of the two particles participating in the collision.

It is clear now that (1.1.2) can be written in the form

$$n^+_{x=L} = n^+_{x=0} \exp (- N\sigma_c L)$$

and that if we know α_c at pressure p, we can calculate σ_c from the equation $\alpha_c = N\sigma_c$.

B. Loss of electrons:

$$X + Y \rightarrow X^+ + e^- + Y$$

A beam of ions X^+ and corresponding neutrals X enters the collision chamber, filled with gas Y (fig. 1.3). By means of a

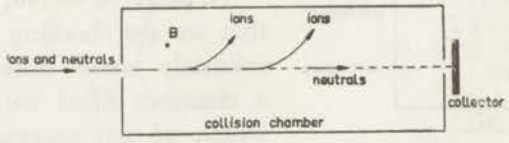

Fig. 1.3.
The loss cross-section determination.

magnetic field B, perpendicular to the plane of the paper, charged particles are deflected at once, so that a neutral which loses an electron in collision with a gas atom, will not reach the collector.

At the collector we determine $n^o_{x=L}$ (= number of neutrals at $x = L$) as a function of the pressure, and we write, by anology with (1.1.2):

$$n^o_{x=L} = n^o_{x=o} \exp(-\alpha_l L) \qquad (1.1.4)$$

$n^o_{x=o}$ is the number of neutrals at the beginning ($x = o$) of the collision chamber.
$n^o_{x=L}$ is the number of neutrals at $x = L$, registered at the collector.
α_l is the probability that the neutral particle loses an electron per unit length.

C. Combination of capture and loss of electrons:

$$X^+ + Y \rightarrow X + Y^+$$
$$X + Y \rightarrow X^+ + e^- + Y$$

Ions X^+ are shot into the collision chamber filled with gas Y (fig. 1.4). Neutrals X are formed by the capture process, but as we do not use a magnetic field in this case, we keep them in the

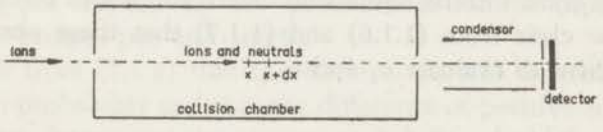

Fig. 1.4.
Combined capture and loss cross-section determination.

beam, so that the beam in the collision chamber contains both ions and neutrals. The neutrals X can experience the loss process, and in this manner ions X^+ are formed again. For the processes between x and $x + dx$ we can write the next equations:

$$\begin{aligned} dn^+_x / dx &= \alpha_l n^o_x - \alpha_c n^+_x \\ dn^o_x / dx &= \alpha_c n^+_x - \alpha_l n^o_x \end{aligned} \qquad (1.1.5)$$

The first of these equations indicates that the number of positive particles at x increases by the loss process for atoms and diminishes by the capture process for ions. The reverse holds for atoms, as

we see in the second equation. By solving these differential equations we can derive the formula of Wien:

$$\alpha = \alpha_c + \alpha_i = 1/L \ln \left(\frac{n^+_{x=L}/n^0_{x=L} + 1}{n^+_{x=L}/n^0_{x=L} - w} \right) \qquad (1.1.6)$$

in which

$$w = n^+_e/n^0_e = \alpha_i/\alpha_c \qquad (1.1.7)$$

The quantities n^+_e and n^0_e are the numbers of ions and neutrals in the equilibrium state of the beam, which is reached at a sufficiently high pressure. In this state the composition of the beam changes no more and is such that as many capture as loss processes occur.

At different pressures the ratio $n^+_{x=L}/n^0_{x=L}$ has to be determined. A detector is used giving the same response on ions and corresponding neutrals. The ratio $(n^+_{x=L} + n^0_{x=L})/n^0_{x=L}$ follows from the response of the detector with and without the ions in the beam. These can be deflected by means of an electrical voltage on the condensor located between collision chamber and detector. At a sufficiently high pressure, further increase of pressure will not change the ratio of ions to neutrals arriving at the detector. The beam has come into its equilibrium state and w can be calculated. It is now clear from (1.1.6) and (1.1.7) that these observations are sufficient to evaluate α_c and α_i.

D. Combination of capture of electrons and ionization:

$$X^+ + Y \rightarrow X + Y^+$$
$$X^+ + Y \rightarrow X^+ + Y^+ + e^-$$

A beam of ions X^+ is shot into a collision chamber filled with gas Y (fig. 1.5). The particles pass along the side electrodes C_1

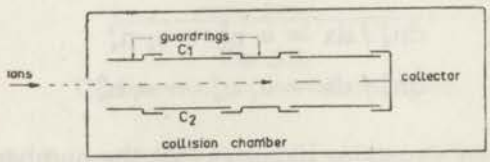

Fig. 1.5.
Combined capture and ionization cross-section determination.

and C_2, flanked by guard rings, and arrive at the collector, so that we can determine the ion intensity $n^+_{x=0}$ in vacuo. Bringing the chamber to a certain gas pressure, slow ions Y^+ will be formed by the capture process, while both ions Y^+ and electrons are created in the gas by the ionization process. By means of a sufficiently high electrical voltage across the side electrodes which hardly influences the linear path of the primary ions, we obtain positive and negative "saturation currents" at C_1 and C_2. If the gas pressure is chosen so low, that on the average in the length of C_1, C_2 no more than one charge exchange collision takes place, one may write the equations

$$\begin{aligned} n^+ &= n_{x=0}\, L\, (\alpha_c + \alpha_i) \\ n^- &= n_{x=0}\, L\, \alpha_i \end{aligned} \tag{1.1.8}$$

n^+ is the slow ion current at the negative electrode of C_1, C_2 and is composed of ions Y^+, which are formed both by capture and ionization.

n^- is the slow electron current at the positive electrode of C_1, C_2 and is composed of electrons which are formed only by ionization.

L is the length of the electrodes C_1 and C_2.

α_c and α_i are respectively the probabilities for the capture and ionization process per unit length.

We see from (1.1.8) that the electron current determines the ionization probability and that the difference of positive and negative current determines the capture probability. At high pressure, Eq. (1.1.8) is no more valid, because the loss process has to be taken into account, so that the formula of Wien (1.1.6) applies.

§ 1.2. Literature review.

The first experiments on charge exchange phenomena were done by Wien[W1], who was active round about 1900.

The method with combined capture and loss cross-section measurements (§ 1.1 section C) and the application of the formula of Wien find their origin in his work. With the unsufficiently technical means at his disposal, Wien was not able to get more than a qualitative view. He determined capture and loss cross-sections for canal rays shot into hydrogen gas. His ion beam contained both hydrogen atomic and hydrogen molecular ions

and the energy of the particles in the beam was not homogeneous, so that we can not set much value on his results.

Ruttenauer[R1] (1921) and Ruchardt[R2] (1923) repeated the capture and loss cross-section measurements for hydrogen ions in hydrogen gas. They used, in the same way as Wien, a thermo-element as detector for ions and neutrals.

An important improvement in these experiments was realized by Bartels[B1] (1930) and Meyer[M1] (1937), by using an analyzing magnetic field for the ions shot into the collision chamber. In this way they got a beam homogeneous in energy and consisting of protons only. Bartels operated with energies between 4 and 30 keV, Meyer with energies between 30 and 200 keV. The protons were not only shot into hydrogen, but also into air, oxygen and nitrogen. As a detector with the same response on ions and corresponding neutrals, they used an ionization chamber, in the meantime constructed by Gerthsen[G1] (1929).

Rudnick[R3] (1931) and Batho[B2] (1932) carried out capture and loss cross-section measurements for rare gas ions shot into rare gases, in the energy region 5—30 keV. Their method is not in principle much different from that of Bartels and Meyer, but the particles were again detected by a thermocouple.

Goldmann[G2] (1931) was the founder of a series of investigations, in which we have a combination of capture and ionization cross-section measurements (§ 1.1 section D). Goldmann shot protons with energies between ½ and 4 keV into hydrogen and argon gas. The method of Goldmann was repeated by Sherwin[S1] (1940), who investigated the capture and ionization for metal ions, shot into hydrogen and helium gas. Keene[K1] (1949) improved the method by giving a lot of attention to secondary effects such as the formation of electrons at the edges of the entrance slit of the collision chamber and the secondary emission of electrons at a side electrode caused by accelerated gas molecular ions. By means of an extra slit, located immediately behind the entrance slit, he suppressed the secondary emission of electrons from the edges of the latter. The extra slit had a larger opening than the other one and was put at a small negative voltage with respect to this entrance slit. The secondary emission at a side electrode, caused by the gas molecular ions, was investigated and suppressed by use of transparent grids. The measure-

ments by Keene deal with H^+, H_2^+, and He^+ ions, shot into hydrogen and helium gas with energies between 3 and 35 keV. In this kind of experiment, Keene was the first investigator, who made mass-spectrometric analysis of the particles formed in the gas. In case of hydrogen gas, he was interested in the question of whether much dissociation appeared as a consequence of the bombardment of the gas molecules by fast ions. The measured dissociation effect seemed to be small. The experiments of Keene were continued by Stedeford[S2] (1954), who started his work with the same apparatus and tried to reproduce some of his results. In case of protons shot into helium he found a capture cross-section which was approximately the half of Keene's value. Stedeford found that the cross-sections determined seemed to depend markedly upon surface conditions, for example state of cleanliness and degree of outgassing. Keene used a second electrode system to determine the proportion of the electrons, collected at the side electrode, which were due to secondary emission, in order to obtain the ionization cross-section. This involved the further assumption that the secondary emission coefficient for the surfaces was the same in these two systems. According to Stedeford, the invalidity of this assumption could be the cause for non reproduction of the results. Stedeford changed the arrangement of Keene in such a way, that the surface effect could not influence the results, but he therefore had to limit himself to capture cross-section determinations only. He shot H^+, H_2^+, and He^+ ions into rare gases with energies between 3 and 40 keV. The experiments of Stedeford formed a continuation of the low energy work of Hasted[H1,2] (1951, 1952), not discussed here. Stedeford has also carried out some measurements for negative atomic hydrogen ions shot into rare gases in the mentioned energy range and he belongs with Hasted among the few workers, who have done experiments about the electron detachment or loss cross-sections of negative ions.

Many recent measurements have been done in the U.S.A., under the direction of Allison[A1] (1953) in Chicago. With these experiments a magnetic field is used in the collision chamber to give the charged particles a curved path. Montague[M2] (1951) carried out loss cross-section determinations (§ 1.1 section B) for H atoms shot into hydrogen between 44.5 and 321 keV. We have seen that the loss cross-section determination performed by

the method in § 1.1 section B is very easy in principle and should be preferred to the indirect determination method of Wien (§ 1.1 section C). However there are some difficulties. Montague has to make a beam of neutral particles and this is done by shooting protons through a thin foil. After having passed the foil, the neutrals which are formed by capture pass into the collision chamber. Especially at energies lower than about 40 keV, the particles leaving the foil, are no longer homogeneous in energy and as a consequence of scattering effects in this foil, their path is not completely defined. It is always a difficult task to construct an accurate detector for neutral particles. Montague used a method, in which the H atoms are registered by measuring the current of secondary emitted electrons at a beryllium- copper plate. Ribe[R4] (1951) carried out capture cross-section determinations (§ 1.1 section A) in the same apparatus as Montague, with a small change in the arrangement. Protons were shot into hydrogen gas with an energy between 34 and 149 keV. The current of the protons was checked by use of a Faraday cylinder. Kanner[K2] (1951) has used the apparatus to determine capture and loss cross-sections for protons shot into air. Snitzer[S3] (1953) carried his beam, consisting of helium ions, into a collision chamber also filled with air. The pressure in this chamber was taken so high, that an equilibrium state in the beam was formed between He^{++}, He^{+} and He^{0} particles. The beam leaving the collision chamber was magnetically analyzed in the same chamber, which his predecessors used for their capture and loss cross-section measurements. To compare the intensities of charged and neutral particles, use was made of thermo-couples. The work of Snitzer was continued by Krasner[K3] (1955), who investigated the loss process for neutral helium atoms shot into hydrogen, helium and air. The particles had an energy between 100 and 450 keV.

At Oak Ridge, also in the U.S.A., Stier[S4] (1954), Barnett and Evans carried out measurements in almost the same manner as Snitzer, determining the equilibrium state in the beam for many ion gas combinations. The energy of the particles was taken between 20 and 250 keV. They made an electrostatic analysis of the beam of particles emerging from the collision chamber and these were again detected by different thermo-couples.

Of great interest are the measurements of Whittier [W2] (1954) in Canada, who shows the importance of the formation of negative H^- ions, when a beam of H^+ particles is shot into hydrogen gas with energies between 4 and 70 keV. After having passed the collision chamber, the magnetic analysis of the beam is made in the so called observation chamber. The positive and negative hydrogen ions are gathered in two different Faraday cylinders, movable longitudinally and symmetrically arranged with respect to the axis of the beam. The currents in the two Faraday cylinders are determined as a function of the pressure in the observation chamber. Whittier used in this respect a method analogous to that of Ribe and Montague, so that (1.1.2) and (1.1.4) can be used to evaluate the capture cross-section for protons and the loss cross-section for negative hydrogen ions. At high pressures in the collision chamber the beam comes into its equilibrium state, and it is found that, at 8.5 keV acceleration of the protons, the equilibrium ratio of the number of H^- to that of H^+ ions amounts to 0.222. In this way Whittier has shown that the formula of Wien (1.1.6) does not hold for the combination H^+, H_2, because the formation of H^- ions is not taken into account. Results of Bartels and Meyer have to be corrected for this effect, as far as negative ions can be formed, which is not the case for accelerated rare gas ions.

Müller [M3] (1954) has performed capture and ionization cross-section measurements for H^+ and H_2^+ ions shot into hydrogen with energies between 1 and 25 keV. In one of his experimental arrangements he has used a magnetic field to analyse the beam which has passed his collision chamber. In this way he can determine the dissociation efficiency for H_2^+ ions. While the fast H^+ and H_2^+ ions are detected with a Faraday cylinder, the slow ions formed in the gas are checked at the side electrodes more or less in the same manner as in Keene's arrangement. The different cross-sections are evaluated by means of a mathematical formalism, which forms an extension of the differential equations of Wien (1.1.5). This formalism is so complicated because the processes both of fast H_2^+ and H^+ ions have to be considered. The dissociation cross-section for the fast H_2^+ ions seemed to be small, being in accordance with the relative small H^+ peak, which Keene found for the slow ions formed in hydrogen gas.

For the sake of completeness we mention the capture cross-section measurements of Smith[S5] (1934), taken for protons in hydrogen and for protons and He^+ ions in helium, in the energy region of 1 to 12 keV.

If we consider our capture, loss and ionization cross-section measurements in connection with this review, we range our capture and loss cross-section determinations among the method of Wien (§ 1.1 section C), though we have applied it in a different experimental way. We range our ionization cross-section determinations more or less among the method of Keene (§ 1.1 section D). As a control on the method of Wien, we determine also the capture cross-section in the same way as Stedeford (§ 1.1 section D). We have used an energy region of 2 to 25 keV.

In short we have summarized the work done on capture, loss and ionization cross-sections for different ion gas combinations in the lower energy region. We can not prefer one method to another one; they all include different experimental possibilities. Till now most work is done on ion and gas particles where the scattering over large angles is so rare that the cross-section measurement is not disturbed. Whether this scattering plays an important part is strongly dependent on the geometrical dimensions of the apparatus. It is in this respect that more ion gas combinations can be investigated with an arrangement as used by Keene and Stedeford, than with the arrangement of Montague and Ribe. The two Americans have used a secondary emittor and a Faraday cylinder, which are closed by a small slit, so that the scattering is permitted over angles not larger than about half a degree compared with a limit of about six degrees in the arrangement of Stedeford. It is clear that more attention has to be paid to the influence of scattering.

No room is left here for such an extensive discussion of the different experiments, as given by Massey[M4] and Burhop (1952). In two tables they give a review of all the ion gas combinations which have been taken in the capture, loss and ionization cross-section measurements. In these tables they have also included the lowest energy work (0—1000 eV) of which that of Rostagni[R5] (1934), Wolf[W3,4,5] (1935—1939) and Hasted is the most important.

§ 1.3. Results.

It is not our intention to summarize all the results, obtained by different observers. By giving a few dates, we will form us an idea about the order of magnitude of the cross-sections and we show that there is often a large discrepancy between the results of the already mentioned investigators.

In fig. 1.6 we have compared the capture cross-section values, which are given by different observers for the process

$$H^+ + H_2 \rightarrow H + H_2^+$$

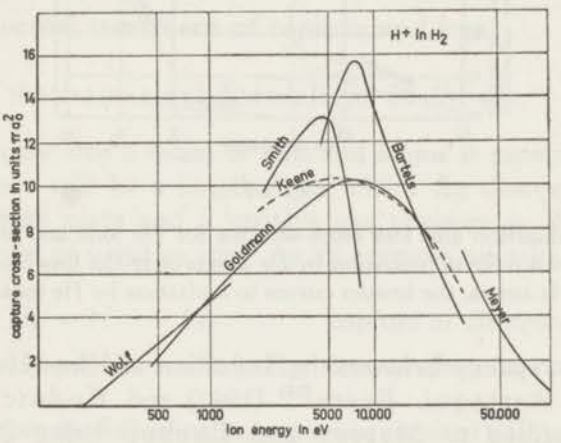

Fig. 1.6.

Capture cross-sections for H^+ in H_2 measured by a number of different observers.

All the curves have the same shape with a maximum for the capture cross-section which is reached at 7 keV, where this cross-section is about 12 π a_o^2. However there is a considerable spread in the observed values, being up to 50% at the maximum of the curve.

Fig. 1.7 illustrates the results of ionization and loss cross-section measurements for the processes

$$He^+ + He \rightarrow He^+ + He^+ + e^- \text{ (ionization)}$$

$$He \quad + He \rightarrow He^+ + e^- \quad + He \text{ (loss or ionization)}$$

For the sake of completeness we remark that Massey and Burhop and other workers do not make a distinction between loss and ionization. Indeed, the loss process is a kind of ionization, namely the ionization of the fast neutrals by a gas molecule or a gas atom. In case of the collision between fast He atoms and He gas atoms, the ionization and loss process are identical in the relative coordinate system and the cross-sections which are found for both processes must be equal to each other.

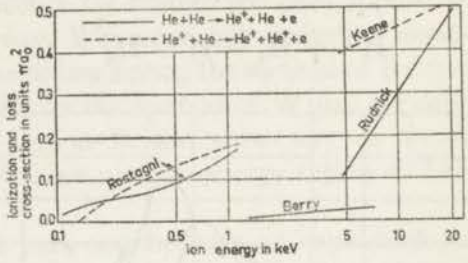

Fig. 1.7.

Measured ionization and loss cross-sections for He ions and atoms in He. The full curves refer to ionization by He atoms or to the loss process for fast He atoms, the broken curves to ionization by He ions.

The discrepancy between the ionization and loss cross-section results of Rostagni, Berry[B3] (1942) and Rudnick is very great, according to Massey and Burhop being due to the different methods used. From our own measurements, discussed in chapter IV, we can understand that it is in general more difficult to do accurate ionization and loss cross-section determinations than corresponding capture ones and so we are not surprised about these large discrepancies. The ionization and loss cross-sections are smaller than the capture cross-sections, as we generally have in our energy region.

CHAPTER II.

GENERAL TREATMENT OF OUR CAPTURE, LOSS AND IONIZATION CROSS-SECTION DETERMINATION.

§ 2.1. Formal treatment of capture and loss.

A. The mathematical formalism of Wien.

We suppose that a beam of ions and atoms is passing through a gas. There will be a length L in which the charge exchange processes take place and a variable gas pressure p. We neglect the formation of negative ions. As an example we take:

$$\begin{aligned} N^+ + H_2 &\rightarrow N \quad + H_2^+ \quad \text{capture of electrons} \\ N \quad + H_2 &\rightarrow N^+ + e^- + H_2 \quad \text{loss of electrons} \end{aligned} \tag{2.1.1}$$

We remember the following important equations (1.1.3) and (1.1.6)

$$\begin{aligned} \alpha_c &= 1/\lambda_c = N\sigma_c;\ \alpha_l = 1/\lambda_l = N\sigma_l \\ \alpha &= \alpha_c + \alpha_l \end{aligned} \tag{2.1.2}$$

α_c and α_l are the probabilities that a particle respectively captures or loses an electron in a length of one centimetre; λ_c and λ_l are the corresponding mean free path lengths.
σ_c and σ_l are the corresponding cross-sections in square centimeters per atom.
N is the number of gas atoms per cc.

Now we consider a beam consisting of n_x^+ ions and n_x^0 atoms at a point x and ask ourselves what is going on between x and x + dx. The number of ions n_x^+ will diminish by capture in dx, but also increase by loss in dx, as we can understand from (2.1.1).

In the same way we find the change in the number of atoms n_x^o. We assume that no beam absorption takes place by scattering over large angles. In this way we can write:

$$\begin{aligned} dn_x^+ / dx &= \alpha_l \; n_x^o \; - \alpha_c \; n_x^+ \\ dn_x^o / dx &= \alpha_c \; n_x^+ \; - \alpha_l \; n_x^o \end{aligned} \qquad (2.1.3)$$

By adding these equations and integrating we obtain:

$$n_x^+ \; + n_x^o = \text{constant} \qquad (2.1.4)$$

If the beam has come into its equilibrium state, so that as many captures as losses occur, dn_x^+/dx and dn_x^o/dx will be zero. From (2.1.3) we derive at once

$$n_e^+ / n_e^o = \alpha_l / \alpha_c \qquad (2.1.5)$$

n_e^+ and n_e^o are respectively the numbers of ions and neutrals in the beam at its equilibrium state. In practice the ratio n_e^+/n_e^o is often represented by w:

$$w = n_e^+ / n_e^o \qquad (2.1.6)$$

When we combine the last equation of (2.1.2), (2.1.4) and (2.1.5), we derive:

$$\begin{aligned} \alpha_c &= \alpha \; n_e^o \; / (n_x^+ \; + n_x^o) \\ \alpha_l &= \alpha \; n_e^+ / (n_x^+ \; + n_x^o) \end{aligned} \qquad (2.1.7)$$

By solving the simultaneous differential equations (2.1.3) and integrating over distance L, we find

$$\begin{aligned} n_{x=L}^+ &= \quad A \exp(-\alpha L) + B \\ n_{x=L}^o &= -A \exp(-\alpha L) + \alpha_c / \alpha_l \; B \end{aligned} \qquad (2.1.8)$$

A and B are determined by the conditions at $x = o$ and $x = \infty$

$$\begin{aligned} n_{x=o}^+ &= A \; + B \\ n_{x=\infty}^+ &= n_e^+ = B \end{aligned}$$

so that we have

$$\begin{aligned} B &= n_e^+ \\ A &= n_{x=o}^+ - n_e^+ \end{aligned} \qquad (2.1.9)$$

We have given the mathematical formalism of Wien and in the next paragraph we shall show how we can apply it in our experiment, in order to determine the capture and loss cross-section.

For the sake of completeness, we treat the special case where $n^o_{x=o} = 0$ and we derive the formula of Wien (see 1.1.6). Under these circumstances a beam consisting of only ions enters the collision chamber. We obtain from (2.1.9) and (2.1.4).

$$\begin{aligned} A &= n^o_e \\ B &= n^+_e \end{aligned} \qquad (2.1.10)$$

Substituting (2.1.10) in (2.1.8) we get:

$$\begin{aligned} n^+_{x=L} &= n^o_e \exp(-\alpha L) + n^+_e \\ n^o_{x=L} &= n^o_e [1 - \exp(-\alpha L)]. \end{aligned} \qquad (2.1.11)$$

Dividing the first of these equations by the second we obtain after some operation the formula of Wien (see also § 1.1 section C)

$$\alpha = \alpha_c + \alpha_i = 1/L \ln \left(\frac{n^+_{x=L} / n^o_{x=L} + 1}{n^+_{x=L} / n^o_{x=L} - w} \right) \qquad (2.1.12)$$

in which

$$w = n^+_e / n^o_e = \alpha_i / \alpha_c$$

B. Simplification of the mathematical formalism of Wien in a special example.

In the special case that a beam consisting of only ions enters the collision chamber and where the gas pressure is so low that we have on the average no more than one charge exchange process in the interval (o, L_2), we can write for the first equation of (2.1.3)

$$dn^+_x / dx = -\alpha_c n^+_x \qquad (2.1.13)$$

For experimental reasons (see § 2.3) we take the integration of (2.1.13) over the interval (L_1, L_2), where $L_1 < L_2$ and $L_2 - L_1 = L'$, getting

$$n^+_{x=L_2} = n^+_{x=L_1} \exp(-\alpha_c L') \qquad (2.1.14)$$

If $\alpha_c L'$ is much smaller than unity, we can write after some operation

$$(n^+_{x=L_1} - n^+_{x=L_2}) / n^+_{x=L_1} = \alpha_c L' \qquad (2.1.15)$$

Taking the pressure low enough and L_1 sufficiently small, we approximately have $n^+_{x=L_1} \sim n^+_{x=0}$, so that we obtain

$$(n^+_{x=L_1} - n^+_{x=L_2}) / n^+_{x=0} = \alpha_c L' \qquad (2.1.16)$$

We shall show in § 2.3 that we can apply (2.1.16) in our experiment in order to determine the capture cross-section independently of the other quantities. We remarked already in § 1.2 that we follow in this way the experimental method of Stedeford.

C. Application of the formalism of Wien in a second example.

We assume that we have a small variation on the circumstances taken in section B of this paragraph, so that we may not neglect a small quantity of neutrals entering the collision chamber and $n^+_{x=L_1}$ can not be approximated by $n^+_{x=0}$. We now take the gas pressure so high that besides first order processes, second order processes will also occur and may not be neglected. We assume that processes of third and higher order take place to a negligible extent. We can now write in stead of (2.1.14)

$$n^+_{x=L_2} = \underbrace{n^+_{x=L_1} \exp(-\alpha_c L')}_{\text{capture}} + \underbrace{n^+_{x=L_1} \left[1 + \frac{\alpha_1 \exp(-\alpha_c L') - \alpha_c \exp(-\alpha_1 L')}{\alpha_c - \alpha_1}\right]}_{\text{first cycle}} + \underbrace{n^0_{x=L_1} [1 - \exp(-\alpha_1 L')]}_{\text{loss}} \qquad (2.1.17)$$

The term indicated by capture represents the number of ions which would be present at $x = L_2$, if the capture process was only taken into account.

The number of neutrals present at $x = L_1$ is responsible for the term indicated by loss. This term equals the number of ions which are formed in the interval (L_1, L_2) by the loss process, increasing the number of ions present at $x = L_2$.
The term indicated by one cycle represents the number of reborn ions which have experienced succeedingly capture and loss. This term is derived as follows:

We assume that a beam is moving along the X axis containing $n^+_{x=o}$ ions at $x = o$ (fig. 2.1). The number of captures taking place at x between x and $x + dx$ is given by $n^+_x \alpha_c dx = n^+_{x=o} \exp(-\alpha_c x)\, \alpha_c dx$. An equal amount of fast atoms is formed, of which a fraction $[(1 - \exp - \alpha_l (L - x)]$ loses an electron before the beam reaches $x = L$. We say now that the reborn ion, having experienced capture and loss successively, has completed one charge exchange cycle. The number of events, the first step of which takes place in the interval $(x, x + dx)$ and the second in (x, L), is given by

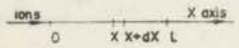

Fig. 2.1.
Beam of ions moving along the X axis.

$$n^+_{x=o} \exp(-\alpha_c x) \cdot \alpha_c dx\, [1 - \exp - \alpha_l (L - x)]$$

By integration of this expression over x in the interval (o, L) we get the number of reborn ions, which are formed in one cycle:

$$n^+_{x=o} \left[1 + \frac{\alpha_l \exp(-\alpha_c L) - \alpha_c \exp(-\alpha_l L)}{\alpha_c - \alpha_l}\right] \qquad (2.1.18)$$

This term equals the term indicated by "first cycle" in (2.1.17), if $n^+_{x=o}$ is replaced by $n^+_{x=L_1}$ and L by L'.

If $\alpha_c L$ and $\alpha_l L$ are much smaller than unity we can develop the exponential powers in (2.1.18) and neglecting third and higher order terms we get

$$n^+_{x=o} (\tfrac{1}{2} \alpha_c \alpha_l L^2) \qquad (2.1.19)$$

In the same manner we simplify (2.1.17) developping all exponential powers and we abtain

$$n^+_{x=L_1} = n^+_{x=L_1} [1 - \alpha_c L' + \tfrac{1}{2} \alpha_c^2 L'^2 + \tfrac{1}{2} \alpha_c \alpha_l L'^2] + n^o_{x=L_1} \alpha_l L'$$

After some operation we change it into

$$(n^{+}_{x=L_1} - n^{+}_{x=L_1})/n^{+}_{x=L_1} = L'\alpha_c[1-\tfrac{1}{2}\alpha L' + (n^{0}_{x=L_1}/n^{+}_{x=L_1})w] \quad (2.1.20)$$

In this experiment it is our intention to show with (2.1.21) to what extent the approximations made with the derivation of (2.1.16) in § 2.1 section B are justified.

§ 2.2. The combined experimental determination of σ_c and σ_l.

A. Introduction.

Our combined capture and loss cross-section determination consists of a measurement of the ion intensity of the beam at a certain distance L from the entrance slit of the collision chamber as a function of the gas pressure. We could do that in the simplest way by measuring the current to a flat electrode, arranged at a distance L from the slit and perpendicular to the beam direction. However, two disturbances will occur at this electrode, namely the secondary emission of electrons and the reflection of fast particles.

In stead of a flat electrode, a shielded Faraday cylinder with small entrance slit is often used in practice. In the experiments of Allison and his co-workers (see § 1.2), the presence of a magnetic field in the collision chamber prevents the escape of secondary electrons from the cylinder. If this field is not present, we must prevent the escape of these electrons by an extra electrode, located immediately before the entrance slit of the Faraday cylinder and with a small negative voltage with respect to this. We shall not discuss the complications which arise in this case and which are caused by the particles in the gas formed by capture and ionization.

Reflection effects will not have an important influence on the current measurement, if the cylinder approximates to a closed form. It is clear, however, that as a consequence of the small entrance slit of the cylinder, its use is only applicable if the scattering of the beam particles is limited to small angles. For this reason many observers do not apply the cylinder in this form. In the next section we show how we have solved this problem.

B. Experimental procedure.

Our collector, located at distance L from the entrance slit, is represented in fig. 2.1, where we have made a schematical design of our electrode system in the collision chamber.

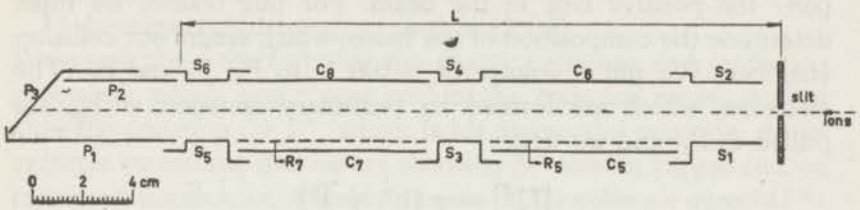

Fig. 2.2.
Schematical design of the electrode system.

The electrodes are flat plates, of which some are bent in a special form, as given in the design. The collector is composed of electrodes P_1, P_2 and P_3. The electrodes S_5 and S_6 are used as guard rings in the same manner as in the experiments of Goldmann, Keene etc. (see § 1.1 section D). We shall explain now the manner in which we carry out the beam intensity measurement with the collector, and to do this we consider separately different gas pressure regions:

Vacuum pressure.

At first we determine the beam current and its composition under vacuum conditions ($p \leq 10^{-5}$ mm Hg).

We apply a voltage of + 100 V to P_3, P_2 and S_6. The beam particles hit P_3. The secondary electrons, formed at P_3, can not leave the collector room and they can only arrive at P_2. A positive current at P_1, which is observed in practice, can only be caused by reflection of particles at P_3.

In this case $I_{P_1} + I_{P_2} + I_{P_3}$ equals the current of beam ions entering the collector room at the beginning of the electrodes P_1 and P_2 (at $x = L$). This collector current is further on represented by I^+, which is proportional to $n^+_{x=L}$ used in (2.1.8). The absolute values of the different currents I, which are used in this chapter, will differ by the same proportion constant from their corresponding n, used in the equations of § 2.1. At vacuum

pressure we have $n^+_{x=L} = n^+_{x=o}$, so that from the collector measurement at x = L the current of ions entering the collision chamber at x = o is known.

In practice we can not realize a beam, which consists only of ions. There are always a small number of neutrals, which accompany the positive ions in the beam. For this reason, we must determine the composition of the beam, which enters our collision chamber. We put a voltage of —100 V to P_3, P_2 and S_6. The electrons, which are formed by secondary emission at P_3, are pulled to P_1, and we write:

$$|I_e^{+o}| = \gamma\,(I^+ + I^o)$$

I^+ and I^o are respectively the currents of ions and neutrals which enter the collector. The secondary emission coefficient at P_3 is represented by γ, having supposed γ equal for ions and corresponding neutrals. I_e^{+o} is the electron current at P_1. The index indicates that this current is caused both by ions and neutrals.

We repeat the measurement, after having removed the ions from the beam before it enters the collision chamber. Only neutrals reach P_3 and we obtain:

$$|I_e^o| = \gamma\, I^o$$

in which I_e^o is the electron current at P_1, which is only caused by the neutrals in the beam.

Combining the two equations we have:

$$I_e^{+o}/I_e^o = (I^+ + I^o)/I^o = (n^+_{x=o} + n^o_{x=o})/n^o_{x=o}$$

As we have measured I^+ and the ratio I_e^{+o}/I_e^o follows from the secondary emission measurements, we can calculate the current of neutrals I^o by means of the last equation. We have again that I^o is proportional to $n^o_{x=L}$, being equal to $n^o_{x=o}$ under vacuum conditions.

Intermediate gas pressures.

The collision chamber is filled with a certain gas at pressure p varying between vacuum and a pressure of about 5.10^{-3} mm Hg. The ion current at the collector is determined in the same way as

under vacuum conditions and we show that in this case the current is also given by

$$I^+ = I_{P_1} + I_{P_2} + I_{P_3}$$

where I^+ is again the current of beam ions, which enter the collector at $x = L$.

I^+ is proportional to $n^+_{x=L}$ used in (2.1.8).

We must proof the fact that the charge exchange and ionization processes, which occur now within the collector room, do not alter the equation for I^+, which holds at vacuum pressure. As an example we assume that we are shooting N^+ ions in H_2 gas and we consider the influence of some processes on the collector current I^+:

1) $N^+ + H_2 \rightarrow N + H_2^+$ (capture)

In stead of registering the fast ion N^+ at P_3, we detect the slow ion H_2^+ at P_2, leaving the sum of currents unchanged.

2) $N^+ + H_2 \rightarrow N^+ + H_2^+ + e^-$ (ionization)

The positive charge unit of H_2^+, drawn to P_2, and the negative charge unit of e^-, drawn to P_1 or P_3, cancel out each other in the sum of currents at P_1, P_2 and P_3.

Similar reasoning can be applied to other processes as well, leaving the equation for I^+ at vacuum and gas pressure the same.

"High" gas pressures.

We increase the gas pressure till the ion current measured at the collector does no more decrease at further pressure rise, being realized at about 5.10^{-3} mm Hg. We have reached the pressure region in which the equilibrium state in the beam is realized. In this state as many captures as losses occur, so that the beam composition of ions and neutrals remains unaltered. The ion current measurement is carried out as before. We find $I^+_{equilibrium}$ being proportional to n^+_e (see 2.1.5 and 2.1.6).

C. Calculation of σ_c and σ_l.

The experimental procedure described in section B is sufficient for a calculation of the capture and loss cross-section, e.g. to find the cross-sections for the processes (2.1.1).

We apply the first equation of (2.1.8):

$$n_{x=L}^{+} = A \exp(-\alpha L) + B$$

where $n_{x=L}^{+}$ is known from the collector measurement at an intermediate gas pressure. A and B are given by equations (2.1.9) in which the quantities are known from the collector measurements at vacuum and high pressures. We can now calculate α being the sum of α_c and α_i.

To find the ratio α_i/α_c we calculate n_e^o as the difference of $(n_{x=o}^{+} + n_{x=o}^{o})$ determined at vacuum pressure and n_e^{+} (see 2.1.4) and we apply equation (2.1.5). The sum and the ratio of α_c and α_i being known, we can evaluate these quantities, which are linearly pressure dependent as we see from (2.1.2). Using this set of equations we find at last σ_c and σ_i.

§ 2.3. The experimental determination of σ_c at low pressures independently of σ_i or w.

A. Experimental procedure.

In these measurements we make use of the electrodes given in fig. 2.3 (see also fig. 2.2). The beam particles pass along the side electrodes C_5, R_5 and C_6 flanked by guard rings S_1, S_2, S_3 and S_4 and they arrive at the collector.

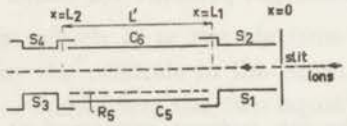

Fig. 2.3.
Electrodes for measuring σ_c.

We assume that we can neglect the number of neutrals present in the beam entering the collision chamber and that the pressure is so low that we can apply equation (2.1.10) in the interval (L_1, L_2) (see § 2.1 section B). In the same manner as discussed in § 2.2 section B we can determine the ion intensity $n_{x=o}^{+}$ at vacuum pressure. In addition we determine the current of slow ions which are formed by the capture process in the interval (L_1, L_2). For that purpose we apply a voltage of +100 V to S_2, C_6 and S_4; this is done in vacuo and at different gas pressures. The primary ions in the beam are so fast (2—25 keV) that the electric field across the side electrodes will alter their path to a negligible extent. At these low pressures two processes are responsible for the formation of slow ions and electrons in the gas, namely the

capture and ionization process. These particles have not generally got an energy larger than ten electron volts, so that we obtain saturation currents at the side electrodes by means of the electrical potential at S_2, C_6 and S_4. Slow ions are drawn to C_5, R_5 and electrons to C_6. If we call these currents respectively i^+ and i^-, their algebraic sum represents the slow ion current arising from the capture process. This is easily understood knowing that the ions and electrons formed by ionization cancel out each other. In the same manner as we have shown in the collector current measurement (§ 2.2 section B), we can explain that such secondary processes as secondary emission of electrons at the side electrodes or secondary ionization by slow ions or electrons do not alter the algebraic sum of i^+ and i^-. We put their absolute values respectively proportional to n^+ and n^-.

B. Calculation of σ_c.

For the calculation of σ_c we use equation (2.1.16). In this equation $n^+_{x=L_1} - n^+_{x=L_2}$ is equal to the number of slow ions, $n^+ - n^-$, formed by the capture process in the interval (L_1, L_2). From our collector measurement in vacuo, $n^+_{x=0}$ is known, so that we are able to calculate α_c. This quantity must be linearly pressure dependent as follows from (2.1.2), of which we use the first equation to evaluate σ_c.

§ 2.4. Formal treatment of ionization.

We assume that we are using the same beam, gas and pressures as in the capture and loss cross-section determinations, and that the ionization occurs in an interval (L_1, L_2).

As a corresponding example we take:

$$\begin{aligned} N^+ + H_2 &\rightarrow N^+ + H_2^+ + e^- \text{ (ionization by positive ions)} \\ N + H_2 &\rightarrow N + H_2^+ + e^- \text{ (ionization by neutrals)} \end{aligned} \qquad (2.4.1)$$

To describe the probabilities of these two processes in the unit length we use respectively α_i^+ and α_i^0. As before we can introduce the cross-sections σ_i^+ and σ_i^0.

We shall consider two cases, in which α_i^+ and α_i^0 are equal and unequal to each other.

A. $\alpha_i^+ = \alpha_i^0 = \alpha_i$.

In a length dx the number of ions or electrons formed by the ionization processes is given by

$$dn_i = \alpha_i (n_x^+ + n_x^0)\, dx \qquad (2.4.2)$$

from which we get after integration over the interval (L_1, L_2)

$$n_i = \alpha_i (n_x^+ + n_x^0)(L_2 - L_1) \qquad (2.4.3)$$

where the ionization is considered between $x = L_1$ and $x = L_2$ $(L_2 > L_1)$.

B. $\alpha_i^+ \neq \alpha_i^0$.

The mathematical treatment is now more complicated than in section A. We shall divide the pressure range into three intervals, one where the pressure is so low that $\alpha L_2 \ll 1$, the second where the pressure is so high that the beam has come into its equilibrium state before it reaches $x = L_1$ and the third with intermediate pressures where the beam composition is strongly alternating between $x = L_1$ and $x = L_2$.

Low pressure region $\alpha L_2 \ll 1$.

If we consider equations (2.1.8) we see that in the interval (L_1, L_2) the beam composition is almost constant and approximately given by $n_{x=0}^+$ ions and $n_{x=0}^0$ neutrals. In this case the ionization is given by

$$n_i = (\alpha_i^+ n_{x=0}^+ + \alpha_i^0 n_{x=0}^0)(L_2 - L_1) \qquad (2.4.4)$$

If we have $n_{x=0}^0 \ll n_{x=0}^+$ we get simply

$$n_i = \alpha_i^+ n_{x=0}^+ (L_2 - L_1) \qquad (2.4.5)$$

which equation determines the ionization probability for ions. The last equation is applied by Keene, Sherwin, Goldmann and other observers.

High pressure region, where the equilibrium state in the beam is reached before it passes $x = L_1$.

We derive the next equation in the same manner as (2.4.4)

$$n_i = (\alpha_i^+ n_e^+ + \alpha_i^0 n_e^0)(L_2 - L_1) \qquad (2.4.6)$$

Intermediate pressure region with alternating beam composition.

If we know the mean numbers of ions and neutrals in the interval (L_1, L_2) responsible for the ionization we can apply an analogous equation as (2.4.4) or (2.4.6). It is easy to calculate these mean amounts by equations (2.1.8) and we obtain:

$$\overline{n^+_{L_1,L_2}} = \int_{L_1}^{L_2} \frac{[A \exp(-\alpha x) + n_e^+]\,dx}{L_2 - L_1} = \\ = -\frac{A \exp(-\alpha L_2) - A \exp(-\alpha L_1)}{\alpha (L_2 - L_1)} + n_e^+ \\ \overline{n^0_{L_1,L_2}} = \int_{L_1}^{L_2} \frac{[-A \exp(-\alpha x) + n_e^0]\,dx}{L_2 - L_1} = \\ = \frac{A \exp(-\alpha L_2) - A \exp(-\alpha L_1)}{\alpha (L_2 - L_1)} + n_e^0 \tag{2.4.7}$$

so that the ionization is given by

$$n_i = (\alpha_i^+ \overline{n^+_{L_1,L_2}} + \alpha_i^0 \overline{n^0_{L_1,L_2}})(L_2 - L_1) \tag{2.4.8}$$

We have given ionization equations in different pressure intervals and we can conclude that if we carry out ionization measurements at two different pressures, α_i^+ and α_i^0 can be calculated by solving two equations with two unknowns.

Measurements at other pressures must give dependent equations and can serve as a control.

§ 2.5. Experimental determination of σ_i^+ and σ_i^0.

A. Introduction.

The ionization measurement is in principle very simple. We can draw the slow ions and electrons formed in the gas to the side electrodes by applying to one of these electrodes a positive or negative voltage of 100 V and by measuring the current at the opposite electrode. As we see from fig. 2.2, we can measure the ionization current at two places in the collision chamber by making

use of the electrodes C_8, C_7, R_7 and C_6, C_5, R_5 with their guard rings S_1, S_2 etc. The grids R_5 and R_7 are used to suppress the secondary emission of electrons, caused by the gas ions which are accelerated to C_5 and C_7. In § 2.4 section A we remarked that the voltage across the side electrodes is sufficiently high to get saturation currents on these and that it does not much influence the path of the fast primary ions.

B. Experimental procedure.

The ionization currents are determined in the same way at the various gas pressures. We explain the method for measuring the ionization between C_6 and C_5 (see also fig. 2.3).

B_1). We apply a voltage of —100 V to R_5, S_1, S_3 and a voltage of —75 V to C_5. We check the negative current at C_6 and call it i_i^-. In this case the ions formed in the gas are drawn to C_5. If secondary emission of electrons takes place at C_5, the electrons will be retarded by the grid and can not reach C_6. The electrons formed in the gas which arrive at C_6 can also cause secondary emission of electrons at C_6, but as a consequence of the negative potential difference $V_{c_5} - V_{c_6}$ the emission is suppressed. Though this measurement would be sufficient for an ionization cross-section determination, we carry out some more measurements, which serve partly as a control and which have also to clear up some phenomena taking place in the collision chamber.

B_2). We increase the voltage of C_5, so that it equals that of R_7, —100 V large. We check the current on C_6, called i^-. The secondary emission of electrons at C_5 is no more suppressed so that we have

$$i^- = (1 + \gamma_{c_5})\, i_i^-$$

where γ_{c_5} represents the secondary emission coefficient of electrons at C_5.

B_3). We apply a voltage of +100 V to C_6, S_2, S_4. We check the sum of currents on C_5 and R_5, called i^+. Only in the case where the beam has reached its equilibrium state before entering the room between C_6 and C_5 we have

$$i^+ = i^-$$

This equation does no longer hold if primary ions hit the side electrodes, for example this can be caused by scattering of these ions over sufficiently large angles.

We remark that we carried out the experimental procedures discussed in section B_2 and B_3 at low pressures to determine σ_c independently of σ_1 or w (see § 2.3).

The measurement under section B_1 should be sufficient for the determination of the ionization cross-section, the beam intensity and composition being known from the experiments on capture and loss. However one complication arises. The current i_i^- is not only composed of electrons formed by ionization (see 2.4.1), but also of electrons formed by the loss process (see 2.1.1). Having determined i_i^- we shall show in the next section how to find the real ionization current i_i. We put them respectively proportional to n_i^- and n_i, the latter quantity being used in the equations (2.4.2) to (2.4.8).

C. Calculation of the real ionization current and the ionization cross-sections.

We shall derive that the number of electrons n_i^-, proportional to i_i^- is given by the next equation:

$$n_i^- = \underbrace{(\overline{n^+_{L_1,L_2}}\,\alpha_i^+ + \overline{n^0_{L_1,L_2}}\,\alpha_i^0)\,(L_2 - L_1)}_{\text{real ionization}} + \underbrace{n^0_{x=L_1}\,\alpha_1\,(L_2 - L_1)}_{\text{loss in equilibrium}} +$$

$$+ \underbrace{(n^+_{x=L_1} - w n^0_{x=L_1})\left[1 + \frac{\alpha_1 \exp(-\alpha_c L') - \alpha_c \exp(-\alpha_1 L')}{\alpha_c - \alpha_1}\right]}_{\text{first cycle}} \qquad (2.4.9)$$

The term indicated by real ionization is equal to n_i and arises from (2.4.8).

To make clear the second term, which is called "loss in equilibrium", we assume that the beam has reached its equilibrium state, before it passes the side electrodes under consideration. In that case the term indicated by "first cycle" is zero, $n^+_{x=L_1}$

being equal to $w n^{o}_{x=L_1}$, so that equation (2.4.9) is changed into a more simple form:

$$n_i^- = \underbrace{(n_e^+ \alpha_i^+ + n_e^o \alpha_i^o)(L_2 - L_1)}_{\text{real ionization}} + \underbrace{n_e^o \alpha_1 (L_2 - L_1)}_{\text{loss in equilibrium}} \qquad (2.4.10)$$

At the equilibrium state the number of neutrals n_e^o is constant in the interval (L_1, L_2) where we measure the electron current. It is clear now that the number of electrons formed by loss is given by the term "loss in equilibrium", so that we have proved the validity of equation (2.4.10).

We have still to explain the term "first cycle" in (2.4.9). If the equilibrium state in the beam has not yet been reached at $x = L_1$, we let correspond to $n^o_{x=L_1}$ a number of positive particles equal to $w n^o_{x=L_1}$. We can say that this part of the beam is already in the equilibrium state at $x = L_1$ and is responsible for the term "loss in equilibrium" in (2.4.9) (see our derivation of 2.4.10).

However at $x = L_1$ the number of positive particles is equal to $n^+_{x=L_1}$, so that we have still to derive how many electrons are formed by the surplus of ions $(n^+_{x=L_1} - w n^o_{x=L_1})$. We can easily show that the number of electrons arising from this surplus is given in (2.4.9) by the term "first cycle". The number of electrons formed in this way is namely equal to the number of reborn ions, which have experienced successively capture and loss in the interval (L_1, L_2), thus achieving the first cycle. In § 2.1 section C we have derived how many ions complete the first cycle, obtaining formula (2.1.18). To get the term "first cycle" in (2.4.9) we have only to replace $n^+_{x=o}$ in (2.1.18) by $(n^+_{x=L_1} - w n^o_{x=L_1})$. We can understand that to calculate all the electrons formed in the interval (L_1, L_2) more cycles should be taken into acount. To examine whether we can do with the first cycle, we assume that both $\alpha_c L'$ and $\alpha_1 L'$ are smaller than one, so that we can develop the exponential powers in (2.1.18). In this way we get the expression

$$n^+_{x=o} [\tfrac{1}{2} \alpha_c \alpha_1 L'^2 \{1 - 1/3 (\alpha_c + \alpha_1) L' + \ldots\}] \qquad (2.4.11)$$

In the same manner we can derive that the first term in the expression for the amount of double cycles in the interval (o, L') is represented by:

$$n^+_{x=o} \cdot 1/4! \, \alpha_c^2 \alpha_1^2 L'^4 \qquad (2.4.12)$$

It is our intention to apply (2.4.9) only at such low pressures, that we can neglect the amount of double cycles taking place in the interval (L_1, L_2). At high pressures where the beam has reached its equilibrium state before passing $x = L_1$, we apply (2.4.10). Having measured i_i^-, proportional to n_i^-, at different pressures we are able to evaluate the part of the current formed by real ionization. As we have seen the probabilities α_i^+ and α_i^o can now be evaluated by means of equations (2.4.3) to (2.4.8). Analogous equations as (2.1.2) give us respectively σ_i^+ and σ_i^o.

Chapter III.

THE APPARATUS.

§ 3.1. Introduction.

We have built an apparatus which enables us to do capture, loss and ionization cross-section determinations in the manner principally described in chapter II.

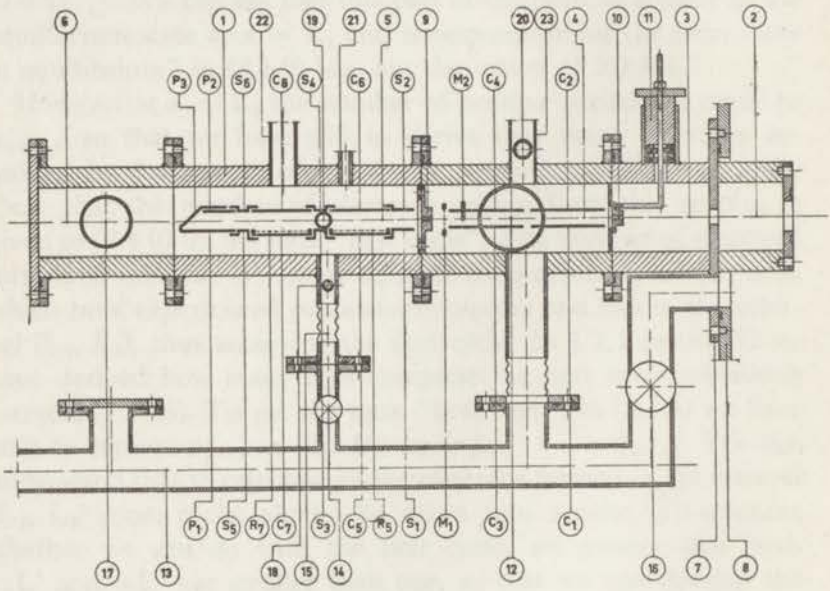

Fig. 3.1.
The apparatus.

We have made a design of the apparatus in fig. 3.1. The apparatus consists of a thick steel tube 1, (inside diameter 95 mm, outside diameter 147 mm), to screen off the stray magnetic field of the separator, which is used as ion source in our experiments. This screening is necessary in order to obtain a linear path for the beam

particles in our apparatus. The tube is divided in different parts 2, 3, 4, 5 and 6 with soldered flanges. The flanges make a vacuum-tight connection with the aid of rubber gaskets.

The apparatus is placed on a trolley, movable from one place to an other. This is necessary because we are using the ions produced by the isotope separator in our experiments. These ions are magnetically analysed in the vacuum chamber of the separator and they enter our apparatus at the collector side of this separator. When we are starting our measurements, the collector is taken off from the separator, our apparatus is taken to its collector side and a vacuum connection is made between flange 7 of our own apparatus and the end flange 8 of the separator. The ions, which can now enter our apparatus, after having described a circular path in the separator, will continue their path almost rectilinearly as a consequence of the screening of the stray magnetic field.

The main part of our apparatus is the collision chamber 5 containing the electrode system discussed in chapter II. We can fill this chamber with the gas, in which we want to investigate the mentioned inelastic collision processes. A narrow slit 9, through which the beam particles enter, forms the connection between the collision chamber and the vacuum chamber 4. At the lower side of the latter chamber, a metal tube 12 leads to an Edwards oil diffusion pump, which is used to evacuate the apparatus. When we are operating, this pump has to maintain a pressure fall at slit 9 and to prevent that the gas in the collision chamber flows into the separator.

The slits 10 and 9 which are arranged at both sides of the vacuum chamber, form the collimating assembly and define the extension of the beam entering our collision chamber.

In the vacuum chamber monitor M_2 is used to eliminate the effects caused by the intensity fluctuations of the beam, so that every current measured in the collision chamber is compared with the current at M_2. Electrodes C_1, C_2, C_3 and C_4 are used to deflect the beam ions, if we want to determine the small proportion of neutrals present in the beam (see § 2.2 section B).

In the following paragraphs we shall discuss in more detail the construction and different parts of the apparatus.

§ 3.2. Screening of the magnetic field of the separator.

Before machining the steel tube, we orientated ourselves about the screening of the stray magnetic field of the separator inside the tube, which was about one metre in length. As we mentioned in the introduction of this chapter, such a screening is important in order that the beam particles describe a linear path in our apparatus. Besides, a magnetic field influences the realization of saturation currents of slow ions and electrons at the side electrodes. To determine this field we have used the Grassot[G3] method. In principle we only measure the induction current arising in a coil after having given it half a turn. The front of the metal tube was located at about ten centimetres from the end flange 8 inside the vacuum chamber of the separator. The largest magnetic field ever used in the separator amounts to about 3150 Gauss in case of uranium separation. If we measure at the axis of the metal tube at thirty five centimetres distance from its front side, we find that this field is reduced to 12 Gauss.

In table 3.1 we have given the magnetic stray field at the tube axis under different circumstances.

TABLE 3.1.

Stray magnetic field of the separator inside the steel tube.

Distance between coil center and front side of metal tube	Stray magnetic field at the tube axis if the magnetic field of the separator is equal to:	
	2000 Gauss	3150 Gauss
5 cm	780 Gauss	1750 Gauss
15	320	1070
25	45	120
35	10	12

We were satisfied with the results of this screening, which would be still better if the metal flanges were attached to the tube.

These measurements were repeated, when the tube had got its definite form. Only the electrodes had still to be placed so that space was left to turn the coil. In table 3.2 we give the stray magnetic field in the vacuum chamber at its front and back side (respectively near slit 10 and 9), and in the collision chamber

where this field does not much alter over its length. For the sake of completeness we mention that a magnetic field of 1500 Gauss in the separator is already reduced to about 20 Gauss in chamber 3 adjoining the separator.

TABLE 3.2.

Stray magnetic field of the separator inside the "definite" steel tube.

Separator	Vacuum chamber		Collision chamber
	Front side	Back side	
3150 Gauss	24.2 Gauss	8.8 Gauss	
3000			5.0 Gauss
2700	16.0	6.6	3.4
2400	7.2	3.3	2.6
2200			2.4
1800			0.9
1500	1.9	1.1	0.4

Further on we shall show by means of the figures in table 3.2 that the stray magnetic field has little influence on the collimation of the beam and on the detection of the saturation currents of the slow ions and electrons in the collision chamber.

§ 3.3. Production and collimation of the beam particles.

The electromagnetic separator produces all kinds of single charged ions which we wish to use in our measurements. This apparatus is described in the thesis of Zilverschoon[21].

In practice the ions in the separator are accelerated by voltages round about twenty kilovolts. For our experiments we have chosen the whole voltage range of the separator lying between 2 and 25 kilovolts. Generally the ion current reaching the collector of the separator is about five milliamperes. The beam has its focussing point near this collector, so that on coming into our apparatus it will diverge. For this reason only a fraction of the current at the collector side of the separator enters our collision chamber.

Before we start our experiments we change the slit at the ion source of the separator for a smaller one than is generally used. We make it 5 mm high and 2 mm wide, so that we get a smaller image at the collector side of the separator. The smaller image is

more in accordance with the dimensions of slit 10 and slit 9, both having a height of 7 mm and a width of 4 mm. In this way we usually obtain a beam current of the order of 10^{-8} amperes in the collision chamber. As we have already mentioned in chapter II (§ 2.2 section B), the beam which enters the collision chamber still contains some neutrals which are formed in the separator.

Zilverschoon[21] remarks that the energy homogeneity of the beam is very good. The energy spread amounts to about 10 volts at an acceleration tension of 25 kV. To be sure that we use the kind of ions, we want for our experiments, a mass spectrogram is always made before the measurements start. We achieve this by measuring the current on electrode P_3 as a function of the magnetic field of the separator.

The slits 9 and 10 at both sides of the vacuum chamber are used for the collimation of the beam. Slit 10 is movable within the vacuum system, for which purpose we have made the construction 11 with two Simmering seals. The main divergence of the beam will occur transversely. If we assume that the focussing point of the beam is at the front of our steel tube, we can calculate the maximum possible extension of the beam in the collision chamber. The opening angle of slit 9 is represented by the quotient of its width (4 mm) and its distance from the front of the tube (500 mm). We find that this angle is about half a degree large. If we know that the distance between slit 9 and the collector at the beginning of electrodes P_1, P_2 is about 250 mm large, we can easily predict a beam width of 6 mm at the collector. In the vertical direction of the slits the beam is nearly parallel and so the extension in this direction is determined by the heights of slits 9 and 10, both seven millimetres high. The distance of the opposite side electrodes in the collision chamber is 24 mm, their height is 60 mm, so that the beam extension (6 mm $\times$ 7 mm) is sufficiently limited.

We might imagine that the collimation could be disturbed by a strong magnetic field. It is easy to show that under the most unfavourable conditions the beam which enters the vacuum chamber is little influenced by the present stray magnetic field. Working with uranium ions at 20 kV, we use a magnetic field of about 3150 Gauss in the separator. The velocity of the single charged ions is equal to 1.4×10^7 cm/sec. and the remaining magnetic field in the vacuum chamber varies between 9 and 24 Gauss as we see from table 3.2.

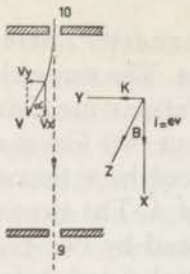

Fig. 3.2.
Path of the beam ions in the vacuum chamber.

The Lorentz force which works on the beam ions is given by $K = 1/10 \frac{Bve}{c}$ dynes.

For the sake of simplification we take the magnetic field 24 Gauss everywhere in the vacuum chamber (see fig. 3.2). We find $K = 5.4 \times 10^{-13}$ dynes. The time interval t in which the acceleration is working in the Y direction, is determined by the distance between the slits 9 and 10, large 25.5 cm and the velocity of the ions, already mentioned.

The path length travelled in Y direction is represented by

$$s_y = \tfrac{1}{2}\, K/m \,.\, t^2 = 2.3 \times 10^{-3} \text{ cm}$$

The exit angle α is equal to the ratio v_y to v_x.

$$v_y = a\, t = 2.6 \times 10^3 \text{ cm/sec}$$
$$v_x = 1.4 \times 10^7 \text{ cm/sec}$$
$$\therefore \alpha = 0.67 \text{ minutes}$$

We have shown by means of this calculation that the beam in the vacuum chamber is influenced by the stray magnetic field only to a negligible extent.

Most of the time the isotope separator is used for the production of stable isotopes, so that we have little occasion to do our experiments with the separator as ion source. Therefore we have built an extra ion source for the preparatory work, which is based on the magnetic discharge principle of Penning. By means of flanges and rubber gaskets we make a vacuum tight connection between this source and our apparatus. In this arrangement an analysing magnet is not yet present, so that if the discharge takes place in hydrogen gas, as well molecular as atomic ions are accelerated into the collision chamber. With this arrangement we only make our apparatus ready for the definitive cross-section measurements at the separator. In this case the currents in the collision chamber are of the same order of magnitude as those being obtained with the separator. In fig. 3.3 we show a design of the so called P.I.G. ion source which is partly an imitation of the source constructed

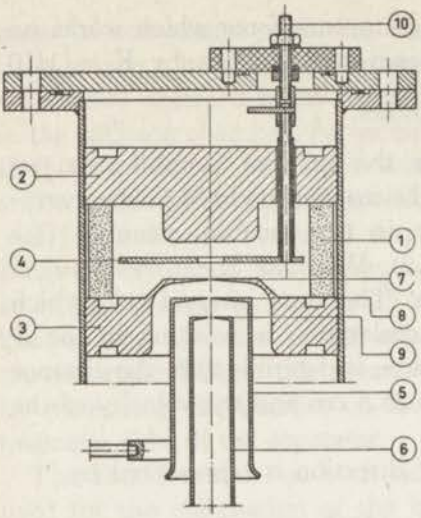

Fig. 3.3.
P.I.G. ion source.

by Barnett[B4], Stier and Evans. The magnetic field in the source has a strength of about 900 Gauss and is produced by a ticonal ring magnet 1. The ticonal ring is flanked by two pieces of soft steel 2 and 3, forming the cathodes. The anode 4 is a ring shaped copper plate. The cathodes are at the same high voltage as the whole ion source, the anode is usually put 200—1000 volts higher. The lens electrode system is formed by the cathode 3, at high voltage, the circular cylinder 5 having about three fourths of this voltage, and cylinder 6 at earth potential. They have circular openings 7, 8 and 9 being respectively 2 mm, 3 mm and 4 mm in diameter. A porcelain cylinder (not present in the figure) isolates the source from our grounded apparatus. The gas being used for the discharge in the source can enter through tube 10 after having passed a needle valve.

§ 3.4. Vacuum system.

The apparatus is evacuated by the Edwards oil diffusion pump being connected with the vacuum chamber by metal tube 12 (see fig. 3.1). To get a low pressure as quickly as possible we also use the reserve pumping line 13 and we open the metal Jenkins valve 14. In this way the collision chamber is also evacuated through tube 15, which has a lower resistance than slit 10.

The front side of the apparatus can be closed in three manners. In the first place we can simply close it by a metal flange and rubber gasket so that we can test the apparatus on leakages. Secondly we have the vacuum connection with the P.I.G. ion source when we are doing our preparatory experiments. In this case we use an extra oil diffusion pump to evacuate this part. Lastly our

apparatus is vacuumtight connected with the separator when the definitive measurements start. For this purpose we use endflange 8 of the separator and flange 7 of our apparatus. If we now evacuate the apparatus we can take advantage of the big oil diffusion pump of the separator by opening Jenkins valve 16, which is always closed when we are carrying out our measurements or when the apparatus is disconnected from the separator.

The Edwards oil diffusion pump has a pumping speed of about sixty litres per second for air. This speed is reduced about a factor three by using a water baffle and a liquid nitrogen trap, located immediately at the upper side of this pump. We usually reach a vacuum of 5×10^{-6} mm Hg. When the experiments start we close valve 14 and this may not considerably influence the vacuum pressure in the collision chamber. In this way we can easily control whether there is a leakage present in the collision chamber when we are operating. Generally we can measure the rate of a leakage when the apparatus is away from the separator or from the P.I.G. ion source and is closed by the metal flange at its front. When we have stopped pumping in this case, we usually measure a pressure rise of 10^{-2} mm Hg in five hours. If we know that the volume of the apparatus amounts to about thirteen litres we calculate that the leakage is about 1/100 mm^3 atmospheric air per second. We shall see later on the reason why it is important that this amount is small.

As a consequence of the use of rubber gaskets as a packing between metal flanges, it is not possible to degas the apparatus by heating. The metal parts will even after a long pumping period degas to a certain amount.

To avoid the influence of oil and mercury vapour we use different cooling traps with liquid nitrogen. By means of trap 17 we get a very "clean" collision chamber which is proved by measuring the ionization current at vacuum pressure. These currents seem negligible with respect to those being measured when we have let gas into the chamber.

The gas, we require for our experiments in the collision chamber is let in by means of a needle valve. The latter is flanked by a liquid nitrogen trap on each side. The high pressure side of the valve is in open connection with a glass supply vessel of about eight litres volume. The low pressure side goes to tube 18 through which the gas enters the collision chamber.

The collision chamber is not closed by a metal foil at its entrance so that an equilibrium in the gas pressure is reached when the gas flow through the needle valve is as large as the gas flow through slit 9 (valve 14 is closed). The rate of flow through slit 9 is determined by its dimensions (7 mm high, 4 mm wide and 15 mm thick) and it has been calculated for air at about one litre per second.

In many of the ion gas combinations we have chosen hydrogen gas in the collison chamber. As an example we assume that we have a hydrogen pressure of 10^{-3} mm Hg in this chamber. About 3.6 litres of gas per second will pass slit 9. An equal quantity is leaving the supply vessel, containing the gas near atmospheric pressure. We calculate that 3.6 litres gas of 10^{-3} mm Hg is equivalent to about 5 mm^3 gas at atmospheric pressure so that the supply vessel loses 5 mm^3 gas per second. In half an hour its contents is diminished with about 2%, so that at one position of the needle valve the pressure in the collision chamber decreases very slowly with the time.

We can also understand that if the gas passes through the needle valve at a rate of 5 mm^3 per second and if we want the gas in the collision chamber at a purity of one percent, the disturbing atmospheric leakage in this chamber may not be larger than 1/20 mm^3 per second. The permitted amount of this atmospheric leakage varies with the working pressure in the collision chamber and the kind of gas used. As we mentioned we obtained a disturbing leakage of about 1/100 mm^3 atmospheric air per second in the collision chamber, which leakage was not localized.

The pumping speed of the Edwards oil diffusion pump, considering its baffle and cooling trap (55 litres/sec for hydrogen), and the rate of flow of the gas through slit 9 (3.6 litres/sec for hydrogen) determine the pressure fall at this slit (valve 14 is closed). We want this fall large so that only a few collision processes occur in the vacuum chamber before the beam enters the collision chamber. In case of hydrogen the ratio of the pressures in the two chambers is equal to 15 to 1. To get better conditions one should make slit 9 smaller, but this has two disadvantages: In the first place the beam intensity in the collision chamber decreases; secondly the gas flows at a smaller rate through the collision chamber so that smaller disturbing leakages are permitted in this chamber. The best solution would be realized by using a pump of higher capacity.

The pressures both in the collision chamber and in the vacuum

chamber can be separately checked with a Mc Leod gauge, calibrated to 1% accuracy. Two leadings 19 and 20 with liquid nitrogen traps and valves make the connection between the Mc Leod gauge and these two chambers. In the course of time we have added a Pirani gauge and an ionization gauge (see leading 21) for a more precise pressure reading between 10^{-4} and 10^{-3} mm Hg in the collision chamber. They are both calibrated for each gas with the Mc Leod gauge. Two Philips ionization gauges are used as a rough pressure indicator in the pressure region 10^{-3} — 10^{-5} mm Hg and they are attached to leadings 22 and 23.

When we are operating with the separator, we have seen that valve 16 is closed so that a very small quantity of gas flows into the separator. This amount of gas is determined by the pumping speed of the Edwards pump and the dimensions of slit 10 being equal to those of slit 9. If we have filled the collision chamber with hydrogen at a pressure of 2×10^{-2} mm Hg and if we know that the rate of pumping in the separator is about 1500 litres/sec, we calculate a pressure rise in the separator of 3×10^{-6} mm Hg. This has little influence on the cross-section measurements, as we shall see in chapter IV.

§ 3.5. The electrode system.

The electrodes we use in our apparatus are made of copper plate two millimetres thick. They usually have a flat form. The electrodes C_1, C_2, C_3 and C_4 which are arranged in the vacuum chamber are ten centimetres long and four centimetres high. As we have seen in the introduction of this chapter, we can deflect the charged particles in the beam by applying a sufficiently high voltage to C_1 and C_3 (about 100—400 volts), so that only the small amount of neutrals can still reach the collision chamber and cause secondary emission of electrons at P_3 (see § 2.2 section B). The vacuum chamber has two monitors being located near slit 9. Though the output of the ion source, the acceleration voltage and the magnetic supply in the separator are very well stabilized, the beam is still a little variable in intensity so that the comparison of a current in the collision chamber with the monitor current is necessary. For that purpose we formerly used grid M_1 with high transparency. This grid has a circular form and is three centimetres large in diameter, while slit 9 is only 4 mm wide. The experiments

have taught us that the beam of the separator was not homogeneous in a small width, so that this monitor was insufficient. We added a second monitor M_2 as wide as slit 9 and with a 5 mm long gap in the centre. When we are operating we apply a tension of +15 V to grid M_1 and to C_3 so that no secondary electrons can hit monitor M_2. These electrons can arise for example at slits 9 and 10. However we advance the emission of electrons from monitor M_2 making its current higher. By this method of comparison we have succeeded in eliminating the beam fluctuations.

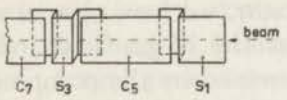

Fig. 3.4.
Electrode C_5 flanked by its guard rings (not drawn on scale).

The electrode system in the collision chamber has already been discussed in chapter II. The "C" electrodes are flat, 8 cm long and 6 cm high. In fig. 3.4 we have made a sketch of a C electrode flanked by its guard rings. These guard rings make the electric field homogeneous between two opposite side electrodes in the direction of the beam.

To investigate the electric field between two side electrodes in a plane perpendicular to the direction of the beam, we have realized a potential distribution at a resistance network (see

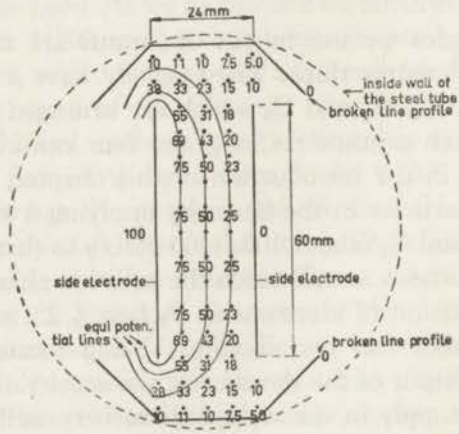

Fig. 3.5.

Potential distribution in a cross-section perpendicular to the beam between two opposite side electrodes respectively at 100 V and 0 V. The numbers give the potential at different places. A part of the circular profile of the inside wall of the steel tube is approximated by a broken line profile, also at 0 V.

Zilverschoon[Z2)]) as given in fig. 3.5. At this network we have approximated a part of the circular profile of the inside wall of the grounded steel tube by a broken line profile. The two side electrodes are represented by straight lines. We apply a potential of 100 V to one of them, while the other electrode and the broken line profiles are on earth potential. At the network we have measured the potential at different points and the results are given by the different numbers in the figure where we have next drawn the equipotential lines. We see that the electric field between the side electrodes is nearly homogeneous along a distance of 36 mm.

The side electrodes of the collector have a special form (see fig. 3.1). We mention that one side of the collector plate P_3 makes an angle of about forty degrees with the arriving beam. This is done to avoid particles reflected at P_3 escaping out of the collector space.

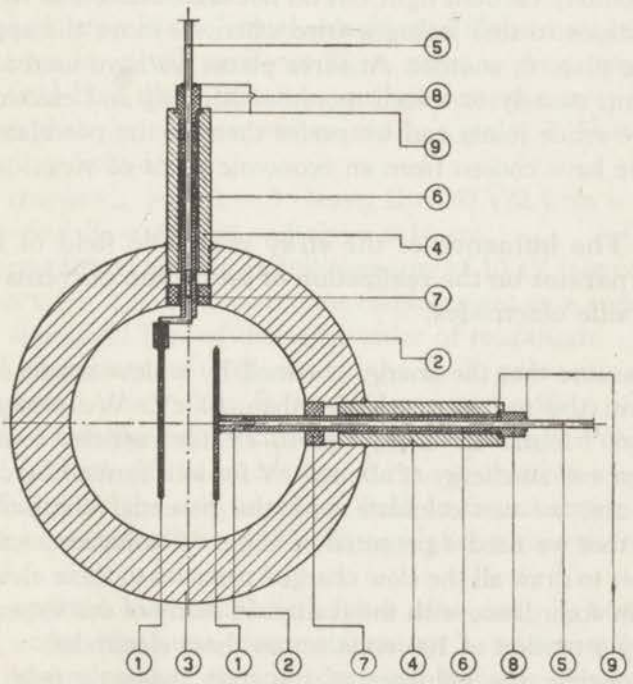

Fig. 3.6.
The insulated and vacuum tight attachment of two opposite side electrodes.

In fig. 3.6 we have made a sketch of the insulated and vacuum tight attachment of two opposite side electrodes. The electrode material used in the vacuum system is polished and carefully cleaned. At the electrodes 1 we have soldered a small brass tube 2 with screw-thread inside. At different places of the steel tube 3 we have soldered steel pipes 4 through which we pass the brass bars 5 making the electrical connection between electrode and cable. For the insulation and the positioning of the electrode we use a porcelain pipe 6, a perspex ring 7 and a porcelain bushing insulator 8. The latter is prepared in a particular way, so that we can attach it with tin solder to the steel pipe and the brass bar. We use small copper rings 9 to simplify the soldering work. In practice it seems difficult to get a perfect vacuum connection between the metal units and the porcelain bushing. To accomplish this operation we smear these connections with amber varnish, having an electrical impedance exceeding 10^{12} Ohm. They are now absolutely vacuum tight but do not seem reliable to mechanical vibrations so that leakages arise when we move the apparatus from one place to another. At three places we have used a Kovar glass joint, namely to attach monitors M_1, M_2 and electrode P_3. They are solide joints and we prefer them to the porcelain joints which we have chosen from an economic point of view.

§ 3.6. The influence of the stray magnetic field of the separator on the realization of saturation currents on the side electrodes.

We assume that the energy obtained by a slow ion or electron formed in the gas is not larger than 10 eV. We remark that Sherwin[S1)] found an energy of 10 eV for particles formed by ionization and an energy of about 1 eV for ions formed by capture. In this case we can calculate with the potential distribution in fig. 3.5, that we need a potential of about 50 volts across the side electrodes to draw all the slow charged particles to these electrodes. This is in accordance with the reality. In many of our experiments we apply a tension of 100 volts across these electrodes.

We consider the influence of the stray magnetic field on the path of a slow particle drawn to a side electrode. For our calculations we choose a stray field of 5 Gauss, the largest field in table 3.2.

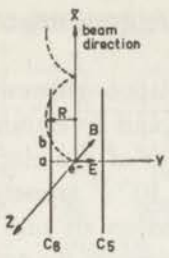

Fig. 3.7.
Trochoidal movement of the electron.

An electron, formed by ionization between the electrodes C_5 and C_6 (see fig. 3.7; for simplification we have omitted R_5) is drawn to electrode C_6 by means of the electric field E. However, if a magnetic field B is present in the Z-direction, as in our case, the electron will carry out a "trochoidal" movement consisting in the description of cycloids. The radius of the rolling circle is given by

$$R = \frac{m_{el.}}{eB}(v_x^2 + v_y^2 + E^2/B^2 - 2E/B.v_x)^{1/2}$$

in which equation e and E are given in electromagnetic units; v_x and v_y are the components of the initial velocity of the electron in the X- and Y-direction.

If the electron has no initial velocity and if the magnetic field B is not present, it will arrive at C_6 in point a. As a consequence of the field B in the Z-direction, a displacement arises in the XY plane so that the electron arrives at C_6 in point b. We calculate the displacement ab.

We choose $v_{el.} = 0$, B = 5 Gauss, E = 50 V/2.4 cm $\sim$ 20 V/cm and we find R = 4.5 cm and ab = 0.16 cm.

It seems that if we take an initial energy of 10 eV into consideration, i.e. $v_{el.} \sim 2 \times 10^8$ cm/sec, the displacement as a consequence of the stray field B is of the same order of magnitude.

A displacement of 0.16 cm in the X-direction in our most unfavourable case, when B = 5 Gauss and with a voltage of 50 volts across the side electrodes is still very small in comparison with the length of the electrodes, 8 cm, so that we may neglect the influence of the stray magnetic field on the saturation currents when we use potentials of 50 volts or higher across the side electrodes.

We omitted our calculation for a slow ion, R being much larger under the same circumstances as a consequence of the much heavier mass of the ion compared with the electron.

§ 3.7. Detection of currents and electronic equipment.

We usually use two current meters, a Kipps galvanometer (type K_c) to detect the current at monitor M_2 and a vacuum tube voltmeter to detect the current at one or more of the electrodes in the collision chamber. At a current of 5×10^{-11} amperes, the Kipps galvanometer undergoes a scale deflection of one millimetre. Its scale is 800 mm long. In most experiments we get more than a hundred millimetres scale deflection and we can thus read these monitor currents within one percent accuracy. The vacuum tube voltmeter has a measuring range between 10^{-6} and 10^{-11} amperes and dependent on the beam intensity we use input resistors of 100 or 1 megohm. Its scale permits a reading within one percent accuracy.

In our case it is only possible to measure the currents at those electrodes to which we have not applied a potential with respect to earth. Therefore we shall explain the manner in which we realize the current measurement at the collector.

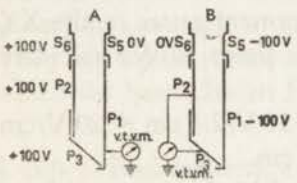

Fig. 3.8.
Collector current measurement.

In § 2.2 section B we have made clear that if we apply at the collector the voltage distribution A, which is given in fig. 3.8, the collector current is represented by $I^+ = I_{P_1} + I_{P_2} + I_{P_3}$. With distribution A we can only measure I_{P_1}, for plate P_1 is at zero potential.

In case B we have lowered the whole voltage level of A a hundred volts, maintaining the same voltage difference between the different electrodes. Because we are working with a beam of particles having energies in the order of kilo electronvolts, we may assume that the current intensity and distribution at the collector electrodes is not changed by this action. With voltage distribution B we measure $I_{P_2} + I_{P_3}$, in this way achieving the collector current measurement.

This measurement is carried out with the circuit given in fig. 3.9. In this circuit switch S is consisting of four sections S_a, S_b, S_c and S_d, being respectively connected with P_1, S_5, $P_2 + P_3$ and S_6. As we see from fig. 3.9 we realize case A if the switch is in position one, case B if it is in position three, while in position two the mentioned electrodes are all at earth potential.

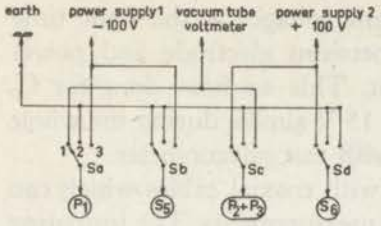

Fig. 3.9.
Electric circuit, used in the collector current measurements.

In an analogous manner we use this switch to determine i^+ and i^- in the experimental determination of σ_c at low pressures (see § 2.3). We find i^+ by applying + 100 V to S_2, C_6, S_4 and measuring the current at C_5, R_5; we find i^- by applying — 100 V to S_1, R_5, C_5, S_3 and measuring the current at C_6. For this purpose we have only to change in our circuit the connections with the switch. We replace P_1, by $C_5 + R_5$, S_5 by $S_1 + S_3$, $P_2 + P_3$ by C_6 and S_6 by $S_2 + S_4$.

The switch is also used for other electrode combinations with similar distributions. However if we require to determine the ionization i_i^- as described in § 2.5 section B_1, we use an other circuit (see fig. 3.10), which enables us to realize every arbitrary potential distribution and current measurement.

In this circuit the tube voltmeter is constantly connected with the current line. In our example of the measurement of i_i^-, we connect R_5, S_1, S_3 with one tension line, and apply to the corresponding power supply a potential of —100 V and C_5 with the other, applying to a second power supply a potential of —75 V. C_6 is connected with the current line so that i_i^- can be read on the tube voltmeter. S_2, S_4 and the electrodes not included in this combination are connected with the earthed lines.

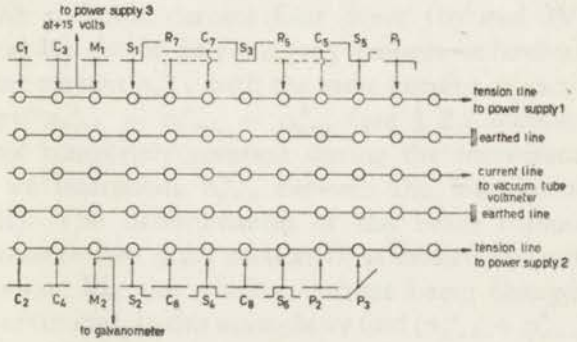

Fig. 3.10.
Electric circuit used in arbitrary voltage distributions and current measurements.

If we need more than two different voltages at the same time we can make a separate contact between electrode and power supply, independently of the circuit. This we have done for C_3 and M_1, which are maintained at + 15 V almost during the whole experiment and for M_2 connected with the galvanometer.

The electrodes are all connected with coaxial cables which can be lead to the circuits we use for our measurements. The insulating resistances between these electrodes and earth exceed 10^{12} Ohm, being sufficiently large in comparison with the input resistor of 10^8 Ohm at our vacuum tube voltmeter.

We have different power supplies at our disposal. Four of these enable us to produce tensions between 0 and 250 volts. They are stabilized with neon tubes (85 A1) and they can be used for the measurements in the collision chamber. If we want to deflect the fast ions in the vacuum chamber, we suffice with a power supply giving tensions between 0 and 2000 volts.

The power supplies are part of the electronic equipment placed in a steel rack. From here cables go through screening tubes in two ways. One tube leads the cables to the place where we are doing our experiments at the separator and the other one leads them to the place where we prepare our definitive measurements by means of the P.I.G. ion source. For the latter a separate high voltage installation (up to 20 kV) is used.

Chapter IV.

EVALUATION OF THE CROSS-SECTIONS FROM THE EXPERIMENTAL RESULTS.

§ 4.1. Combined capture and loss cross-section measurement.

In § 2.1 section A we have described the mathematical formalism of Wien we use in these measurements and in § 2.2 we have explained our experimental method.

For illustration we give our experimental dates of the combination N^+, H_2 at 10 kV in table 4.1 (see page 60) and we show in this table how we calculate the capture and loss cross-section.

We have measured the collector current I^+ at different gas pressures in the collision chamber (see § 2.2 section B). These currents are divided by the corresponding monitor currents measured on M_2 (see § 3.5) and the quotients are given in column IV of table 4.1 by $n'^+_{x=L}$ in arbitrary units. By means of the accent we indicate that the values $n'^+_{x=L}$ have to be corrected for a pressure dependent monitor effect (column V) which is explained in § 4.6 section B. At vacuum pressure ($\pm 5 \times 10^{-6}$ mm Hg) we have checked the collector current four times (column IV number 1, 10, 15 and 20). At the different gas pressures we have to compare the collector current $n'^+_{x=L}$ with the same current at vacuum pressure, where $n'^+_{x=L} = n^+_{x=L} = n^+_{x=0}$ (see § 2.2 section B). The latter is not completely constant during the measurements and therefore we interpolate $n^+_{x=0}$ between the four known values (column II). The determination of the beam composition at vacuum pressure (see § 2.2 section B) is carried out without the use of monitor M_2, the monitor current being changed by the deflection of the ions. In this example we find $(n^+_{x=0} + n^0_{x=0})/n^0_{x=0} = 19.6$, from which we calculate $(n^+_{x=0} + n^0_{x=0})/n^+_{x=0} = 1.054$. Knowing the $n^+_{x=0}$ values in column II, we can now find the corresponding $n^+_{x=0} + n^0_{x=0}$ values in column III. The values $n'^+_{x=L}$

TABLE 4.1.

Combined capture and loss cross-section measurement for N^+, H_2 at 10kV.

Arc tension in the ion source of the separator 185 V. Temperature 20° C.

	I	II	III	IV	V	VI	VII	VIII	IX
no.	pressure in mm Hg	$n^+_{x=0}$ interpolated (arbitrary units)	$n^+_{x=0}+n^o_{x=0}$ (arbitrary units)	$n'^+_{x=L}$ (arbitrary units)	monitor correction in percent	$n^+_{x=L}$ (arbitrary units)	$[n^+_{x=L}]$	αL[2]) (L = 26.8 cm)	Evaluation of α_c and α_l σ_c and σ_l
1	5×10^{-6}	3.19	3.36	3.19	0	3.19	0.949		At 10^{-3} mm Hg
2	4.0×10^{-4}	3.21	3.38	2.53	— 0.3	2.52	0.745	0.276	$\alpha L = 0.706$
3	6.0×10^{-4}	3.23	3.40	2.19	— 0.4	2.18	0.641	0.454	$\alpha = 0.0264$ cm^{-1}
4	9.0×10^{-4}	3.25	3.42	1.96	— 0.7	1.95	0.570	0.596	$\alpha_c = \alpha[n^o_e] = 0.0237$ cm^{-1}
5	1.39×10^{-3}	3.27	3.44	1.44	— 1.0	1.43	0.415	1.00	$\alpha_l = \alpha[n^+_e] = 0.00274$ cm^{-1}
6	1.92×10^{-3}	3.29	3.46	1.14	— 1.4	1.12	0.323	1.35	
7	2.74×10^{-3}	3.31	3.48	0.812	— 2.0	0.796	0.229	1.91	At 10^{-3} mm Hg and
8	3.77×10^{-3}	3.33	3.51	0.600	— 2.8	0.584	0.166	2.61	T = 20° C
9	4.24×10^{-3}	3.36	3.54	0.480	— 3.1	0.465	0.131	3.44	$N = 0.659 \times 10^{14}$ atoms/cm^3
10	5×10^{-6}	3.39	3.57	3.39	0	3.39	0.949		
11	5.53×10^{-3}	3.37	3.55	0.440	— 4.0	0.422	0.119	4.03	$\sigma_c = 36.0 \times 10^{-17}$ cm^2/at
12	6.76×10^{-3}	3.35	3.53	0.400	— 4.8	0.381	0.108[1])		$\sigma_l = 4.16 \times 10^{-17}$ cm^2/at
13	9.00×10^{-3}	3.33	3.51	0.260	— 6.2	0.244	0.0695		
14	1.24×10^{-2}	3.31	3.49	0.400	— 8.3	0.367	0.105[1])		
15	5×10^{-6}	3.29	3.47	3.29	0	3.29	0.949		
16	1.46×10^{-2}	3.31	3.49	0.420	— 9.6	0.380	0.109[1])		
17	1.68×10^{-2}	3.33	3.51	0.380	— 10.6	0.340	0.0968[1])		
18	2.00×10^{-2}	3.35	3.53	0.410	— 12.0	0.361	0.102[1])		
19	2.44×10^{-2}	3.37	3.55	0.420	— 13.5	0.364	0.103[1])		
20	5×10^{-6}	3.39	3.57	3.39	0	3.39	0.949		

$(n^+_{x=0} + n^o_{x=0})/n^o_{x=0} = 19.6 \rightarrow (n^+_{x=0} + n^o_{x=0})/n^+_{x=0} = 1.054$

$[n^+_{x=0}] = 0.949$

$[n^o_{x=0}] = 0.051$

$[B] = [n^+_e] = 0.104$

$1 - [n^+_e] = [n^o_e] = 0.896$ $\Big\}$ w = 0.116

$[A] = [n^+_{x=0}] - [n^+_e] = 0.845$

[1]) $[n^+_e]$ is equal to the mean value of the numbers with accent [1]) in column VII.

[2]) $\alpha L = -\ln([n^+_{x=L}] - [n^+_e])/[A]$.

are transformed into $n^+_{x=L}$ (column VI) by applying the monitor correction (column V); these $n^+_{x=L}$ values are next divided by the corresponding $n^+_{x=o} + n^o_{x=o}$ (column II). The results are given in column VII by $[n^+_{x=L}]$. By the bracket notation used in this chapter we indicate that the quantity, in this case $n^+_{x=L}$, is divided by $n^+_{x=o} + n^o_{x=o}$.

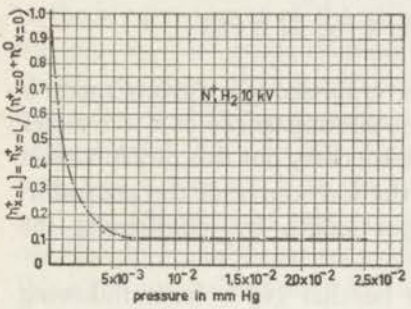

Fig. 4.1.
Relative collector ion intensity as a function of the pressure.

In fig. 4.1 we show the pressure dependence of $[n^+_{x=L}]$. At vacuum pressure this quantity is almost one, a few neutrals being present in the beam. At higher gas pressures $[n^+_{x=L}]$ decreases strongly. The capture process is responsible for the decrease which continues till a gas pressure of about 7×10^{-3} mm Hg is reached. With still increasing pressure $[n^+_{x=L}]$ remains constant, the equilibrium state in the beam being realized. The constant part of the curve determines $[n^+_e]$ (column VII).

We continue our calculation by applying (2.1.8) in the next form:

$$[n^+_{x=L}] = [A]e^{-\alpha L} + [B]$$

[A] and [B] are evaluated by means of (2.1.9) so that we can calculate αL (column VIII) at the different pressures.

In fig. 4.2 we see that αL or α is linearly pressure dependent as we suspected from (2.1.2). By determining the slope of the straight line in fig. 4.2 we can find α reduced at 10^{-3} mm Hg in our case; we have $\alpha L = 0.706$ at 10^{-3} mm Hg. We have taken $L = 26.8$ cm, as explained in § 4.6 section A, so that we find $\alpha = 0.0264$ cm^{-1}. In order to calculate α_c and α_i (column IX) we apply (2.1.7) in which $[n^+_e]$ is known and from (2.1.4) we derive $[n^o_e]$ which is given by $[n^o_e] = 1 - [n^+_e]$. We

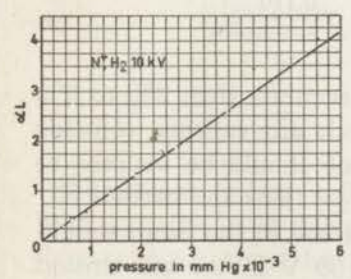

Fig. 4.2.
Pressure dependence of αL.

get $\alpha_c = 0.0237\ cm^{-1}$ and $\alpha_l = 0.00274\ cm^{-1}$ at 10^{-3} mm Hg and T = 20° C. Under these circumstances the number of atoms per cc, N, equals to 0.659×10^{14} for hydrogen gas. We find at last by application of (2.1.2):

$$\sigma_c = 36.0 \times 10^{-17}\ cm^2/at$$
$$\sigma_l = 4.16 \times 10^{-17}\ cm^2/at$$
$$w = [n_e^+]/[n_e^0] = \sigma_l/\sigma_c = 0.116$$

The combined capture and loss cross-section measurement is sometimes repeated under different circumstances in the manner we have described. In the first place we carry out this measurement with two different arc voltages in the ion source of the separator. Secondly we vary the effective gas length by lengthening the collector.

Shooting with N^+ ions it may be that $N_2^{+\,+}$ ions, following the same path in the separator, or excited N^+ ions are also present in the beam entering our apparatus. Their presence will influence the cross-section values. Their share in the beam is dependent on the arc voltage (= voltage difference of anode and cathode) in the ion-source and therefore we compare two cross-section measurements with different arc voltages. We have got the following results:

N^+, H_2 10 kV.

arc voltage	100 V	200 V
σ_c	33.4	33.0
σ_l	3.70	3.91
w	0.111	0.119

Our results being generally no more accurate than 2% to 5% we see that the cross-sections with both arc voltages coincide within the limit of error. From this, one should be inclined to conclude that a negligible quantity of $N_2^{+\,+}$ ions and excited N^+ ions are present in the beam, for their share in the beam should alter considerably with a variation of 100 V in the arc tension and give corresponding variable cross-sections. However, more critical studies taught us that many metastable N^+ ions are present

in the beam and that under certain conditions the same holds for $N_2^{+\,+}$ ions.

In our mass-spectrometer it is found that the ratio $^{14}N_2^{+\,+}$ to $^{14}N^+$ is equal to 1.7, determined from the ratio of the peaks at mass 14.5 and mass 15. In this case a Nier ion source is used with an arc voltage of 80 V. We can not draw a complete conclusion from this for our experiment, because for example the circumstances in the arc ion-source of the separator differ from those in the Nier ion-source. The interpretation of our results with the adiabatic theory indicates that many excited N^+ ions are present in the beam (see § 5.7). So it seems strange that the change of the arc voltage from 100 V to 200 V does not effect our results. However a change of 0 to 100 V in the arc tension would alter for a greater part the efficiency of ionizing the gas by electrons and in this case one should probably get remarkable changes in the cross-sections. We have not realized such low arc voltages in our experiment because of the strong decrease in the intensity of the collector current.

The lengthening of the collector is done by replacing P_1 by C_7, R_7, S_5, P_1 electrically connected together and P_2, P_3 by C_8, S_6, P_2, P_3 similarly connected. S_3 and S_4 are now used as guard rings. In this case the effective gas length is equal to 16.6 cm (see § 4.6 section A). Comparing the results of the collectors with effective gas length 26.8 cm and 16.6 cm, respectively called short and long collector, we get:

N^+, H_2 10 kV.

	short collector	long collector
arc voltage	200 V	200 V
effective gas length	26.8 cm	16.6 cm
σ_c	33.0	33.4
σ_l	3.91	3.78
w	0.119	0.114

The results in both collectors coincide within the limit of error. Both systems have different opening angles, about 2.7° in the short collector, about 4.6° in the long collector, so that we conclude that the disturbing influence of the scattering over large angles is negligible.

§ 4.2. The determination of σ_c at low pressures independently of σ_i or w.

In § 2.1 section B we have described the mathematical formalism we use in these measurements and in § 2.3 we have explained our experimental method.

We illustrate our results for the combination N^+, H_2 at 10 kV in table 4.2 and we calculate the capture cross-section.

TABLE 4.2.

Capture cross-section measurement at low pressures independently of σ_i or w for N^+, H_2 at 10 kV.

Arc tension in the ion source of the separator 200 V.
Temperature 25.5° C.

	I	II	III
no.	pressure in mm Hg	$n^+ - n^-$ in (L_1, L_2) (arbitrary units)	Evaluation of α_c and σ_c by means of $\alpha_c L' = (n^+ - n^-)/n^+_{x=0}$
1	2×10^{-5}	0.089	$n^+_{x=0} = (6.52 + 6.24)/2 = 6.38$
2	1.2×10^{-4}	0.203	$L' = 8.3$ cm
3	1.5×10^{-4}	0.233	The slope of the straight line
4	1.9×10^{-4}	0.260	in fig. 4.3 corresponds with
5	2.3×10^{-4}	0.335	$n^+ - n^- = 1.06$ per 10^{-3} mm Hg
6	3.0×10^{-4}	0.380	$\alpha_c = 0.0200$ cm^{-1} at 10^{-3} mm Hg
7	4.1×10^{-4}	0.515	and T = 25.5° C
8	5.0×10^{-4}	0.591	$\sigma_c = 30.9 \times 10^{-17}$ cm^2/at
9	5.5×10^{-4}	0.653	

We have measured the currents i^+ and i^- respectively on the side electrodes C_5, R_5 and C_6 (see § 2.3 section A) at different low gas pressures in the collision chamber. These currents are divided by the monitor currents just as in § 4.1 so that we find the corresponding $n^+ - n^-$ in the interval (L_1, L_2). We have made a graph of these values as a function of the pressure (fig. 4.3) and we get a linear dependence in accordance with (2.1.16) and (2.1.2). The slope of the straight line corresponds to $n^+ - n^- = 1.06$ per 10^{-3} mm Hg. We have seen in § 2.3 section B that $n^+ - n^- = n^+_{x=L_1} - n^+_{x=L_2}$. The vacuum intensity $n^+_{x=0}$ is determined as the mean value of the two collector currents respectively checked at the beginning and the end of this measurement.

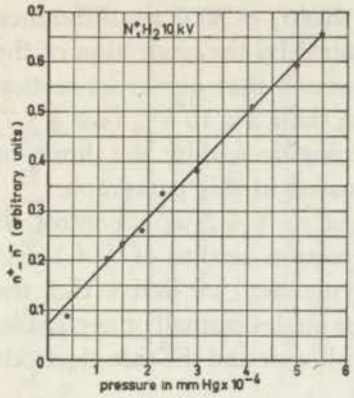

Fig. 4.3.

Pressure dependence of $n^+ - n^-$.

In our case $L_2 - L_1 = L' = 8.3$ cm. It is now possible to apply (2.1.16) and we find that (see column III) $\alpha_c = 0.0200$ cm^{-1} at 10^{-3} mm Hg. The temperature in this measurement being 25.5° C we calculate by means of (2.1.2) that $\sigma_c = 30.9 \times 10^{-17}$ cm^2/at.

§ 4.3. Comparison of the capture cross-sections or probabilities determined by the two different methods.

We shall explain that the capture cross-section found in § 4.2 must be smaller than that in § 4.1. In (2.1.16) we neglect the second order processes and now we shall investigate their influence by means of (2.1.20) derived in § 2.1 section C.

In our example the measurements on the collector (§ 4.1) and on the side electrodes (§ 4.2) were taken with the same beam composition in vacuum, given in table 4.1 by $[n^+_{x=0}]$ and $[n^0_{x=0}]$.

With our consideration of the second order effects we make use of our capture and loss cross-sections found in § 4.1. Further we choose a gas pressure of 5×10^{-4} mm Hg, the linear dependence in fig. 4.3 being no more realized at some higher pressures in our experiments.

We compare (2.1.20) with (2.1.16). In the left hand side of (2.1.20) we have $n^+_{x=L_1}$ in the denominator in stead of $n^+_{x=0}$ in (2.1.16). With our results in table 4.1 and with an effective gas length $L_1 = 6.1$ cm (see § 4.6 section A) we find by application of (2.1.8) that $[n^+_{x=L_1}] = 0.894$ at 5×10^{-4} mm Hg and 25.5° C. In table 4.1 we see that $[n^+_{x=0}] = 0.949$ so that by replacing $n^+_{x=L_1}$ by $n^+_{x=0}$ we make in our calculation α_c or σ_c 6.7% too small. In the right hand side (2.1.20) has a factor between brackets extra, given by $[1 - \frac{1}{2}\,\alpha L' + (n^0_{x=L_1}/n^+_{x=L_1})\,w]$. We find this factor 0.960 large, so that if we omit this term α_c is taken 4.2% too small.

Neglecting second order effects we find thus that α_c at 5×10^{-4} mm Hg is taken 6.7 + 4.2 = 11% too small. Having

found in § 4.1 that $\sigma_c = 36.0$, in § 4.2 that $\sigma_c = 30.9$, the difference of 17% in these values is partly explained by the neglection of the second order effects in § 4.2. We remark that our cross-section results are generally no more accurate than 2% to 5% (see § 4.7) so that both cross-sections almost coincide within the limit of error if we apply the correction discussed in this paragraph.

We generally use the measurement in § 4.2 as a control. If the difference in the capture cross-section results of § 4.1 and § 4.2 can be explained in the given manner, we derive that the disturbing effect of scattering over large angles is small or negligible. In this case the opening angles of the collector and the side electrode system are respectively 2.7° and 16°.

§ 4.4. Ionization cross-section measurement.

In § 2.4 we have described them athematical formalism we use in this measurement and in § 2.5 we have explained our experimental method and the evaluation of the real ionization current.

For illustration we give our experimental dates of the combination N^+, H_2 at 10 kV in different tables.

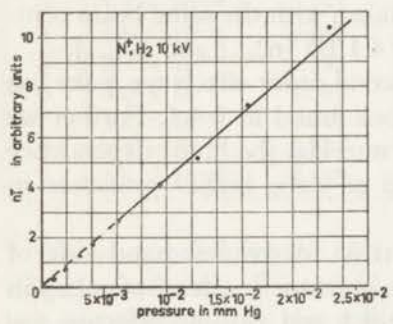

Fig. 4.4.
Pressure dependence of n_i^-.

In table 4.3 we have gathered our results determined in the manner explained in § 2.5 section A, B_1 and B_2. In this table we find $n_i'^-$ (column II) by dividing the currents i_i^- by the corresponding monitor currents. Applying the monitor correction (column V) for these values we get n_i^- (column VI). We have made a graph of these values as a function of the gas pressure and at sufficiently high gas pressures we get a linear dependence. In this pressure region of the curve the beam passing along the side electrodes C_8 and C_7, R_7 is in its equilibrium state. If the linear part of the curve is extrapolated (broken line) it passes through the origin. We deduce from this that in the equilibrium state of the beam $n_i^- = 0.436$ reduced to $p = 10^{-3}$ mm Hg and with

TABLE 4.3.

Ionization cross-section measurement with electrodes C_7, R_7, C_8, S_3, S_4, S_5, S_6 for N^+, H_2 at 10 kV.
Arc tension in the ion source of the separator 200 V. Temperature 27.5° C.

	I	II	III	IV	V	VI	VII
no.	pressure in mm Hg	n'_i— (arbitrary units)	n'— (arbitrary units)	$1+\gamma$	monitor correction in percent	n_i— (arbitrary units)	Evaluation of α_i and σ_i by means of $[n_i^-]/L' = \alpha_i + [n_e^0]\ \alpha_1$
1	5×10^{-6}	0.0642			0	0.0642	In the equilibrium state of the beam
2	2.3×10^{-4}	0.109	0.141	1.29	0	0.109	$n_i^- = 0.436$ reduced to
3	6.5×10^{-4}	0.225	0.313	1.39	— 0.5	0.224	$p = 10^{-3}$ mm Hg.
4	10^{-3}	0.331	0.437	1.32	— 0.7	0.328	$n^+ + n^0 = (12.6 + 12.4)/2 = 12.5$
5	1.92×10^{-3}	0.726	0.979	1.33	— 1.4	0.716	$[n_i^-] = 0.0348$ at 10^{-3} mm Hg
6	3.10×10^{-3}	1.30	1.48	1.14	— 2.3	1.27	and 27.5° C
7	4.11×10^{-3}	1.77	2.00	1.13	— 3.0	1.72	$[n_i^-] = 0.0357$ at 10^{-3} mm Hg
8	6.15×10^{-3}	2.80	3.14	1.12	— 4.4	2.68	and 20° C
9	9.51×10^{-3}	4.43	4.88	1.10	— 6.5	4.15	$L' = 8.3$ cm
10	1.24×10^{-2}	5.61	6.34	1.13	— 8.3	5.15	$[n_i^-]/L' = 0.00430\ cm^{-1}$
11	1.65×10^{-2}	8.07	8.65	1.07	— 10.5	7.22	$[n_e^0]\ \alpha_1 =$
12	2.29×10^{-2}	11.9	11.9	1.00	— 13.0	10.4	$(0.900 \times 0.00246) = 0.00221\ cm^{-1}$ —
							$\alpha_i = 0.00209\ cm^{-1}$
							$\sigma_i = 3.16 \times 10^{-17}\ cm^2/at$

$T = 27.5°$ C. To calculate the ionization cross-section we apply (2.4.10) in the following form:

$$[n_i^-]/L' = ([n_e^+]\,\alpha_i^+ + [n_e^0]\,\alpha_i^0) + [n_e^0]\,\alpha_l$$

and we replace $([n_e^+]\,\alpha_i^+ + [n_e^0]\,\alpha_i^0)$ by α_l, the ionization probability per beam particle in its equilibrium state ($L' = L_2 - L_1 = 8.3$ cm). In our calculation (column VII of table 4.3) we find that

$$\alpha_i = 0.00209 \text{ cm}^{-1} \text{ at } 10^{-3} \text{ mm Hg and } 20° \text{ C}$$
$$\sigma_i = 3.16 \times 10^{-17} \text{ cm}^2/\text{at.}$$

and we remark that we have taken $[n_e^0] = 0.900$ and $\alpha_l = 0.00246$, being both the values of these quantities determined in a preceding combined capture and loss cross-section measurement.

In column III of table § 4.3 we have given our n'^- values and from § 2.5 section B_2 we know that

$$n'^- = n_i'^- (1 + \gamma)$$

so that $(1 + \gamma)$ (see column IV) can be calculated from the values in column II and III.

The secondary emission of electrons at C_7 can be caused by slow ions formed in the gas, which are accelerated by the tension of 100 V across the side electrodes to C_7 and it may be that a very small quantity of primary particles hits the side electrodes causing also the emission of electrons.

In the appendix of table 4.3 we have calculated the ionization cross-section in the intermediate pressure region (see § 2.4) where the beam has not yet reached its equilibrium state before entering between the side electrodes C_7, R_7, C_8. We have seen in equation 2.4.8 that the real ionization is given by

$$n_i = (\alpha_i^+ \overline{n^+_{L_1, L_2}} + \alpha_i^0 \overline{n^0_{L_1, L_2}})\, L'$$

where $\overline{n^+_{L_1, L_2}}$ and $\overline{n^0_{L_1, L_2}}$ are given by (2.4.7). We have calculated these quantities per incident beam particle and given them in column X and XI of the appendix table. In order to find the real ionization from our experimental n_i^- or $[n_i^-]$ values (column VI of table 4.3 and column II of the appendix), we apply equation (2.4.9) at the different pressures. We have a rather large $[n_i^-]$ at "zero pressure" (5×10^{-6} mm Hg), so that we correct all $[n_i^-]$

APPENDIX OF TABLE 4.3.

Calculation of the ionization cross-section in the intermediate pressure region.

	I	II	III	IV	V	VI	VII	VIII	IX	X	XI
no.	pressure in mm Hg	$[n_i^-]$ (arbitrary units)	$[n_i^{-*}]$	[1) loss in equilibrium]	[2) first cycle]	[3) n_i]	$[n_i]$ reduced to $p = 10^{-3}$ mm Hg	$\alpha_i^{+0} = [n_i]/L'$ at $p = 10^{-3}$ mm Hg	σ_i^{+0} in 10^{-17} cm²/at	$\overline{[n^+_{L_1, L_2}]}$	$\overline{[n^0_{L_1, L_2}]}$
1	5×10^{-6}	0.00513	0							1	0
2	2.3×10^{-4}	0.00872	0.00359	0.000549	0.829×10^{-4}	0.00296	0.0129	0.00156	2.44	0.934	0.066
3	6.5×10^{-4}	0.0179	0.0128	0.00308	0.000544	0.00918	0.0141	0.00171	2.66	0.778	0.222
4	10^{-3}	0.0263	0.0212	0.00647	0.00111	0.0136	0.0136	0.00164	2.56	0.669	0.331
5	1.92×10^{-3}	0.0571	0.0520	0.0192	0.00265	0.0301	0.0157	0.00189	2.94	0.458	0.542
6	3.10×10^{-3}	0.101	0.0961	0.0403	0.00416	0.0524	0.0169	0.00204	3.18	0.304	0.696
7	4.11×10^{-3}	0.137	0.132	0.0607	0.00470	0.0666	0.0162	0.00195	3.04	0.227	0.773

Note: In this calculation we have taken:

$\left.\begin{aligned} \alpha_c &= 0.0216 \\ \alpha_1 &= 0.00246 \end{aligned}\right\}$ at 10^{-3} mm Hg $\quad n^+ + n^0 = 12.5$, $[n^+_{x=0}] = 0.955$

$\left.\begin{aligned} [n_e^+] &= 0.101 \\ [n_e^0] &= 0.899 \end{aligned}\right\}$ $w = 0.113$ $\quad L_1 = 16.6$, $L_2 = 24.9$, $L_2 - L_1 = L' = 8.3$

1) [loss in equilibrium] $= [n^0_{x=L_1}]\, \alpha_1 L'$

2) [first cycle] $= \left([n^+_{x=L_1}] - w\,[n^0_{x=L_1}]\right)\left(1 + \dfrac{\alpha_1 \exp(-\alpha_c L') - \alpha_c \exp(-\alpha_1 L')}{\alpha_c - \alpha_1}\right)$

3) $[n_i] = [n_i^{-*}]$ — [loss in equilibrium] — [first cycle]

by substracting from them the $[n_i^-]$ value at 5×10^{-6} mm Hg. In this way we obtain $[n_i^{-*}]$ (column III), which is substituted for $[n_i^-]$ in (2.4.9). In this equation the two last terms (column IV and V) are calculated with our results in the combined capture and loss cross-section measurement (see the note in the appendix). In this manner we find $[n_i]$ values (column VI) which we reduce to 10^{-3} mm Hg (column VII). We calculate then a_i^{+o} (column VIII) and σ_i^{+o} (column IX) given by

$$\left.\begin{aligned} a_i^{+o} &= a_i^+ \overline{[n^+_{L_1, L_2}}] + a_i^o \overline{[n^o_{L_1, L_2}]} \\ \sigma_i^{+o} &= \sigma_i^+ \overline{[n^+_{L_1, L_2}]} + \sigma_i^o \overline{[n^o_{L_1, L_2}]} \end{aligned}\right\} \quad a_i^{+o} = N\sigma_i^{+o}$$

As a consequence of a large zero effect in column II our σ_i^{+o} values at the lowest pressures are rather unreliable. At higher pressures (see number 5, 6, 7) the dates of σ_i^{+o} do not show a large change with the variation of the average beam composition and are near σ_i in table 4.3, so that it seems that there is not much difference between σ_i^+ and σ_i^o. The determination is not accurate enough to give reliable σ_i^+ and σ_i^o cross-section results.

In § 2.5 section B_3 we have shown the importance of the determination of $i^+ + i^-$ at such high pressures that the beam passing the side electrodes is in its equilibrium state. In table 4.4 and in fig. 4.5 we have given the results of this measurement in the usual way, both on electrodes C_5, R_5, C_6 and on electrodes C_7, R_7, C_8. In fig. 4.5 we have drawn two curves showing the relation between $[n^+] - [n^-]$ and the pressure. In this figure we see that $[n^+] - [n^-]$ is smaller than 0.01 in both cases at sufficiently high gas pressure. This value is reached at a lower pressure for C_7, R_7, C_8 than for C_5, R_5, C_6, the equilibrium state in the beam being obtained at a lower pressure between the first side electrodes.

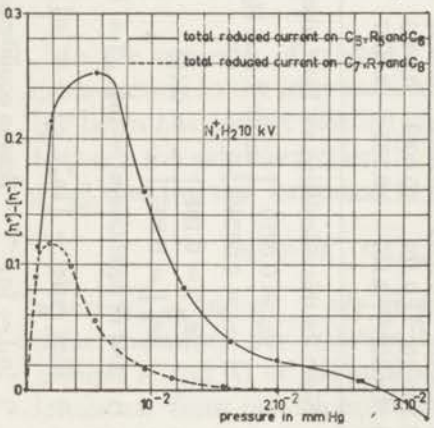

Fig. 4.5.
Pressure dependence of $[n^+] - [n^-]$.

TABLE 4.4.

Sum current measurements on the side electrodes for N^+, H_2 at 10 kV.

Arc tension in the ion source of the separator 200 V. Temperature 26° C.

Measurement on C_5, R_5 and C_6

	I	II	III
no.	pressure in mm Hg	$n^+ - n^-$ (arbitrary units)	$[n^+]-[n^-]$
1	5×10^{-6}	0.122— 0.039= 0.083	0.0066
2	10^{-4}	0.472— 0.072= 0.400	0.0318
3	5×10^{-4}	1.15 — 0.137= 1.01	0.0801
4	9×10^{-4}	1.70 — 0.26 = 1.44	0.114
5	1.92×10^{-3}	3.34 — 0.64 = 2.70	0.214
6	3.77×10^{-3}	4.03 — 1.55 = 2.48	0.197
7	5.53×10^{-3}	5.48 — 2.44 = 3.04	0.252
8	9.43×10^{-3}	6.60 — 4.61 = 1.99	0.158
9	1.26×10^{-2}	7.50 — 6.48 = 1.02	0.0810
10	1.63×10^{-2}	9.55 — 9.05 = 0.50	0.040
11	2.00×10^{-2}	10.8 —10.5 = 0.3	0.02
12	2.68×10^{-2}	14.7 —14.6 = 0.1	0.008
13	3.20×10^{-2}	17.7 —18.0 = —0.3	—0.02

Measurement on C_7, R_7 and C_8

	I	II	III
no.	pressure in mm Hg	$n^+ - n^-$ (arbitrary units)	$[n^+]-[n^-]$
1	5×10^{-6}	0.071— 0.057 = 0.014	0.0011
2	2×10^{-4}	0.575— 0.125 = 0.450	0.0357
3	7.52×10^{-4}	1.43 — 0.30 = 1.13	0.0896
4	1.92×10^{-3}	2.28 — 0.81 = 1.47	0.117
5	3.65×10^{-3}	2.99 — 1.74 = 1.25	0.0992
6	5.53×10^{-3}	3.57 — 2.87 = 0.70	0.0555
7	9.51×10^{-3}	5.00 — 4.79 = 0.21	0.0167
8	1.16×10^{-2}	6.02 — 5.96 = 0.06	0.005
9	1.58×10^{-2}	8.15 — 8.13 = 0.02	0.002
10	2.00×10^{-2}	10.5 —10.5 = 0.0	0.0
11	2.65×10^{-2}	14.4 —13.9 = 0.5	0.04

$$n^+_{x=0} + n^0_{x=0} = 12.6$$

Since the difference of $[n^+] - [n^-]$ is smaller than 0.01 in both cases at sufficiently high gas pressures, we may conclude that the amount of scattered or reflected ions of the primary beam reaching the side electrodes is negligibly small; otherwise we should have a large positive value for $[n^+] - [n^-]$ in this pressure region.

§ 4.5. Secondary emission coefficient γ and reflection coefficient R at collector plate P_3.

In § 2.2 section B we have seen that with the determination of the beam composition at vacuum pressure we make use of the secondary emission of electrons at P_3. The primary beam hits electrode P_3, where the secondary emission of electrons takes place and where some of the primary particles are reflected in the direction of P_1. It is not our intention to realize an accurate measurement of γ and R. We should use a different apparatus for such experiments which would be carried out in a vacuum of about 10^{-9} mm Hg. We are working with a vacuum of about 5×10^{-6} mm Hg at which pressure oxide layers are easily formed on an electrode surface. We are nevertheless interested in the order of the mentioned processes accompanying our cross-section measurements and we shall discuss our results about them.

In § 2.2 section B we have written the equation

$$| I_e^{+o} | = \gamma (I^+ + I^o)$$

Neglecting the relatively small amount of neutrals present in the beam we get

$$| I_e^{+o} | \sim \gamma I^+$$

In this way we find in our example where N^+ ions of 10 keV hit electrode P_3 that $\gamma = 3.3$. In this calculation we have supposed that I_e^{+o} is equal to I_{P_1} with the given voltage distribution. In reality we have

$$| I_{P_1} | = | I_e^{+o} | - | I^{r+} |$$

I^{r+} being the current of ions on P_1 which are reflected from P_3. I^{r+} seems to be very small with respect to $| I_e^{+o} |$ so that we have

$$I_{P_1} \sim I_e^{+o}$$

The reflection coefficient R is roughly estimated from the positive current arriving on P_1, if we apply a tension of +100 V to P_3, P_2 and S_6 at vacuum pressure. In our case we define R as the number of ions and neutrals reflected from P_3 per incident ion. We thus include the ions which have become neutral by capturing an electron on the surface of P_3 and which return as a neutral to P_1.

We have per definition

$$R = (I^{r+} + I^{ro})/I^{+}$$

I^{r+} and I^{ro} representing respectively the currents of reflected ions and neutrals. For the sake of simplification we write

$$I^{r} = I^{r+} + I^{ro}$$

and we assume that all reflected particles arrive on electrode P_1. We can now represent the current on P_1 measured with the mentioned voltage distribution by

$$I_{P_1} = I^{r+} + I_e^{r}$$

I_e^{r} being the current of secondary electrons leaving P_1 in consequence of the reflected particles hitting P_1.

In order to realize a rough approximation about the reflection, we assume two cases:

a) all particles reflected from P_3 are positive.

b) all particles reflected from P_3 are neutral.

Case a): $I_{P_1} = I^{r+} + |I_e^{r}|$ changes into $I_{P_1} = I^{r} + |I_e^{r}|$. If we call the mean secondary emission coefficient on P_1 per reflected particle γ^* we have

$$I_{P_1} = (1 + \gamma^*)\, I_r \text{ or}$$
$$R = I^{r}/I^{+} \sim I_{P_1}/I^{+}(1 + \gamma^*)$$

In evaluating R we do not know the value we have to take for γ^*. The reflected particles have a spread in energy varying between the energy of the primary particles and zero. We can only give the lower and upper limit for R taking respectively $\gamma^* = 0$ and $\gamma^* = \gamma$ and we find in our example where $\gamma = 3.3$ that

$$0.042 < R < 0.17$$

Assuming that R is of the same order of magnitude as the mean value of these limits, in this case equal to 0.11, we get an idea about the importance of the reflection in our measurements.

Case b): $I_{P_1} = I^{r+} + |I_e^r|$ changes into $I_{P_1} = |I_e^r|$. Just in the same manner as in case a) we find

$$R = I^r/I^+ = I_{P_1}/I^+ \gamma^*$$

Assuming that γ^* is the same for ions and neutrals, for example $\gamma^* = 1.65$ we get $R = 0.17/1.65 \sim 0.10$ compared with $R = 0.17/2.65 \sim 0.064$ in case a). We may conclude from this that the value of R obtained in case a) will be too small if neutrals are present in the beam and the smaller γ^*, the larger the difference between case a) and case b).

One could imagine that radiation could arrive from P_3, the radiation causing secondary emission of electrons at P_1. However, Shekhter (see Hagström[H3]) has shown that the probability of neutralization of an ion near a metal surface accompanied by radiation is very low ($\sim 5 \times 10^{-7}$). The probability of any radiative process is expected to be low because the lifetime of radiation ($\sim 10^{-8}$ sec) is very long compared to the time which even a thermal particle spends within a few angströms of the surface (10^{-12} sec).

One can also show that the secondary emission of electrons at P_1 due to "bremsstrahlung" formed in the target material of P_3 is negligible. This radiation arises when the beam particles are stopped in the copper material of P_3.

The method of collector current measurement (§ 2.2 section B) is only justified if we keep the particles reflected at P_3 inside the collector space. For that purpose we have given one side of electrode P_3 a slope of about 40 degrees with respect to the direction of the arriving beam. In practice we find negligible reflection currents at S_5 or C_7 with respect to the vacuum collector current, in the order of some pro milles, so that it seems that we have succeeded to hold almost all reflected particles inside the collector space.

Notwithstanding this we show with our rough estimation of R that it is important to take into account reflection effects. In an arrangement as that of Keene[K1], with the end electrode of the Faraday box perpendicular to the primary beam, reflected particles have a larger chance to go back into the collision chamber than in our case and they will participate there in the different collision processes for a second time.

§ 4.6. Corrections.

A. Effective length.

In § 4.1 we have described the collector current measurement with different hydrogen pressures in the collision chamber. The beam passes over a length of 243.5 mm in the collision chamber before entering the collector room formed by P_1, P_2 and P_3. We have $L_a = 243.5$ mm (see fig. 4.6).

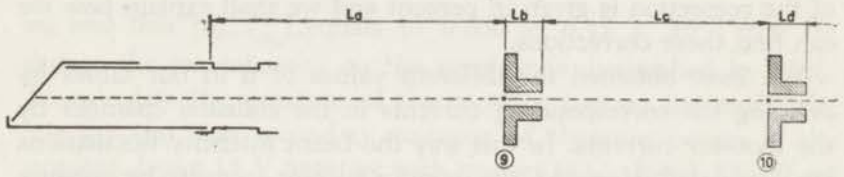

Fig. 4.6.
The effective length (not drawn on scale).

As we have seen in § 3.4 the pressure fall at slit 9 is not so large that we can neglect the presence of gas in the vacuum chamber with $L_c = 240$ mm.

With different hydrogen pressures in the collision chamber we have determined the ratio of the gas pressure in the collision chamber and the vacuum chamber. We take the mean value of these dates and we find

$$p_{\text{vac. chamber}} = 0.0647 \times p_{\text{coll. chamber}}$$

The correction of L_a does not only include the gas length of the vacuum chamber, but also that of slits 9 and 10 (fig. 4.6). We assume a linear pressure fall in these slits both with a geometrical length of 15 mm. We reduce the geometrical lengths L_b, L_c and L_d (fig. 4.6) to the gas pressure in the collision chamber in such a way that for instance

$$L_c \times p_{\text{vac. chamber}} = L_c^r \times p_{\text{coll. chamber}} \text{ (r means reduced)}$$

We find an effective length L by adding to L_a the reduced lengths:

$$\begin{aligned} L &= L_a^r + L_b^r + L_c^r + L_d^r = \\ &= (243.5 + 8.0 + 15.5 + 1.0) \text{ mm} \\ &= 243.5 \text{ mm} + 24.5 \text{ mm} = 268 \text{ mm} \end{aligned}$$

In case of hydrogen gas we have a length correction of 24.5 mm which must be added to the gas length 243.5 mm in the collection chamber. This correction must also be applied to other gas lengths in the collision chamber.

B. Monitor effect.

In table 4.1 and 4.3 we have corrected respectively $n'_{x=L}$ and $n'_{\bar{i}}$ for a monitor effect, dependent on the pressure. The magnitude of the correction is given in percent and we shall explain how we can find these corrections.

We have obtained the different values of n in our tables by dividing the corresponding currents in the collision chamber by the monitor currents. In this way the beam intensity fluctuations are eliminated. However, the monitor current seems to be pressure dependent. If we are taking a hydrogen gas pressure p in the collision chamber, the gas pressure in the vacuum chamber is equal to $0.0647 \times p$, as we have seen in section A of this paragraph. The capture process occurs also in the vacuum chamber, so that the monitor current will decrease if we increase the pressure in the collision chamber. As a consequence of the fluctuations in the beam intensity we can not always observe this decrease directly, so that we need calculations for the monitor correction.

In practice we start a capture and loss cross-section calculation without monitor correction using the same scheme as in table 4.1. Having found the uncorrected cross-sections we use these values to evaluate the monitor correction at different pressures. For this purpose we apply also equations (2.1.8). The beam passes over a length of 200 mm in the vacuum chamber, before it reaches monitor M_2. Assuming a linear pressure fall in slit 10, which is 15 mm thick, we get $L_{M_2} = (200 + \frac{1}{2} \times 15)$ mm $= 208$ mm. This value is substituted for the length in 2.1.8, taking the uncorrected α' at the pressure in the vacuum chamber.

As an example we calculate the monitor correction for N^+, H_2 at 10 kV, with a hydrogen gas pressure of 10^{-2} mm Hg in the collision chamber. We have found the following uncorrected values which we need in this calculation from our experimental dates in column I and IV of table 4.1:

At 10^{-3} mm Hg $\quad \alpha_c' = 0.0251 \ \text{cm}^{-1} \quad [A'] = 0.834$

$\alpha_1' = 0.00328 \ \text{cm}^{-1} \quad [B'] = 0.115$

$\alpha' = 0.0284 \ \text{cm}^{-1}$

A hydrogen pressure of 10^{-2} mm Hg in the collision chamber corresponds to a pressure of 6.47×10^{-4} mm Hg in the vacuum chamber. Applying the first equation of (2.1.8) in the form

$$[n^+_{x=L_{M_3}}] = [A'] \, e^{-\alpha' L_{M_3}} + [B']$$

we find that $[n^+_{x=L_{M_3}}]$ equals to 0.660 at 6.47×10^{-4} mm Hg and so the ion intensity on the monitor is diminished by 34%. To calculate the decrease of the monitor current we must take into account that secondary emission of electrons occurs at the monitor, being 15 V negative with respect to C_3 (see § 3.5). If we assume that the secondary emission coefficient γ (see § 4.5) is the same for the monitor and electrode P_3, both made of copper, we calculate that we still keep a fraction of the vacuum current on the monitor given by

$$\frac{I_{M_3 (p = 6.47 \times 10^{-4} \text{mm Hg})}}{I_{M_3 (\text{vacuum pressure})}} = \frac{[n^+_{x=L_{M_3}}]_{6.47 \times 10^{-4} \text{ mm Hg}} + \gamma}{[n^+_{x=L_{M_3}}]_{\text{vacuum pressure}} + \gamma} =$$

$$= \frac{0.660 + 3.3}{0.949 + 3.3} = 0.932$$

in which we have taken $[n^+_{x=L_{M_3}}]_{\text{vacuum pressure}}$ equal to $[n^+_{x=0}]$ (see § 4.1 and table 4.1).

In this case the monitor current change amounts to —6.8%. In fig. 4.7 we have drawn a full curve describing the monitor current change calculated as a function of the gas pressure in the collision chamber. The monitor corrections in table 4.1 and 4.3 are read from this curve.

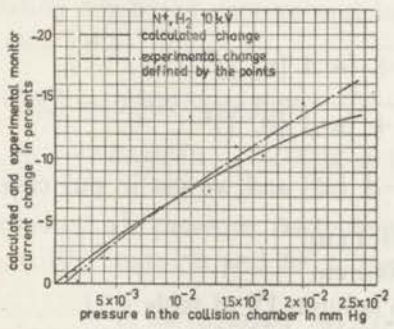

Fig. 4.7.
Monitor correction.

Accidentally there were small intensity fluctuations in the beam when we carried out our cross-section measurement

for N^+, H_2 at 10 kV given in table 4.1, so that we succeeded in finding the experimental monitor current change, given in fig. 4.7 by the broken line. This line is estimated from the differently determined points in the graph. The calculated and experimental curve almost coincide.

We have calculated that in our example 2% of the beam intensity is lost in the separator as a consequence of increasing the hydrogen gas pressure in the collision chamber with 2×10^{-2} mm Hg. In our pressure region this loss of particles is linearly pressure dependent. If we use our experimental curve in fig. 4.6 for monitor correction we must correct the experimental monitor current change by + 0.1% per 10^{-3} mm Hg.

§ 4.7. Sources of error

At first we consider the capture and loss cross-section results in table 4.1. We determine the mean square root error in our σ_c and σ_l, or α_c and α_l values.

We estimate the error in αL reduced at 10^{-3} mm Hg (see fig. 4.2 and column VIII and IX in table 4.1) from the scatter of points in fig. 4.2 giving the pressure dependence of αL. Then we calculate the mean square root error in the $[n_e^+]$ value (see column VII table 4.1). In this way we find that
(α, α_c, α_l, $\Delta\,\alpha$, $\Delta\,\alpha_c$ and $\Delta\,\alpha_l$ are all reduced to $p = 10^{-3}$ mm Hg):

$$\alpha L = 0.706 \pm 0.010 \text{ or } \alpha = (0.0264 \pm 0.0004)\ \text{cm}^{-1}$$
$$[n_e^+] = 0.0986 \pm 0.0018$$

In order to calculate $\Delta\,\alpha_c$ and $\Delta\,\alpha_l$ we apply the following equations derived from (2.1.7)

$$\Delta\,\alpha_c = \sqrt{([n_e^0]\,\Delta\,\alpha)^2 + (\alpha\,\Delta\,[n_e^0])^2}$$
$$\Delta\,\alpha_l = \sqrt{([n_e^+]\,\Delta\,\alpha)^2 + (\alpha\,\Delta\,[n_e^+])^2}$$

We remark that $\Delta\,[n_e^+] = -\Delta\,[n_e^0]$ and we get in our case:

$$\alpha_c = (0.0237 \pm 0.0003)\ \text{cm}^{-1}$$
$$\alpha_l = (0.00274 \pm 0.00006)\ \text{cm}^{-1}$$

and from this we obtain (see also column IX of table 4.1)

$$\sigma_c = (36.0 \pm 0.5) \times 10^{-17}\ \text{cm}^2/\text{at}$$
$$\sigma_l = (4.16 \pm 0.09) \times 10^{-17}\ \text{cm}^2/\text{at}$$

In this calculation we have only taken into account errors due to fluctuation of experimental conditions. reading errors etc. These errors are essentially random. There are, however, several sources of systematic error, discussed below.

In an analogous manner we can calculate the mean square root error in our σ_c or α_c value given in table 4.2. We estimate the error in $n^+ - n^-$ per 10^{-3} mm Hg (see fig. 4.3 and table 4.2) from the scatter of points in fig. 4.3 giving the pressure dependence of $n^+ - n^-$. We find in our case $n^+ - n^- = 1.06 \pm 0.02$ per 10^{-3} mm Hg. We have the same relative error in σ_c so that we get at last (see also column III in table 4.2) $\sigma_c = (30.9 \pm 0.5) \times 10^{-17}$ cm^2/at.

Thirdly we consider the ionization cross-section of the beam in its equilibrium state, calculated in table 4.3. We estimate the error in n_i^- reduced to 10^{-3} mm Hg (see fig. 4.4 and column VI and VII in table 4.3) from the scatter of points in fig. 4.4, giving the pressure dependence of n_i^-. We have

$$n_i^- = 0.436 \pm 0.006$$

For α_i we have written (see § 4.4)

$$\alpha_i = [n_i^-]/L' - [n_e^o]\,\alpha_l$$

so that we derive from this equation

$$\Delta\,\alpha_i = \sqrt{(\Delta\,[n_i^-]/L')^2 + ([n_e^o]\,\Delta\,\alpha_l)^2 + (\alpha_l\,\Delta\,[n_e^o])^2}$$

For $[n_e^o]$ and α_l we have taken the values determined in a preceding combined capture and loss cross-section measurement (see also § 4.4)

$$[n_e^o] = 0.900 \quad \pm 0.007$$

$$\alpha_l \quad = 0.00246 \pm 0.00022 \text{ at } 10^{-3} \text{ mm Hg and } 20^\circ \text{ C}$$

Reducing all pressure dependent values in the equation for $\Delta\,\alpha_i$ to 10^{-3} mm Hg and 20° C, we find at last:

$$\alpha_i = (0.00209 \pm 0.00021) \text{ cm}^{-1} \text{ or}$$

$$\sigma_i = (3.16 \pm 0.31) \times 10^{-17} \text{ cm}^2/\text{at}$$

In order to consider the reproducibility of the results some measurements were repeated under the same circumstances. We give our σ_c, σ_1 (taken with the short collector) and σ_i results in case of N^+, H_2 at 10 kV. The errors given represent standard deviations determined either by external or internal consistency which ever is larger.

	$\sigma_c \times 10^{-17}$cm²/at	$\sigma_1 \times 10^{-17}$cm²/at	$\sigma_i \times 10^{-17}$cm²/at
	36.0 ± 0.5	4.16 ± 0.09	2.91 ± 0.38
	34.0 ± 0.8	4.09 ± 0.28	3.16 ± 0.31
	33.4 ± 0.5	3.70 ± 0.14	
Average	34.6 ± 0.9	4.02 ± 0.14	3.05 ± 0.24

Besides the random errors, we mention several possible sources of systematic error, of which the following are probably the most important:

A. Monitor current correction.

Having realized a good correspondence between the calculated and experimental monitor correction in case of the combination N^+, H_2 at 10 keV (see § 4.6 section B), we estimate the correction generally accurate within 2% at the highest pressures used. At these pressures the deviation of 2% will mainly influence the $[n_e^+]$ values so that we may expect a corresponding systematic error of about 2% in our α_1 or σ_1 value. As a consequence of this error in α_1, which probability is used in the calculation of α_i or σ_i, we estimate the systematic error in the latter quantity to be at least as large as 2%.

B. Mc Leod gauge calibration and surface tension effect.

The Mc Leod gauge was calibrated by measuring the volumes of its bulb and capillary. The experimental error in the calibration was less than one percent. Since an error in the Mc Leod gauge calibration effects all the measured cross-sections by the same

percentage, this means that it causes a systematic error in the cross-sections smaller than one percent. However there are indications that due to variations of the surface tension by unknown reasons systematic errors in the pressure determination can occur of a few percents.

C. The scattering of beam particles over "large" angles.

In § 4.1 we have remarked that the opening angle of our short collector amounts to 2.7°. If the scattering occurs over larger angles than 2.7°, equation (2.1.4) is no more valid for the short collector. The scattering causes that $[n_c^+]$ is calculated too small, so that we can understand from (2.1.7) that in this case we find α_1 or σ_1 smaller, α_c or σ_c larger than their real values.

We have carried out different measurements for the combination N^+, H_2 at 10 kV, from which we have deduced that in this case the scattering over large angles influences the results to a negligible extent (see our comparison of the cross-sections obtained with the short and long collector in § 4.1, our comparison of the capture cross-sections obtained with different methods in § 4.3 and our explanation of fig. 4.5 in § 4.4).

D. The reflection of beam particles at P_3 out of the collector space.

Particles reflected out of the collector space can pass the side electrodes for a second time and participate in the collision processes anew. As a consequence of this we will have systematic errors in our capture cross-section determined at low pressures (§ 4.2) and in our ionization cross-sections (§ 4.4), getting larger values than the real cross-sections. We can not predict the influence on the capture and loss cross-section obtained by the combined method (§ 4.1). This depends on the pressure dependence of the reflection at P_3.

From different measurements it seems that in case of N^+, H_2 at 10 kV the influence of reflection on the cross-section results is negligible (see our remark in § 4.5 that the reflection currents at S_5 and C_7 are in the order of pro milles with respect to the vacuum collector current and our explanation of fig. 4.5 in § 4.4).

The total estimated systematic error.

We can not predict in general the influence of scattering and reflection for different combinations on the systematic error. This has to be considered for the different cases apart. It seems that their influence in case of N^+, H_2 is negligible (see section C and D).

The systematic error in the capture cross-section is mainly determined by the error discussed in section B and we estimate it to be smaller than 4%.

The systematic error in the loss cross-section will be larger as a consequence of the error in section A, so that it may be 6% large or smaller. From our method of evaluation of the ionization cross-section it follows that the systematic error in this will also be of the order of 6%, but can be larger.

Chapter V.

GENERAL SURVEY AND DISCUSSION OF OUR EXPERIMENTAL RESULTS.

§ 5.1. Introduction.

We have shot many ions into hydrogen gas and determined the capture, loss and ionization cross-sections for these combinations in the energy range 2—25 keV. Intentionally we have started these experiments with a light atom in the collision chamber to avoid the scattering effect. Later on we have taken some other ion-gas combinations at one acceleration voltage in order to compare our measurements with those of other observers. In the next paragraph we shall give our results, which are calculated by means of our methods explained in chapter IV.

§ 5.2. Results.

We have given our results in different graphs followed by corresponding tables of cross-sections. In these graphs we plot our capture and loss cross-sections taken with the short collector (see § 4.1), our capture cross-sections found with the method of Stedeford[S2] (see § 4.2) and our ionization cross-sections for the beam in its equilibrium state (see § 4.4) and we compare them with the available results of other observers. We did not find a remarkable change of the cross-section in any combination when we altered the arc tension in the ion source from 100 to 200 V so that we plot the values with different arc tensions together. The ion-gas combinations with one acceleration voltage are only given in a table. We give the mean square root error in the cross-sections (see § 4.7) only in case of the combination N^+, H_2. Generally the mean square root errors in the other combinations are of the same order of magnitude, that is about 3% for σ_c, 6% for σ_l and 8% for σ_i. Systemetic errors have already been discussed in § 4.7.

We summarize the symbols used in the following tables and graphs:

Symbols used in the tables:

kV acceleration voltage of the ions;

$\sqrt{eV}$ square root of the energy of these ions;

σ_c^s capture cross-section determined with the short collector;

σ_l^s loss cross-section determined with the short collector;

$w^s = \sigma_l^s/\sigma_c^s$;

σ_c^* capture cross-section determined with the method of Stedeford;

σ_i ionization cross-section for the beam in its equilibrium state;

σ_c^l capture cross-section determined with the long collector;

σ_l^l loss cross-section determined with the long collector;

$w^l = \sigma_l^l/\sigma_c^l$;

σ_i^+ and σ_i^0 ionization cross-sections for ions and neutrals.

All the cross-sections are given in units 10^{-17} cm^2/at.

In table 5.1 we have written some cross-section dates with an index number; for example with index ④ we indicate that the value is determined four times under the same circumstances. In this case we give the average of the four dates and the corresponding standard deviation. In case of only one cross-section determination we give the mean square root error in the observations leading to this cross-section (see § 4.7).

Symbols used in the graphs

$\sigma_c \rightarrow \square$; $\sigma_c^* \rightarrow \blacksquare$; $\sigma_l \rightarrow \bullet$; σ_i^+, σ_i^0 or $\sigma_i \rightarrow$ o

H_c, H_l and H_i correspond respectively to capture, loss and ionization cross-sections of our own group.

G_c, Ha_c, St_c and W_c correspond respectively to capture cross-sections of Gilbody, Hasted, Stedeford and Wolf. The dates of Gilbody and some of Hasted were obtained by private communication. W_{i+} corresponds to the ionization cross-section of positive ions in case of Wolf's experiments.

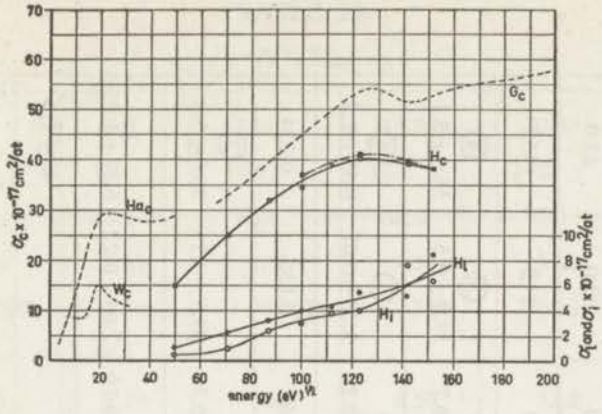

Fig. 5.1.
Cross-sections for the combination N^+, H_2.

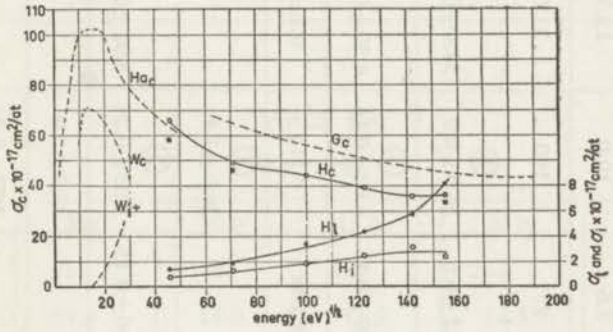

Fig. 5.2.
Cross-sections for the combination A^+, H_2.

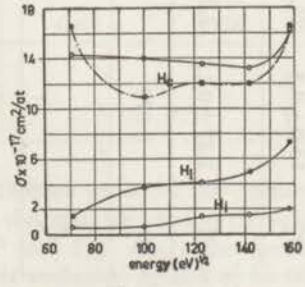

Fig. 5.3.
Cross-sections for the combination Kr^+, H_2.

TABLE 5.1.

N^+, H_2.

kV	2.5	5.0	7.6	10.0	12.5	15.0	20.0	23.0
$\sqrt{eV}$	50	71	87	100	112	123	142	152
σ_c^s	15.0±0.3	24.8±0.6	32.2±0.6	③ 34.6±0.9	38.9±0.8	④ 40.4±0.7	③ 38.8±0.5	④ 36.6±5.1
σ_i^s	1.17±0.12	2.26±0.10	3.30±0.15	③ 4.02±0.14	4.39±0.13	④ 5.50±0.22	③ 5.28±0.07	④ 8.55±1.2
w^s	0.078	0.091	0.103	0.115	0.113	0.136	0.136	0.234
σ_c^*				② 36.6±1.4		41.2±0.7	39.6±0.5	② 36.6±6.6
σ_i	0.55±0.13	1.03±0.10	2.46±0.15	② 3.05±0.24	3.92±0.19	4.08±0.19	7.65±0.22	6.37±1.05
σ_c^l				33.7±2.0				48±1.3
σ_i^l				3.77±0.34				6.04±0.67
w^l				0.111				0.126

TABLE 5.2.

A^+, H_2.

kV	2.1	5.0	10.0	15.0	20.0	24.0
$\sqrt{eV}$	46	71	100	123	142	155
σ_c^s	66.0	48.8	43.8	38.5	35.3	36.1
σ_l^s	1.38	1.87	3.36	4.38	5.68	8.14
w^s	0.0209	0.0383	0.0767	0.114	0.161	0.225
σ_c^*	58.2	46.1				33.0
σ_i	0.70	1.24	1.85	2.50	3.12	2.38
σ_c^l		60.0			40.4	
σ_l^l		2.08			9.70	
w^l		0.0346			0.240	

TABLE 5.3.

Kr^+, H_2.

kV	5.0	10.0	15.0	20.0	25.0
$\sqrt{eV}$	71	100	123	142	158
σ_c^s	14.3	14.0	13.5	14.5	16.2
σ_l^s	1.53	3.73	4.17	5.00	7.29
w^s	0.107	0.266	0.309	0.344	0.450
σ_c^*	16.5	10.9	12.1	12.0	16.5
σ_i	0.61	0.62	1.38	1.50	2.03
σ_c^l	13.1				14.7
σ_l^l	1.39				7.34

Note: With the long collector we could not determine the equilibrium ratio in the beam. In this case we have to increase the gas pressure higher than 2×10^{-2} mm Hg where the measurements seem no more reliable. We have evaluated σ_c^l and σ_l^l by taking w^l equal to w^s.

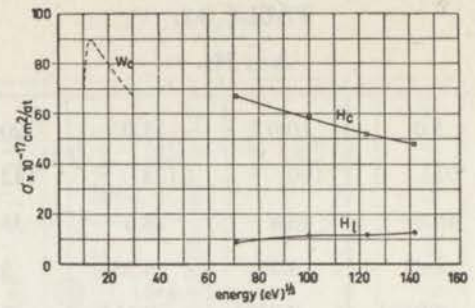

Fig. 5.4.

Cross-sections for the combination N_2^+, H_2.

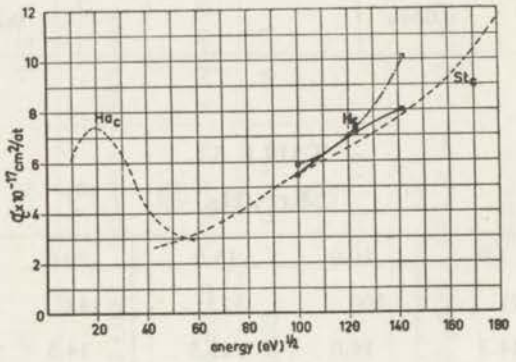

Fig. 5.5.

Capture cross-sections for the combination He^+, H_2.

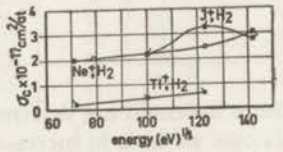

Fig. 5.6.

Capture cross-sections for three different combinations.

TABLE 5.4.

N_2^+, H_2.

kV	5.0	10.0	15.0	20.0
$\sqrt{eV}$	71	100	123	142
σ_c^s	66.9	58.5	52.1	47.6
σ_1^s	8.78	11.2	11.7	12.6
w^s	0.131	0.192	0.224	0.264

Note: In this combination incidentally we have only taken cross-section determinations with the short collector. Properly the method of Wien is not applicable to molecular ions. However, our curve of the collector ion intensity against the gas pressure shows an equilibrium value, so that the dissociation of N_2 seems rare. The dissociation is namely the reason that the formalism of Wien is no more applicable.

TABLE 5.5.

He^+, H_2.

kV	10.0	15.0	20.0
$\sqrt{eV}$	100	123	142
σ_c^s	5.4	7.1	8.0
σ_c^*	5.85	7.26	10.1

Note: As in other combinations with small cross-sections we could not realize the equilibrium state in the beam. In order to calculate σ_c^s we estimate w^s from our experimental results and we find it roughly equal to 0.25 at the taken acceleration voltages. In this case we can not obtain a sufficiently accurate σ_1 value to determine σ_i from the ionization measurements.

TABLE 5.6[1].

Ne^+, H_2.

kV	5.0	6.2	15.0	20.0
$\sqrt{eV}$	71	79	123	142
σ_c^s		2.06	2.44	2.98
σ_c^*	1.98			3.06

TABLE 5.6[2].

J^+, H_2.

kV	10.0	15.0	20.0
$\sqrt{eV}$	100	123	142
σ_c^*	2.10	3.23	2.75

TABLE 5.6[3].

Tl^+, H_2.

kV	5.0	10.0	15.0
$\sqrt{eV}$	71	100	142
σ_c^*	0.26	0.44	0.66

Note: In these three combinations which have small cross-sections we could not realize the equilibrium state in the beam. In case of Ne^+, H_2 we estimate w^s equal to 0.1 in our energy region. The combination J^+, H_2 can not be treated with the formalism of Wien because of the formation of negative J^- ions. We have obtained the smallest capture cross-sections in case of Tl^+, H_2 as we can expect from theoretical considerations (see § 5.7).

TABLE 5.7.

Ions in argon gas at 10 kV acceleration voltage.

ion	He^+	N^+	Ne^+	A^+	Kr^+
σ_c^s	69.6	107	35.8	181	55.5
σ_l^s	5.78	21.2	6.46	26.4	16.1
w^s	0.083	0.198	0.181	0.146	0.290
σ_c^*	53.1	93.5	22.8	183	32.3
σ_l				24.6	

TABLE 5.8.

Ions in neon gas at 10 kV acceleration voltage.

ion	N^+	Ne^+	A^+	Kr^+
σ_c^s	4.30	79.0	6.72	11.4
σ_l^s		18.5		
w^s	0.7[1])	0.234	0.05[1])	0.3[1])
σ_c^*	2.30	86.5	1.40	2.80
σ_i		18.8		

[1]) They are estimated w^s values, the equilibrium state in the beam not being realized.

TABLE 5.9.

Some cross-section results, in our case taken at one acceleration voltage only, compared with those of other observers.

ion-gas combination	energy keV	observer	his cross-section values			our cross-section values		
			σ_c	σ_l	σ_c^*	σ_c	σ_l	σ_c^*
He^+, A	10	Stedeford			63	69.6		53.1
Ne^+, A	10	Gilbody			4.4	35.8		22.8
A^+, A	10	Gilbody			132	181	26.4	183
		Batho	84.3	5.4				
Ne^+, Ne	10	Gilbody			74	79.0	18.5	86.5
		Batho	37.4	5.5				
H_2^+, H_2	20	Stedeford			57			61
H^+, H_2	17.5	Stedeford			26	35.2	3.48	
		Keene			31			
		Bartels	39	9.7				

§ 5.3. Discussion of the results.

For the combinations N^+, H_2, A^+, H_2 and Kr^+, H_2 we have determined the capture and loss cross-section for both short and long collector (see § 5.2) at some energies. The agreement between σ_c^s and σ_c^l and between σ_l^s and σ_l^l is sometimes reasonable, of the order of 5%, but we find also differences of about 25% which is beyond the error limit. The experimental conditions are more favourable in a measurement with the short collector and we rely most on these results.

In the combinations with hydrogen where we have measured both σ_c and σ_c^* ; the agreement between the corresponding cross-sections is rather good, in many cases within 5%, so that we may conclude that in these cases the scattering over large angles influences the capture cross-section determination to a negligible extent (see § 4.3). However, in the ion-argon and ion-neon combinations we find σ_c^* much lower than σ_c^s, except in the symmetrical combinations A^+, A and Ne^+, Ne with large σ_c. We shall show in § 5.4 and § 5.5 that this difference is due to scattering over large angles. Its influence on the σ_c value will be relatively larger, if σ_c is smaller, as we see in case of the ion-neon combinations.

Our capture cross-section results agree in many cases rather well with those of the English group (Keene, Hasted, Stedeford and Gilbody). As we see from theoretical considerations in § 5.7 the determination is influenced by the presence of metastable ions in the beam and their share will vary in the different experiments. For this reason we think that the agreement in the capture cross-section for different combinations, varying from about 5% to 30%, is not too bad. As we see the tendency in the $\sigma_c - \sqrt{eV}$ curves is always the same and for example in N^+, H_2 a maximum in σ_c at 15 kV is found both by our group and Gilbody. Measurements of Wolf and Batho do not seem reliable.

As for loss and ionization not so much work is done by other observers and we can compare only a few of our results with other dates. For A^+, A and Ne^+, Ne the agreement with Batho in the σ_l value is bad. In our own experiment σ_l and σ_i nearly coincide in both combinations, just as one would expect.

§ 5.4. The disturbance by scattering.

In § 5.3 we have seen that in case of ion-argon and ion-neon combinations σ_c^* is often lower than σ_c^s. We shall show that this difference is due to scattering over large angles.

In fig. 5.7 we have given the pressure dependence of $[n^+] - [n^-]$ on C_7, R_7, C_8 for some ions in hydrogen and some ions in

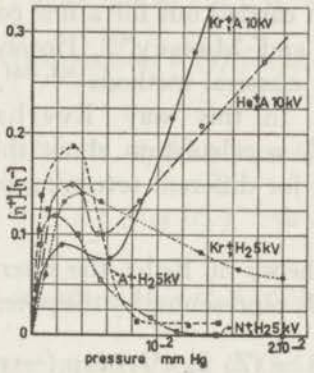

Fig. 5.7.
Pressure dependence of $[n^+] - [n^-]$ on C_7, R_7, C_8 in different ion-gas combinations.

argon (see also § 4.4). In hydrogen where we have generally found agreement between σ_c and σ_c^*, all curves give a low value of $[n^+] - [n^-]$ in the higher pressure region so that the disturbance by scattering on the cross-section measurement seems negligible. However in argon we have a remarkable rise of the value of $[n^+] - [n^-]$ in the higher pressure region and this effect can only be due to scattering. Having shown that the scattering over large angles is important in case of ion-argon combinations, we can expect that we find σ_c^s larger than σ_c^*, in agreement with the reality and the same seems to hold for the ion-neon combinations. In these ion-neon combinations we have small σ_c values so that the scattering effect is relatively much larger.

If we have an important disturbance by scattering we can rely more on our σ_c^* than on our σ_c values; w, σ_l and σ_i are still more effected by the scattering, so that they may differ much from their real values. Notwithstanding it is remarkable that for the symmetrical combinations Ne^+, Ne and A^+, A, σ_l^s and σ_i are close together.

§ 5.5. Theoretical interpretation of the disturbing scattering.

From our experience about scattering shown in § 5.4, it is clear that the geometry of the electrode system to be chosen, depends on the disturbance by scattering. For this reason one ought to calculate the angle distribution of the scattered particles for any taken combination before building the electrode system. Accurate calculations about these problems are very complicated. They have only been carried out for a few combinations and are described in Mott and Massey[M5]. However, one can obtain some information by classical methods [M4, M5], using the screening theory of Bohr[B5]. In this way Everhart[E1], Stone and Carbone have made a calculation about the differential cross-section for scattering for different screening parameters.

In the screening theory of Bohr the interaction between two atoms is approximately represented by the potential energy function

$$V(r) = (Z_1 Z_2 e^2/r) \exp(-r/a) \tag{5.5.1}$$

The first factor is the Coulomb potential energy function between two nuclei of charges $Z_1 e$ and $Z_2 e$. The exponential factor takes into account the electronic screening, whose extent is determined by the screening length a.

$$a = a_0/(Z_1^{2/3} + Z_2^{2/3})^{1/2} \qquad (a_0 = 0.53 \times 10^{-8} \text{ cm}) \tag{5.5.2}$$

Classical calculation of the differential cross-section is valid when:

a) the de Broglie wavelength λ of the incident particle is very small compared with the dimension of the scattering center.

b) the collision is well defined within the limitations of the uncertainty principle

$$\lambda = h/mv \tag{5.5.3}$$

in which m is the reduced mass of the system, and v the relative velocity of the collision. Condition a) requires that

$$\begin{cases} \lambda/2\pi < a \\ \lambda/2\pi < b \end{cases} \tag{5.5.4}$$

in which b is the distance of closest approach in a "head on" collision of the bare nuclei and it is given by

$$b = Z_1 Z_2 e^2/(\tfrac{1}{2} mv^2) \tag{5.5.5}$$

Condition b) leads to a lower limit on the scattering angle, namely

$$\begin{cases} \theta^* \sim \lambda/2\pi a \text{ or} \\ \theta^* \sim b/a = \zeta \text{ if } \zeta \ll 1 \end{cases} \tag{5.5.6}$$

The differential cross-section $\sigma(\theta)$ for scattering is calculated classically from

$$\sigma(\theta) = p/\sin\theta \,.\, dp/d\theta \text{ where} \tag{5.5.7}$$

$$\theta = \pi - 2\int_{r_0}^{\infty} (r\,\Phi(r))^{-1}\, dr \text{ and} \tag{5.5.8}$$

$$\Phi(r) = \{r^2/p^2 - 1 - r^2 V(r)/\tfrac{1}{2} mv^2 p^2\}^{\frac{1}{2}} \tag{5.5.9}$$

Here r_0 is the largest positive root of (5.5.9).

By the classical method Everhart c.s. have evaluated the differential cross-section $\sigma(\theta)$ over b^2 as a function of θ for different screening parameters b/a. The results have been plot in a graph. Deducing integral cross-section curves from the differential cross-section curves and transforming these curves from the relative coordinate system into the laboratory coordinate system, we are able to make estimations about the scattering in our own combinations. For example with a collector of opening angle 3°, we want to know the integral scattering cross-section for scattering over angles larger than 3°.

Though our calculations about these problems are in a preliminary state, we shall give some of our results. We shall consider some interesting examples:

A. H, H_2 at 10 keV or $v = 1.39 \times 10^8$ cm/sec.

Taking H_2 as an atom with $Z_2 = 2$ and $m_2 = 2$ atomic units we calculate that

$$\begin{cases} b = 4.32 \times 10^{-11} \text{ cm} \\ a = 3.30 \times 10^{-9} \text{ cm} \end{cases} \quad \zeta = b/a = 0.013$$

Bohr shows that in case of $\zeta \ll 1$, we can use the classical Rutherford scattering for angles larger than ζ radials. Here $\zeta = 0.013$ radials $\sim 0.8°$. The Rutherford scattering is pronounced over small angles and given by

$$\sigma(\theta) = b^2/16 \,.\, \mathrm{cosec}^4\, \theta/2. \tag{5.5.10}$$

By integration we find an integral scattering cross-section between θ_2 and θ_1 given by

$$Q_{\theta_1}^{\theta_2} = 2\pi \int_{\theta_1}^{\theta_2} \sigma(\theta) \sin\theta \, d\theta = \left[\pi b^2/4 \,.\, \sin^{-2}(\theta/2)\right]_{\theta_2}^{\theta_1} \tag{5.5.11}$$

In this way we find for scattering over angles larger than $\theta = 4°$

$$Q(\theta > 4°) = 1.2 \times 10^{-18}\ \mathrm{cm^2/mol} = 0.6 \times 10^{-18}\ \mathrm{cm^2/at}$$

If the angle Φ in the laboratory system corresponds with the angle θ in the relative coordinate system, we have the following relation:

$$\mathrm{tg}\, \Phi = \frac{\sin\theta}{\cos\theta + m_1/m_2} \tag{5.5.12}$$

where m_1 is the mass of the fast particle and m_2 the mass of the gas particle. In this example we find that for $\theta = 4°$, $\Phi \sim 3°$ so that with an opening angle of 3° in our collector one will obtain a negligible disturbance by scattering, $Q(\Phi > 3°)$ being equal to 0.6×10^{-18} cm²/at. This result is in agreement with capture and loss cross-section experiments done with H^+, H_2 by different observers, which experiments do not show a scattering effect.

B. Tl, H_2 at 10 keV or $v = 9.7 \times 10^6$ cm/sec.

This example forms an extreme contrast with the Rutherford scattering, which is pronounced over small angles and decreases rapidly with increasing angle. This combination has an uniform scattering over large angles in the relative coordinate system. We calculate that

$$\begin{cases} b = 2.40 \times 10^{-7}\ \mathrm{cm} \\ a = 1.19 \times 10^{-9}\ \mathrm{cm} \end{cases} \quad \zeta = b/a = 202$$

We have a case with very large screening parameter, the colliding atoms will not be able to penetrate each other and the best approximation is obtained by the hard sphere model, worked out by Massey and Burhop. We give their result:

$$\begin{cases} \sigma(\theta) = {}^1/_4\,\varrho^2\,\{k^2\varrho^2 - (k^2\varrho^2 - 1)\,(k\varrho\,\theta/\pi)\} & \text{for } \theta < \pi/k\varrho \\ \sigma(\theta) = {}^1/_4\,\varrho^2 & \text{for } \theta > \pi/k\varrho \end{cases} \qquad (5.5.13)$$

where $k = 1/\lambda$ and (ϱ is the sum of the radii of the two colliding particles, of the order 10^{-8} cm). With rough approximation Massey and Burhop find by integration $Q^{\pi}_{\pi/k\varrho} \sim \pi\varrho^2$ and $Q^{\pi/k\varrho}_{o} \sim \pi\varrho^2$ ($\pi\varrho^2 \sim 30 \times 10^{-17}$ cm^2/mol).

In our example $\lambda/2\pi = 3.18 \times 10^{-13}$ cm and we calculate $\theta = \pi/k\varrho \sim (10^{-3})^{\circ}$. Generally an uniform scattering as in this example for angles larger than $\theta = \pi/k\varrho$ is very unfavourable in our experiment. However, having a heavy primary particle with respect to the gas particle, the maximum angle of scattering in the laboratory coordinate system is given by

$$\sin \Phi_{max} = m_2/m_1 = 1/102 \qquad (5.5.14)$$

and we obtain $\Phi_{max} \sim 0.6^{\circ}$ so that with an opening angle of 3° in our collector we will obtain a negligible disturbance by scattering.

C. Classical scattering in different combinations.

In table 5.10 (page 98) we give our results for integral scattering which we have obtained by making use of the dates calculated by Everhart c.s. In this table we have also included H^+, H_2 and Tl^+, H_2, just discussed in section A and B. In our beam we have both ions and atoms, but the screening theory describes the interaction between two atoms. We assume that the ions are scattered in the same way as the atoms, which will be approximately true if many screening electrons are present.

In column II of table 5.10 we have given the screening parameter ζ for different combinations at 10 keV. With larger ζ the frequency of small angle deflections will be less pronounced and the scattering may approach a spherical symmetrical angular distribution in the relative coordinate system. In column III we have changed the energy in some combinations in such a way that we obtain corresponding values of ζ for which Everhart c.s. have determined

TABLE 5.10.

Estimations about some integral cross-sections for classical scattering.

I	II	III	IV	V	VI	VII
Combination	$b/a = \zeta$ at 10keV	energy in keV	ζ	$Q(\theta > 3°)$ in 10^{-17} cm²/mol	θ if $\Phi = 3°$	$Q(\Phi > 3°)$ in 10^{-17} cm²/mol
He^+, A	0.31	6	0.5	6.6	3°	6.6
Kr^+, A	23	23	10	10	9°	5.9
H^+, H_2	0.013	10	0.013	0.21	4°	0.12
N^+, H_2	0.70	7	1	9.5	25°	1.8
A^+, H_2	5.9	12	5	18	90° ($\Phi_{max} \sim 3°$)	0
Kr^+, H_2	29	29	10	15	— ($\Phi_{max} \sim 1^1/_2°$)	0
Tl^+, H_2	202	10	202	30	— ($\Phi_{max} \sim 0.6°$)	0

the differential cross-section curves for scattering. In column V we have given the integral cross-section for scattering over angles larger than $\theta = 3°$. However, as for the collector we are interested in the scattering over angles larger than $\Phi = 3°$. Therefore we determine the corresponding angle θ in the relative coordinate system by using (5.5.12) for every combination. For example if we take Kr^+, H_2 we have $\theta = 9°$ if $\Phi = 3°$. From our integral cross-section curve for scattering in the relative coordinate system we read $Q(\theta > 9°)$ and this is equal to $Q(\Phi > 3°)$ in column VII. For Kr^+, H_2 and Tl^+, H_2 the maximum angle of scattering in the laboratory coordinate system is smaller than 3°, so that for these combinations $Q(\Phi > 3°) = 0$. The same is true for A^+, H_2 with $\Phi_{max} \sim 3°$. In practice the effective integral cross-section will be smaller than found in column VII, because the beam, on its way to the collector, approaches it with an increasing opening angle. Comparing the dates with the experimental results in fig. 5.7, we see that the disturbance by scattering experimentally found in He^+, A and Kr^+, A corresponds to the combinations with the largest integral cross-section $Q(\Phi > 3°)$ in table 5.10, including all combinations of fig. 5.7.

The considerations about scattering, given here, are incomplete, neglecting for example multiple scattering effects. However we have shown the importance of scattering in these experiments and have given indications for the solution of the problem.

§ 5.6. The adiabatic hypothesis.

We shall apply the so-called adiabatic hypothesis (see Massey[M4] and Burhop) in order to give a theoretical interpretation of our results and therefore we first discuss its principle. As an example we consider the capture process

$$N^+ + A \rightarrow N + A^+ - 1.22 \text{ eV}.$$

In this case the internal energy exchange, ΔE, amounts to 1.22 eV. This is the difference of the ionization energies of N and A, respectively 14.54 eV and 15.76 eV. We suppose that the capture electron can be present in two energy states. One level corresponds to the state N^+, A, the other to the state N, A^+. By applying the correspondence principle the transition of the electron corresponds with a so-called transition frequency ν, equal to $\Delta E/h$, where h is the constant of Planck. We define a corresponding time of vibration given by $t = 1/\nu = h/\Delta E$. We first consider a collision with a gradual character, in which the two particles are approaching each other with a velocity very small compared with that of the atomic electrons. The latter have therefore plenty of time to readjust themselves to the slowly changing conditions without a transition taking place. We say that this impact is nearly adiabatic. Slow velocity of the atoms corresponds with a large collision time τ. This time τ is of the order a/v, where a is the range of interaction between the particles and v their relative velocity. In our example the condition for weak capture becomes $\tau \gg t$ or $a/v \times \Delta E/h \gg 1$.

In case of $\tau < t$ the relative velocity is so large or the collision time τ so small, that the particles have little time to disturb each other and we find ourselves in a region where the capture probability decreases with increase of the relative velocity. Between the two regions mentioned where $\tau \sim t$ we may expect a so-called resonance maximum and we write in this case

$$a/v \times \Delta E/h \sim 1$$

We have taken ΔE as the internal energy exchange in a capture process, but the consideration is similar for every excitation process.

A special case of resonance is that where $\Delta E = 0$ being realized in the example

$$A^+ + A \rightarrow A + A^+$$

Here we have a case of so-called exact resonance where a maximum capture occurs at zero velocity or energy and where the capture decreases constantly with increasing energy.

§ 5.7. Interpretation of our results with the adiabatic hypothesis.

In order to apply this theory to our results, we assume that the resonance maximum is given by $a/v \times \Delta E/h = 1$ and replacing v by $\sqrt{2eV/m}$ we change this equation into:

$$a = (h/\Delta E)\ (eV_{max}/150\ M)^{\frac{1}{2}} = 0.57 \times 10^{-8} \sqrt{V_{max}}/\Delta E\sqrt{M}$$

V_{max} is the acceleration voltage of the ions at which the maximum cross-section occurs, given in volts; ΔE is the internal energy exchange in eV and M is the mass of the accelerated ion in atomic units.

Hasted[H4] and his group have determined a for many ion-gas combinations by measuring V_{max} for the corresponding capture process and they have plot the results in a graph, giving the relation between V_{max} and $\Delta E\sqrt{M}$. They get a so-called adiabatic straight line for which we deduce the adiabatic relation.

$$\log \sqrt{V_{max}} = 1.09 + 1.01 \log \Delta E\sqrt{M}$$

so that we can find that on the average a is near 7.2×10^{-8} cm in our energy region.

Near the end of this paragraph we have given V_{max} and a $\Delta E/hv$ at 10 kV, calculated for the capture, loss and ionization cross-sections of different ion-gas combinations (table 5.11 and 5.12), making use of the adiabatic relation. The excitation energies corresponding to different atomic and molecular states in table 5.13 are needed for the evaluation of ΔE.

We shall now discuss our experimental curves.

A. The interpretation of σ_c—$eV^{1/2}$ curves.

1. N^+, H_2: In this case $\Delta E = -0.94$ eV and omitting the negative sign we obtain $\Delta E\sqrt{M} = 3.52$. We deduce from the adiabatic relation that $V_{max} = 1.9$ kV. Both Hasted and Wolf find a maximum in the low energy region near 0.53 kV, so that there is a small deviation with the estimated acceleration voltage where the maximum occurs. However, the maximum cross-section has a rather low value in comparison with many other obtained resonance maxima and a second maximum arises both in our and Gilbody's curve at $\sqrt{V_{max}} = 123$ or $V_{max} = 15$ kV. This maximum can not be explained with a transition energy of —0.94 eV. A more critical study shows that the second maximum may arise from metastable N^+ ions in the beam entering the collision chamber. They may be in the $^1S_0$ state, $\Delta E = 3.12$ eV and we calculate $V_{max} = 21$ kV, not far from the experimental maximum. The transition may even be more complicated, the metastable ions changing after capture into excited N atoms. In this case the following reactions are important:

$$N^{+\prime}\,(^1D_2) + H_2 \rightarrow N'\,(^2P^o_{1/2,\,1\,1/2}) + H_2^+ - 2.61\text{ eV with } V_{max} = 16\text{ kV and}$$

$$N^+ + H_2 \rightarrow N'\,(^2D^o_{1\,1/2,\,2\,1/2}) + H_2^+ - 3.32\text{ eV with } V_{max} = 24\text{ kV}.$$

From our results in the combination N^+, Ne it seems that the metastable part of the beam consists mainly of $N^{+\prime}$ ($^1D_2$) ions (see number eight of this section).

After the explanation of one example we can understand that the difference between the absolute values of the capture cross-sections of different observers can partly be due to a different share of metastables in the primary ion beam. This share is dependent on the situation in the ion source and the path length between ion-source and collision chamber if the time of flight is of the same order of magnitude as the lifetime of a metastable ion. The lifetime varies from about 10^{-5} — 10^{-2} second while the time of flight lies between $3 \times$ to 0.3×10^{-5} sec (the path length in the separator is about 3 meter). These factors differ in each experimental arrangement and may explain many discrepancies.

2. A^+, H_2: A resonance maximum is found by Hasted and Wolf near 0.23 kV. This maximum corresponds to a transition between the ground states of ions and atoms, where we have $\Delta E = 0.28$ eV and we find $V_{max} = 0.48$ kV near the experimental value.

3. N_2^+, H_2: In the same manner as in the last combination we have $\Delta E = 0.16$ eV, we calculate $V_{max} = 0.11$ kV, which is not far from the experimental maximum of Wolf at 0.17 kV.

4. Kr^+, H_2: This is our second example where the metastable ions in the beam play an important part. The transition between ground states corresponds with $\Delta E = -1.48$ eV, $V_{max} = 29$ kV. If metastable $Kr^{+'}$ ($^2P_{½}$) ions are present we have $\Delta E = -0.82$ eV, $V_{max} = 9.0$ kV. Our $\sigma_c - eV^{½}$ curve does not show a maximum in the energy range 5—25 kV, but the rather flat form of the curve can be explained very well with the two different maxima.

5. He^+, H_2: The low energy maximum obtained by Hasted[H2)], is explained by him with the formation of a H_2^+ ion into an excited state. Such cases with molecular excitation are generally complicated and need both more experimental and theoretical investigation.

6. Tl^+, H_2, J^+, H_2 and Ne^+, H_2: With Tl^+, H_2 we find ourselves in the adiabatic region. We have a large $\Delta E = 9.37$ eV and a large atomic mass $M = 204$, so that $\Delta E\sqrt{M} = 134$ is large in comparison with preceding values. We find $V_{max} = 2900$ kV, so that we are far below the resonance energy and only a few capture transitions occur, in accordance with the very low σ_c values obtained by us. In Ne^+, H_2 and J^+, H_2 our energy region is also below the resonance energy, being respectively equal to 120 kV and 500 kV and we find corresponding low experimental σ_c values.

7. Ions in argon: Generally we may expect that the capture cross-sections in the ion-hydrogen and ion-argon combinations are of the same order of magnitude if we have the same primary ion, because the ionization energy of A and H_2 does not differ much (see table 5.13) and the same holds for ΔE. In order to compare the capture cross-section in the molecular gas H_2 with that in the atomic gas A, we must multiply the first by two because we have given everywhere the cross-section per gas atom.

In table 5.11 we see that nitrogen and krypton ions give in both gases capture cross-sections of the same order of magnitude,

TABLE 5.11.

V_{max} and a $\Delta E/hv$ at 10 kV, calculated for the capture cross-sections of different ion-gas combinations.

combination	ΔE in eV	$\Delta E\sqrt{M}$	V_{max} in kV	a $\Delta E/hv$ at 10kV	σ_c at 10kV in 10^{-17} cm²/at	σ_c^* at 10kV in 10^{-17} cm²/at
He^+, H_2	9.10	18.2	53	2.30	5.4	5.85
N^+, H_2	—0.94	3.52	2.0	0.45		
$^1S_0$ $N^{+\prime}$, H_2	+3.12	11.7	19	1.48	34.5	36.6
$^1D_2$ $N^{+\prime}$, H_2	2.61 ($N'\,^2P^o_{1/2,3/2}$)	9.75	16	1.24		
N^+, H_2	—3.32($N'\,^2D^o_{3/2,5/2}$)	12.4	24	1.55		
A^+, H_2	0.28	1.77	0.48	0.22	43.8	
Kr^+, H_2	—1.48	13.6	29	1.70	14.0	10.9
$^2P_{1/2}$ $Kr^{+\prime}$, H_2	—0.82	7.52	9.0	0.95		
J^+, H_2	10.44	57.0	500	7.10		2.10
Tl^+, H_2	6.11	134	2900	17.0		0.44
He^+, A	8.82	17.6	50	2.23	69.6	53.1
He^+, A	—4.6 ($A^{+\prime}\,^2S_{1/2}$)	—9.2	13	1.16		
N^+, A [1]	—1.22	4.55	33	0.57	107	93.5
$^1S_0$ $N^{+\prime}$, A	2.84	10.6	18	1.34		
Ne^+, A	6.20	27.8	130	3.60	35.8	22.8
Kr^+, A	—1.76	16.1	40	2.02	55.5	32.3
$^2P_{1/2}$ $Kr^{+\prime}$, A	—1.10	10.1	16	1.28		
N^+, Ne [1]	—7.02	26.2	110	3.32	4.30	2.30
$^1S_0$ $N^{+\prime}$, Ne	—2.96	11.1	20	1.40		
A^+, Ne	—5.80	36.6	220	4.70	6.72	1.40
Kr^+, Ne	—7.56	69.5	790	8.90	11.4	2.80
$^2P_{1/2}$ $Kr^{+\prime}$, Ne	—6.90	63.2	640	8.00		

[1]) Note: In the combinations N^+, A and N^+, Ne we have only taken the metastable $^1S_0$ state in the N^+ ion.

but with He^+ ions σ_c for He^+, A is much larger than for He^+, H_2. A metastable state in He^+ should effect both combinations in the same sense, so that the explanation must be found in argon. More critical study shows that an argon ion can be formed in the excited $^2S_{1/2}$ state, with $\Delta E = -4.6$ eV, responsible for a high capture cross-section. Such an explanation is also given by Hasted[H2].

Our large σ_c value for Ne^+, A can not be explained with the adiabatic theory and is not in agreement with Gilbody (§ 5.2).

8. Ions in neon: The examples with neon gas generally have a large ΔE so that at 10 kV acceleration voltage we are far below V_{max} and we may expect small capture cross-sections in agreement with the experiments. We have one exception in case of nitrogen where the maximum due to $N^{+'}$ ($^1S_0$) metastables is predicted at 19 kV. However, we find a very low capture cross-section in this case, so that the metastable part of the beam will mainly consist of $N^{+'}$ ($^1D_2$) ions (see number one of this section). For these ions $V_{max} = 63$ kV.

B. The interpretation of $\sigma_l - eV^{1/2}$ and $\sigma_i - eV^{1/2}$ curves.

In our energy region many loss and ionization cross-sections are small in comparison to the corresponding capture cross-sections and this is explained as follows: If we take for example the combination A^+, H_2, the ionization energy of H_2 represents the internal energy exchange if the ionization process is considered and we have always $|\Delta E_{ion.}| > |\Delta E_{capt.}|$ if $\Delta E_{capt.}$ corresponds to charge transfer between the ground states. In case of A^+, H_2 we have $\Delta E_{ion.} = -15.48$ eV and calculate $V_{max} = 1540$ kV (table 5.12), while we have found for the capture process with $\Delta E_{capt} = 0.28$ eV that $V_{max} = 0.53$ kV. In case of the ionization process we are far below the resonance energy so that the low ionization cross-sections experimentally found are in correspondence with the theory. If we calculate $a\Delta E/hv$ at 10 kV both for capture and ionization we find respectively 0.23 and 12.5, so that for capture we have passed the resonance energy, but for ionization we are more or less in the adiabatic region where few excitations occur.

Similar reasoning can be applied to the loss process, which is a kind of ionization. In our example $\Delta E_{loss} = 15.76$ eV and we calculate $V_{max} = 1600$ kV and $a\Delta E/hv$ at 10 kV is equal to 12.6 (table 5.12).

TABLE 5.12.

V_{max} and a $\Delta E/hv$ at 10 kV, calculated for the loss and ionization cross-sections of different ion-gas combinations.

combination	process	ΔE in eV	$\Delta E\sqrt{M}$	V_{max} in kV	a $\Delta E/hv$ at 10kV	σ_i or σ_l in 10^{-17} cm²/at at 10kV
N, H_2	ionization	15.48	58.0	540	7.4	3.04
	loss	14.54	54.4	476	6.9	3.98
A, H_2	ionization	15.48	98.0	1520	12.4	1.85
	loss	15.76	99.5	1590	12.6	3.36
Kr, H_2	ionization	15.48	142	3250	18.0	0.62
	loss	14.00	128	2650	16.3	3.73
Ne, Ne	ionization	21.56	96.5	1500	12.3	18.8
	loss	21.56	96.5	1500	12.3	18.5
A, A	ionization	15.76	99.5	1600	12.6	24.6
	loss	15.76	99.5	1600	12.6	26.4

TABLE 5.13.

Excitation energy for the formation of the ions and excited atoms.

Particle	Excitation energy in eV	Particle	Excitation energy in eV
H^+	13.60	N_2^+	15.64
H_2^+	15.48	Ne^+	21.56
He^+	24.58	A^+	15.76
N^+	14.54	$A^{+\prime}$ ($^2S_{1/2}$)	29.15
$N^{+\prime}$ ($^1S_0$)	18.60	Kr^+	14.00
$N^{+\prime}$ ($^1D_2$)	16.44	Kr^+ ($^2P_{1/2}$)	14.66
N' ($^2P^o_{1/2,3/2}$)	3.57	J^+	10.44
N' ($^2D^o_{3/2,5/2}$)	2.38	Tl^+	6.11

In table 5.12 we see that for N, H_2, A, H_2 and Kr, H_2 the ionization cross-section is smaller the larger the adiabatic parameter (>1) in agreement with the theory. However the corresponding loss cross-sections are about of the same magnitude indepently of this parameter.

The symmetrical combinations Ne, Ne and A, A show both an ionization and loss cross-section larger than twice the corresponding cross-section in case of ion-hydrogen combinations, even where these combinations have a smaller adiabatic parameter.

§ 5.8. Deviations from the adiabatic theory.

On ground of theoretical considerations one may expect deviations from the adiabatic theory. If we have

$$X^+ + Y = X + Y^+ + \Delta E$$

the adiabatic theory neglects the dependence of ΔE on the distance of the particles. We can understand that it is possible that ΔE is strongly dependent on distance r as given in fig. 5.8. We have taken $\Delta E_{minimum}$ equal to ΔU and the distance in which ΔE differs remarkably from $\Delta E_{asymptotic}$ (large r) equal to 1. If we have $\Delta U \ll \Delta E$ and l is of the same order of magnitude as a, then we may expect a strong deviation from the normal adiabatic character. In this case it is possible that $a\,\Delta E/h\nu \gg 1$ (normally corresponding to the adiabatic region), but that $l\,\Delta U/h\nu \sim 1$ so that an adiabatic region may not be present at all and we get a deviation from the normal adiabatic curve indicated in fig. 5.9

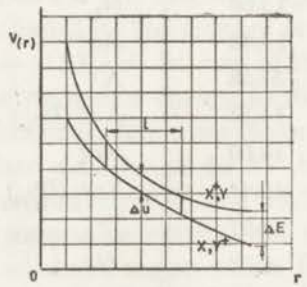

Fig. 5.8.
The potential curves for X^+, Y and X, Y^+ showing an energy difference dependent on r.

by the broken line. Such deviations are found by Hasted (private communication) for capture in the combinations A^+, Kr and C^+, Kr and are expected in some loss processes. In our measurements the loss cross-section in case of Kr, H_2 seems to show such a behaviour.

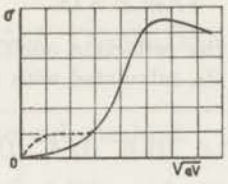

Fig. 5.9.
$\sigma - \sqrt{eV}$ curve with adiabatic deviation represented by the broken line.

§ 5.9. Secondary emission and reflection.

In order to determine the composition of the beam entering our collision chamber in vacuo, we determine the secondary emission of electrons at P_3 (§2.2 section B). In § 4.5 we have explained the determination of the secondary emission coefficient γ for N^+ ions on the copper electrode P_3. In table 5.14 we have given γ for different ions.

TABLE 5.14.

The secondary emission coefficient γ for ions on copper electrode P_3.

kV	2.0	2.5	5.0	6.2	7.6	10.0	12.5	15.0	17.5	20.0	24.0	25.0
H^+									3.1			
He^+						2.9				3.4		
N^+		1.5	2.0		2.8	3.4	3.1	3.5		4.1		
N_2^+			3.2			4.1		4.6		5.5	6.7	
Ne^+			2.3	2.2		2.4		3.1		3.3		
A^+	0.96	2.3				3.3		3.9		4.5	4.8	
Kr^+			1.4			2.4		3.1		3.5		4.9
J^+						2.4		2.8		3.4		
Tl^+			0.75					2.1				

In § 4.5 we have proved the importance of the reflection of beam particles at P_3. In table 5.15 we give the limits between which R is lying for different ions on the copper electrode P_3, calculated with method a) in § 4.5 (see also method b)).

TABLE 5.15.

The limits between which the reflection coefficient R is lying for ions on copper electrode P_3, calculated with method a) in § 4.5.

kV	2.0	2.5	5.0	6.2	7.6	10.0	12.5	15.0	17.5	20.0	24.0	25.0
H^+									0.008			
									0.034			
He^+						0.017		0.017		0.009		
						0.064		0.051		0.041		
N^+		0.041	0.046		0.045	0.035	0.042	0.043		0.036		
		0.10	0.14		0.17	0.16	0.17	0.19		0.18		
N_2^+			0.042			0.049		0.050		0.050	0.048	
			0.18			0.25		0.28		0.32	0.37	
Ne^+				0.049		0.058		0.059		0.055		
				0.15		0.20		0.24		0.24		
A^+	0.038		0.051			0.051		0.064		0.065	0.080	
	0.075		0.16			0.27		0.31		0.33	0.45	
Kr^+			0.046			0.064		0.072		0.066		0.057
			0.11			0.22		0.29		0.29		0.34
J^+						0.078		0.086		0.087		
						0.26		0.33		0.38		
Tl^+			0.052					0.075				
			0.091					0.23				

Chapter VI.

CRITICAL CONSIDERATIONS.

§ 6.1. The experimental method.

By using the method of Wien for the combined capture and loss cross-section determination, we need a rather complicated mathematical formalism, so that much calculation work has to be done before obtaining the cross-section results. One can use this method only for positive single charged ions and atoms, where the formation of positive double charged or negative ions can be neglected. In our arrangement the loss cross-section is proportional to the number of ions in the equilibrium state of the beam (2.1.7 and 2.1.2). This number becomes smaller if the scattering over large angles disturbs the measurement and this process may cause a large error in the determination of the loss cross-section.

Stedeford [S2] has applied a much simpler method for the determination of the capture cross-section (§ 1.2). We have used this method as a control on the combined capture and loss cross-section measurement. In this case one can also use double charged ions and molecular ions. One works with a lower gas pressure and a shorter gas length, which is preferable from a point of view of the disturbing scattering. However, one obtains only the capture cross-section. The loss cross-section can now be deduced from the equilibrium state in the beam. This state is sometimes determined by magnetic or electrostatic analysis of the beam which has passed the collision chamber. A detector must be found giving the same response on ions and neutrals. In this respect good results are obtained with a thermo-couple by some coworkers of Allison [A1] and by Stier [S4], Barnett and Evans (§ 1.2). The scattering will not disturb these measurements if ions and neutrals are scattered in the same extent. From the screening theory of Bohr [B5] as well as from these experiments this condition seems approximately realized.

Our ionization cross-section determination corresponds with that of Keene[K1]. At low pressures one can determine the ionization cross-section for positive ions. In this case the mathematical formalism is very simple. We have also taken higher pressures where neutrals are present in the beam so that we get a combination of the ionization by ions and atoms. Deriving the ionization from the saturation electron currents we must take into account electrons from the loss process. The mathematical formalism used to calculate the ionization cross-section for ions and atoms apart is complicated. In our experiment the ionization cross-section determinations with the equilibrium state in the beam are the most reliable. We have to refine our experimental conditions to find reliable ionization cross-section values for the ions and atoms apart.

§ 6.2. Experimental conditions.

For our definitive measurements we always used the isotope separator, having no analyzing magnet in our preparatory arrangement and so we could only make a run of measurements when the production of isotopes stopped. It is necessary to add a magnet in the preparatory arrangement so that we can carry out cross-section measurements independently of the separator.

Our energy range is limited to a small region (2—25 keV) and from a theoretical point of view it should be interesting to go up to 100 keV or 200 keV.

The construction of the apparatus can be improved so that it is simpler to change the structure of the electrode system. This can be done by mounting all the electrodes of the collision chamber on an end flange so that they are taken out off the apparatus together. Our insulated attachment of these electrodes must be changed, either by means of glass joints or by an other design.

In connection with scattering and reflection effects it is preferable to use a more closed electrode system for the collector. This is done in Stedeford's[S2] case by connecting the side electrodes of the collector by micalex plates which are covered with colloidal graphite. These plates have a resistance of $\frac{1}{2}$ MΩ.

From experimental evidence it seems that better electron saturation currents will be obtained if no secondary emission of electrons occurs on the frame of the transparent grids. These grids are used to suppress the secondary emission of electrons on a side electrode,

caused by the slow positive ions which are accelerated to this electrode (see § 2.4 section B_1). To improve the transparency of the grid as a whole, a guard ring construction has to be chosen in which the frame is partly located behind the guard rings.

The electronic detection on the collector can be made simpler by isolating the power supply and measuring the current on P_1, P_2, P_3 together. The same system can be applied for current measurements on the opposite side electrodes.

A balancing current measurement is preferable to the measurement of currents in the collision chamber and the monitor current apart.

The apparatus will give a cleaner high vacuum, if degassing by heating is possible.

The pressure fall between the collision and the vacuum chamber is low (a factor 15) so that we have to correct in our calculations for the collision processes in the vacuum chamber. This causes a lot of extra calculation work. We can improve the conditions by taking a pump of much higher capacity and by taking a smaller slit between the chambers. However, as a consequence of a smaller slit the currents are becoming smaller in the collision chamber.

We have chosen a slit with canal shape in order to increase the pressure fall. A slit of knife shape which has however less resistance for a flow of gas, seems more advicable. Not much is known about the charge exchange or reflection effects in the canal of the slit.

§ 6.3. Continuation and extension of the experiment.

In connection with the adiabatic theory and deviations from this theory it seems important to do more work about capture, loss and ionization, especially more accurate measurements about the two last processes. More attention has to be paid to the disturbance by scattering and by reflection in connection with the geometry of the electrode system. For the interpretation of the results it is desirable to work with a beam of fast ions without metastable states.

Molecular cases can be more seriously investigated. When an atomic ion is shot into a molecular gas, a mass-spectromatric analysis can be made of the formed gas particles. In this manner one gets information about the dissociation of the gas.

If the primary beam is molecular, the dissociation of the beam

particles can be determined by analyzing the beam which has passed the collision chamber.

In our laboratory we are intending to make a spectroscopic study of the different collision processes, in order to learn more about the excitation processes in the collision chamber. Not much work is done in this region and the last experiments about this subject date from about 1940.

SAMENVATTING.

In dit proefschrift worden de verschillende botsingsverschijnselen onderzocht, welke plaats hebben in de vacuum ruimte van de Amsterdamse electromagnetische isotopen separator. Deze verschijnselen zijn van grote invloed op het produktie proces van isotopen. Bij onze onderzoekingen welke in het energie gebied 2—25 keV plaats hebben, beperken we ons tot de zogenaamde ladingsoverdracht verschijnselen: vangst van electronen waarbij het snelle ion een electron overneemt van het gasmolecuul en neutraal wordt, verlies van electronen waarbij het snelle atoom bij botsing met een gasmolecuul een electron verliest en ionisatie van de gasmoleculen hetzij door snelle ionen of atomen. Wij bepalen voor deze processen de waarschijnlijkheid dat zij over de afstand van één centimeter plaats vinden, α, of de werkzame doorsneden per atoom, σ, waarbij $\alpha = N\sigma$ als N het aantal atomen voorstelt per cc gas.

Wij hebben een apparaat geconstrueerd om deze verschijnselen te onderzoeken, welke ook een belangrijke invloed hebben op het remmend vermogen van een gas. Het onderzoek vormt een onderdeel van het research programma van de Stichting voor Fundamenteel Onderzoek der Materie en werd mogelijk gemaakt door de financiële steun van de Nederlandse Organisatie voor Zuiver Wetenschappelijk Onderzoek en van de Philips Gloeilampen Fabrieken in Eindhoven.

In hoofdstuk I wordt een beknopt overzicht gegeven van de methoden welke gebruikt worden om de vangst, verlies en ionisatie doorsneden te bepalen en in een literatuur overzicht worden de belangrijkste onderzoekers genoemd.

Wij passen zelf de methode van Wien toe in een gewijzigde experimentele vorm, om een gecombineerde vangst en verlies doorsnede bepaling uit te kunnen voeren. Onze ionisatie doorsnede bepaling geschiedt min of meer op dezelfde wijze als bij Keene, terwijl we tevens in staat zijn de werkwijze van Stedeford voor

de bepaling van de vangst doorsnede te gebruiken als een controle op de methode van Wien.

In hoofdstuk II wordt het mathematisch formalisme besproken, dat wij voor de uitwerking van onze metingen gebruiken. Tevens worden de experimentele methoden schematisch aangegeven.

De gecombineerde bepaling van de vangst en verlies doorsnede verloopt als volgt: De bundel, die de botsingskamer binnentreedt, bestaat bijna uitsluitend uit ionen. De botsingskamer wordt gevuld met een te kiezen gas en bij verschillende drukken meten wij de ionen stroom van de bundel op de collector, welke op zekere afstand van de intree spleet van deze kamer is opgesteld. Bij stijgende druk neemt de collector stroom af, want tengevolge van het vangst proces komen er meer neutralen in de bundel. Bij voldoende hoge druk verandert de collector stroom niet meer bij verdere druk verhoging. De bundel is in de evenwichtstoestand gekomen, waarbij het vangst en verlies proces even vaak optreden. Het mathematisch formalisme van Wien wordt gebruikt om uit deze bepalingen de vangst en verlies doorsneden te berekenen.

De bepaling van de ionisatie doorsnede bestaat uit de detectie van langzame electronen, gevormd in het gas. De verzadigingsstroom van electronen wordt verkregen met behulp van een spanningsveld tussen twee tegenover elkaar liggende electroden, welke geflankeerd zijn door schermplaten. Als wij bedenken dat electronen ook door het verlies proces gevormd worden, kunnen wij begrijpen dat het formalisme voor de berekening van de ionisatie doorsnede ingewikkeld is.

Zoals wij reeds opmerkten bepalen wij de vangst doorsnede ook met de methode van Stedeford, als controle op onze gebruikelijke werkwijze. Hierbij meet men de algebraische som van de positieve en negatieve verzadigingsstromen welke op twee tegenover elkaar liggende zijelectroden worden verkregen. Men houdt de gas druk echter zo laag dat een ion uit de bundel gemiddeld niet meer dan één omlading uitvoert, d.w.z. het verlies proces is te verwaarlozen. Men krijgt nu op de zijelectroden een positief ionen overschot afhankelijk van de vangst doorsnede.

In hoofdstuk III wordt ons apparaat beschreven. Dit bestaat uit een dikke stalen buis, om het strooi magneetveld van de isotopen separator of te schermen, welke als ionenbron gebruikt wordt in ons experiment. De buis is verdeeld in enkele onderdelen met gesoldeerde flenzen, welke met behulp van rubber pakkingen een

vacuum dichte verbinding geven. De separator is vaak in gebruik voor de produktie van isotopen. Daarom hebben wij een extra ionen bron voor het voorbereidend werk. Deze bron is gebaseerd op het gasontladings principe van Penning. In deze opstelling is nog geen analyserende magneet aanwezig.

Het belangrijkste onderdeel van het apparaat is de botsingskamer waarin het electrode systeem met behulp van elektrisch geisoleerde vacuum doorvoeringen is aangebracht. Deze kamer wordt met het gewenste gas gevuld en is aan de bron zijde afgesloten door een nauwe spleet, waardoor de ionen bundel binnen treedt. De vacuum kamer welke aan deze spleet grenst, is verbonden met een olie diffusie pomp welke het hele apparaat evacueert. Wanneer wij de experimenten uitvoeren, moeten wij met behulp van deze pomp een druk verval handhaven tussen botsings en vacuum kamer en voorkomen dat het gas uit de eerste kamer in de separator kan stromen.

Elke stroom, met een buisvoltmeter gemeten op een of meer elektroden in de botsingskamer, wordt vergeleken met de stroom van de bundel op de monitor in de vacuum kamer (gemeten met een galvanometer), om op deze wijze de intensiteits fluctuaties van de bundel te elimineren.

In hoofdstuk IV worden alle soort bepalingen uitvoerig besproken voor de combinatie N^+, H_2 bij 10 keV. Hierbij wordt het mathematisch formalisme van hoofdstuk II in toepassing gebracht. De gas druk waarmee men werkt varieert ruw genomen van 10^{-4} — 2×10^{-2} mm Hg, de gas lengte van ongeveer 6—27 cm. Voor de lengte 27 cm bereikt de bundel zijn evenwichtstoestand bij ongeveer 5×10^{-3} mm Hg. De vangst doorsnede, verkregen met de methode van Stedeford, blijkt redelijk overeen te stemmen met het resultaat van de gecombineerde vangst en verlies doorsnede bepaling. De ionisatie doorsnede wordt bepaald voor de bundel in evenwichtstoestand. Er blijkt verder weinig verschil te bestaan tussen de ionisatie doorsnede voor de bundel ionen en atomen afzonderlijk. Een methode wordt aangegeven om met de bundel in evenwichtstoestand de storende strooiing te onderzoeken. Deze blijkt verwaarloosbaar voor de genomen combinatie N^+, H_2. Wij meten de secundaire emissie van elektronen in de collector, veroorzaakt door de primaire ionen bundel en wij tonen aan dat er een belangrijke reflectie optreedt. De gereflecteerde deeltjes blijven echter grotendeels in de collector

ruimte, zodat de doorsnede metingen niet gestoord worden. De middelbare fout in de verschillende doorsneden is ongeveer 5%; de systematische fout is van dezelfde orde. De reproduceerbaarheid der waarnemingen is zeer bevredigend.

In hoofdstuk V wordt een overzicht gegeven van alle meetresultaten. Wij hebben de vangst, verlies en ionisatie doorsneden bepaald voor verschillende ionen in waterstof gas. Om meer aanpassing bij andere onderzoekers te verkrijgen, hebben wij nog enkele metingen uitgevoerd in argon en neon gas. Alleen bij de combinaties in argon en neon vinden wij een verschil tussen de vangst doorsneden bepaald met de twee reeds eerder aangeduide methoden. Wij tonen aan dat dit verschil veroorzaakt wordt door strooiing over hoeken groter dan 3°. Er is redelijke overeenstemming tussen onze vangst doorsneden en die van de Engelse groep in Londen (Hasted, Gilbody, Stedford, Keene). Bij de verlies en ionisatie doorsneden hebben wij weinig aanpassing bij andere onderzoekers kunnen vinden.

De resultaten worden geinterpreteerd met de adiabatische theorie. Wanneer de adiabatische parameter $a\Delta E/hv$ (a = atoom diameter $\pm 10^{-8}$ cm, ΔE = de verandering van inwendige energie welke in geval van ionisatie gelijk is aan de ionisatie energie, h = constante van Planck, v = relatieve snelheid) van de orde één is, wordt er een zogenaamd resonantie maximum in de doorsnede verwacht. In overeenstemming met de qualitatieve theorie kunnen wij begrijpen dat onze verlies en ionisatie doorsneden in het algemeen kleiner zijn dan onze vangst doorsneden. De toepassing van de theorie wordt gecompliceerd door het bestaan van aangeslagen toestanden in het primaire ion en in het gevormde gas ion.

Er worden resultaten gegeven over secundaire emissie en reflectie op de koperen eind electrode van de collector.

In hoofdstuk VI geven wij enkele kritische beschouwingen. De methode van Wien kan slechts toegepast worden voor enkelvoudig positief geladen ionen en atomen, waarbij de vorming van dubbel geladen of negatief geladen ionen is te verwaarlozen. De methode van Stedeford heeft een eenvoudiger mathematisch formalisme, maar men bepaalt hier alleen maar de vangst doorsnede. Het is wenselijk deze methode te combineren met een analyse van de bundel welke in evenwichtstoestand de botsingskamer verlaat. Uit de samenstelling van de bundel volgt de verhouding van vangst

en verlies doorsnede. Men moet echter een goede detector hebben die op dezelfde manier op geladen en neutrale deeltjes reageert.

Het is wenselijk de constructie van het apparaat te verbeteren. Vereenvoudigingen kunnen aangebracht worden in het stroom meet systeem en men kan het vacuum systeem verbeteren door o.a. een hogere pomp capaciteit in te voeren.

In verband met de theorie zijn verdere vangst, verlies en ionisatie doorsnede bepalingen belangrijk.

Wij zullen de experimenten uitbreiden door de botsingsprocessen spectroscopisch te onderzoeken en op deze manier meer te leren over de aangeslagen toestanden.

REFERENCES

A 1. Allison S. K. and Warshaw S. D., Rev. Mod. Phys. **25** (1953) 779.
B 1. Bartels H., Ann. d. Phys. **6** (1930) 957 and **13** (1932) 373.
B 2. Batho H. F., Phys. Rev. **42** (1932) 753.
B 3. Berry H. W., Phys. Rev. **62** (1942) 378.
B 4. Barnett C. F., Stier P. M. and Evans G. E., Rev. Sci. Instr. **24** (1953) 394.
B 5. Bohr N., Kgl. Danske Videnskab. Selskab, Mat-fys. Medd. **18** (1948) 8.
E 1. Everhart E., Stone G. and Carbone R. J., Phys. Rev. **99** (1955) 1287.
G 1. Gerthsen Chr., Ann d. Phys. **3** (1929) 394.
G 2. Goldmann F., Ann d. Phys. **10** (1931) 460.
G 3. Grassot M. E., J. Phys. **4** (1904) 696.
H 1. Hasted J. B., Proc. Roy. Soc. **A 205** (1951) 421.
H 2. Hasted J. B., Proc. Roy. Soc. **A 212** (1952) 235.
H 3. Hagstrum H. D., Phys. Rev. **96** (1954) 336.
H 4. Hasted J. B., Proc. Roy. Soc. **A 227** (1955) 476.
K 1. Keene J. P., Phil. Mag. **40** (1949) 369.
K 2. Kanner H., Phys. Rev. **84** (1951) 1211.
K 3. Krasner S., Phys. Rev. **99** (1955) 520.
M 1. Meyer H., Ann. d. Phys. **30** (1937) 635.
M 2. Montague J. H., Phys. Rev. **81** (1951) 1026.
M 3. Müller W., Dissertation, Karelsruhe 1954.
M 4. Massey H. S. W. and Burhop E. H. S., Electronic and Ionic Impact Phenomena, Clarendon Press., Oxford 1952.
M 5. Mott N. F. and Massey H. S. W., The Theory of Atomic Collisions, Clarendon Press, Oxford 1949.
R 1. Ruttenauer A., Z. f. Phys. **1** (1920) 385 and **4** (1921) 267.
R 2. Rüchardt E., Ann. d. Phys. **71** (1923) 377.
R 3. Rudnick P., Phys. Rev. **38** (1931) 1342.
R 4. Ribe F. L., Phys. Rev. **83** (1951) 1217.
R 5. Rostagni A., Z. f. Phys. **88** (1934) 55.
S 1. Sherwin C. W., Phys. Rev. **57** (1940) 814.
S 2. Stedeford J. B., Proc. Roy. Soc. **A 227** (1955) 466.
S 3. Snitzer E., Phys. Rev. **89** (1953) 1237.
S 4. Stier P. M., Barnett C. F. and Evans G. E., Phys. Rev. **96** (1954) 973.
S 5. Smith R. A., Proc. Cambridge Phil. Soc. **30** (1934) 514.
W 1. Wien W., Ann. d. Phys. **39** (1912) 528.
W 2. Whittier A. C., Can. J. of Phys. **32** (1954) 275.
W 3. Wolf F., Ann. d. Phys. **23** (1935) 285.
W 4. Wolf F., Ann. d. Phys. **27** (1936) 543.
W 5. Wolf F., Ann. d. Phys. **34** (1939) 341.
Z 1. Zilverschoon C. J., Dissertation, Amsterdam 1954.
Z 2. Zilverschoon C. J., Ned. T. Natuurk. **16** (1950) 323.

CONTENTS

Introduction. 9

Chapter I Historical review of the experiment.

§ 1.1. Experimental methods 12
§ 1.2. Literature review 17
§ 1.3. Results 23

Chapter II General treatment of our capture, loss and ionization cross-section determination.

§ 2.1. Formal treatment of capture and loss 25
§ 2.2. The combined experimental determination of σ_c and σ_l 30
§ 2.3. The experimental determination of σ_c at low pressures independently of σ_l or w 34
§ 2.4. Formal treatment of ionization 35
§ 2.5. Experimental determination of σ_i^+ and σ_i^0 . 37

Chapter III The apparatus.

§ 3.1. Introduction 42
§ 3.2. Screening of the magnetic field of the separator 44
§ 3.3. Production and collimation of the beam particles 45
§ 3.4. Vacuum system 48
§ 3.5. The electrode system 51
§ 3.6. The influence of the stray magnetic field of the separator on the realization of saturation currents on the side electrodes 54
§ 3.7. Detection of currents and electronic equipment 56

Chapter IV Evaluation of the cross-sections from the experimental results.

§ 4.1. Combined capture and loss cross-section measurement 59
§ 4.2. The determination of σ_c at low pressures independently of σ_i or w 64
§ 4.3. Comparison of the capture cross-sections or probabilities determined by the two different methods 65
§ 4.4. Ionization cross-section measurement . . . 66
§ 4.5. Secondary emission coefficient γ and reflection coefficient R at collector plate P_3 72
§ 4.6. Corrections. 75
§ 4.7. Sources of error. 78

Chapter V General survey and discussion of our experimental results.

§ 5.1. Introduction 83
§ 5.2. Results 83
§ 5.3. Discussion of the results 92
§ 5.4. The disturbance by scattering. 93
§ 5.5. Theoretical interpretation of the disturbing scattering 94
§ 5.6. The adiabatic hypothesis. 99
§ 5.7. Interpretation of our results with the adiabatic hypothesis 100
§ 5.8. Deviations from the adiabatic theory . . . 106
§ 5.9. Secondary emission and reflection 107

Chapter VI Critical Considerations.

§ 6.1. The experimental method 109
§ 6.2. Experimental conditions 110
§ 6.3. Continuation and extension of the experiment 111

Samenvatting 113

References. 118

STELLINGEN.

1. Het verdient aanbeveling meer aandacht te besteden aan de strooiingsverschijnselen van snelle ionen en atomen in gassen in verband met de methode en de geometrie van het systeem van electroden voor de electronen vangst, verlies en ionisatie doorsnede metingen.

Hoofdstuk I, V en VI van dit proefschrift.

2. In het energiegebied lager dan ongeveer 25 keV is een directe meting van de electron verlies doorsnede voor atomen in het algemeen moeilijk uitvoerbaar. Het gebruik van een bepaling langs indirecte weg verdient daarom in vele gevallen de voorkeur.

J. H. Montague, Phys. Rev. 81 (1951) 1026.

3. De methode welke Foster gebruikt om de ionen dichtheid in de gasontlading van de hoogvacuum ionenpomp te berekenen is aanvechtbaar en voert tot een te hoge waarde voor deze dichtheid.

J. S. Foster, thesis, Berkeley (California) 1953.

4. Een statistische analyse van de precisie massabepalingen van Scolman, Quisenberry en Nier geeft aanleiding te veronderstellen dat de door hen opgegeven fouten een grootte-orde te klein zijn.

T. T. Scolman, K. S. Quisenberry en A. O. Nier.
Bull. Amer. Phys. Soc. 30, no. 7 (1955) E 10-11.

5. De bepaling door Rasmussen van de kernspin van de twee hafnium isotopen met oneven massagetal is onbetrouwbaar. Ze dient herhaald te worden met gescheiden isotopen, mede met het oog op de recente ontwikkeling in het schillenmodel van de kern.

E. Rasmussen, Naturwiss. 23 (1935) 69.
B. R. Mottelson en S. G. Nilsson, Phys. Rev. 99 (1955) 1615.

6. Uit de negatieve resultaten van de neutronen diffractie proeven van Bacon en Street voor Mn As in het temperatuurgebied 40—130 °C kan men nog niet concluderen dat er geen anti-ferromagnetische structuur bestaat in dit gebied.

G. Bacon en R. Street, Nature 175 (1955) 518.

7. Hoewel de registratie van harttonen belangrijke informaties kan geven, over de tijdsrelaties maakt zij het auscultéren allerminst overbodig; te trachten de weergave karakteristiek van het registrerende instrument vergelijkbaar te maken met de karakteristiek van het oor is mede daarom zinloos.

8. De Saha vergelijking voor een thermodynamisch temperatuur-druk evenwicht geeft toegepast op het inwendige van de zon onwaarschijnlijke resultaten.

S. CHANDRASEKHAR, Astrophysics (J. A. Hynek), 1951, blz. 606-608.

9. De wijze waarop Becker de optimale druk afleidt voor isotopen scheiding door thermodiffusie is onjuist. De formule voor deze druk is fout.

E. W. BECKER, Ullmanns Enc. der techn. Chem. 1 (1951) 360.

10. De additieve eigenschappen die Dunkel toekent aan de molaire cohaesie λ en de constante B voor alkanen en mono-substitutie producten van alkanen hebben slechts een beperkte toepasbaarheid. Een uitbreiding van de theorie is voor massaspectrometrische doeleinden zeer gewenst.

M. DUNKEL, Z. Phys. Chem. 138 (1928) 42.

11. Het nut van de exermano wordt door vele musici ten onrechte onderschat.